Russian Chemical Reviews **74** (7) 587 – 618 (2005) © 2005 Russian Academy of Sciences and Turpion Ltd

DOI 10.1070/RC2005v074n07ABEH000903

Nanotubes and related nanostructures of d-metal oxides: synthesis and computer design

G S Zakharova, V L Volkov, V V Ivanovskaya, A L Ivanovskii

Contents

I.	Introduction	587
II.	Synthesis and properties of nanotubes and related nanostructures of metal oxides	588
III.	Computer design of structures and electronic properties of oxide nanotubes	607
IV.	Conclusion	613

Abstract. State-of-the-art studies on the synthesis, properties and the computer design of nanotube forms of transition metal oxides are analysed. Main methods for the preparation of oxide nanotubes and related quasi-one-dimensional nanostructures (nanobundles, nanoribbons, *etc*.) are discussed. Data on the morphology and physicochemical properties of these materials and prospects for their technological applications are summarised. The results of the computer design of atomic structures and results of quantum-chemical calculations of electronic structures and chemical bond parameters of Ti, V and Mo oxide nanotubes and their fullerene-like molecules are considered. The bibliography includes 427 references.

I. Introduction

The discovery (in 1991) of quasi-one-dimensional (1D) nanostructures, *viz*., carbon nanotubes (NT),[1] and the design of nanomaterials with unique properties [2–28] have stimulated theoretical and experimental studies aimed at searching for and preparing analogues of such materials based on other simple substances and inorganic compounds. The advances made in this field by the early 20th century have been covered in reviews.[29–39]

Nanotubes of numerous inorganic compounds were synthesised. Nanotubes of MoS_2,[40] other layered d-metal dichalcogenides MX_2 (M = Mo, W or Ta; X = S or Se) [41–55] and hexagonal boron nitride (BN), boron carbide (BC_x) and boron carbonitride ($B_xC_yN_z$) were among the first to be prepared.[56–63] Nanotube forms of numerous chalcogenides were synthesised: InS,[64] ZnS,[65] Bi_2S_3,[66] ReS_2,[67] $W_xMo_yC_zS_2$,[68] ZrS_2, HfS_2,[69,70] $NbSe_2$,[71–73] TiS_2, $TiSe_2$,[74–76] $MoTe_2$,[77] WSe_2,[78] $MoS_{2-x}I_y$,[79] CdS, CdSe,[80,81] Ag_2S [82] and Li_zMoS_2.[83] The synthesis of $NiCl_2$ nanotubes was also documented.[84–86] Tubular forms of semiconducting materials, such as SiGe, InAs/GaAs, InGaAs/GaAs, SiGe/Si and InGeAs/GaAs,[87–89] are also known.

Cobalt,[90] antimony,[91] tellurium [92–94] and bismuth [95–97] nanotubes were synthesised. The atomic structures, electronic properties, stability factors and possible procedures for the preparation of nanotubes of metals (Na, Cu,[98] Ni,[99] Ag, Au [100,101] and Bi [102,103]), boron,[104] silicon,[105] metal diborides MB_2 (M = Mg, Al, Sc, Ti and Zr),[106–110] $CaSi_2$,[111] ternary silicides with AlB_2: $Sr(Ga_xSi_{1-x})_2$ and $Ca(Al_xSi_{1-x})_2$ structures,[112] layered metal halide nitrides β-MNX (M = Zr or Hf; X = Cl or Br) [113] and high-temperature superconducting complex ceramics [114] were theoretically predicted.

In recent years, p-, d- and f-metal (Al, Ge, Ti, Nb, Ta, Zr, V, Mo, Dy, Tb, *etc*.) oxides, along with the above-mentioned substances and compounds, have found wide application in the design of nanostructured functional materials as films, nanorods, mesoporous systems, nanoclusters and nanocrystallites and their various associates. Some of these nanosized materials can be prepared with the use of carbon nanotubes. For example, these compounds can be prepared as nanofibres and nanotubular ceramics by filling inner (and intertubular) cavities in carbon tubes (or their bundles) with oxides V_2O_5, MoO_3, PbO or Bi_2O_3 followed by the removal of the carbon shell by chemical methods. The design of various nanocomposites based on or involving metal oxides has attracted considerable attention.

One of the main lines of investigation of nanostructured metal oxides is the preparation of their nanotube forms. Phases, which have (like graphite) layered (quasi-two-dimensional, 2D) structures and are characterised by pronounced anisotropy of interatomic interactions, are generally considered as substances or compounds promising for the preparation of such tubular forms.[6–9,18,29–39] The anisotropy of interatomic interactions is determined by a combination of strong covalent (or covalent-ionic) bonds and weak van der Waals interactions between the layers. These structural features and characteristics of chemical bonding are less typical of metal oxides than, for example, of d-element dichalcogenides. Hence, methods for the preparation of metal oxide nanotubes have essential distinguishing features and often produce hollow nanotubes along with a broad range of other quasi-one-dimensional nanostructures (nanorods, nanoribbons, *etc*.)

It should be noted that data on the synthesis, structures, properties and fields of application of carbon NT are summarised in monographs [3–7] and numerous reviews,[8–32] whereas publications, in which the results of studies of non-carbon nanotubes were generalised, are scarce [29–39] and were devoted primarily to the most well-studied groups of such materials, *viz*., nanotubes (and fullerene-like clusters) of graphite-like boron nitrides, carbides and carbonitrides and d-metal dichalcogenides. Selected results of the synthesis and investigations of oxide NT were included in the reviews.[37,38] The review [39] dealt with practical procedures for the

G S Zakharova, V L Volkov, V V Ivanovskaya, A L Ivanovskii Institute of Solid State Chemistry, Urals Branch of the Russian Academy of Sciences, ul. Pervomaiskaya 91, 620219 Ekaterinburg, Russian Federation.
Fax (7-343) 374 44 95, tel. (7-343) 349 30 09, e-mail: volkov@ihim.uran (G S Zakharova, V L Volkov), tel. (7-343) 349 33 87, e-mail: viktoria@ihim.uran.ru (V V Ivanovskaya), tel. (7-343) 374 53 31, e-mail: ivanovskii@ihim.uran.ru (A L Ivanovskii)

Received 3 February 2004
Uspekhi Khimii **74** (7) 651 – 685 (2005); translated by T N Safonova

preparation and modelling of titanium and vanadium oxide nanotubes.

In the present review, we consider the state-of-the art studies of all known nanotube forms of transition metal oxides. Main methods for the preparation of oxide nanotubes and related quasi-one-dimensional nanostructures (nanofibres, nanorods, nanoribbons, *etc*.) are summarised. Data on the morphology and physicochemical properties of such materials are discussed. The possible fields of technological applications are considered. The results of computer design of atomic structures and quantum-chemical calculations of electronic structures and chemical bond parameters of Ti, V and Mo oxides nanotubes and related fullerene-like molecular clusters are analysed.

It should be noted that the known nanotube forms of oxides are not limited to transition metal oxides considered below. Nanotubes and nanotube composites of p-element (aluminium, silicon and gallium) oxides have attracted considerable attention.[115–125] The studies aimed at synthesising nanotubes of f-element oxides (for example, Tb_2O_3 [126] and Dy_2O_3 [127]) are presently underway. However, data on the structures and properties of 1D forms of these oxides are scarce, and analysis of such materials is beyond the scope of the present review.

II. Synthesis and properties of nanotubes and related nanostructures of metal oxides

The classification of nanosized materials used in the literature and their principal geometric parameters are given in Table 1. Nowadays, the main lines of investigation of nanostructured metal oxides are as follows: the development of methods for their synthesis and study of the morphology and physicochemical characteristics of the products. Progress in the synthesis of oxide nanotube materials with reproducible properties determines to a large extent the prospects of their practical use.

Table 1. Structural types of nanosized materials and their geometric parameters.

Structural type	Description [a]
Nanotubes	tubular structures with an outer diameter of up to 100 nm, $L < 1$ μm
Nanorods	quasi-one-dimensional cylindrical structures, $D < 100$ nm, $L < 1$ μm
Nanowire	the same, $D < 100$ nm, $L > 1$ μm
Nanofibres	threads, $D \leqslant 50$ nm, $L > 1$ μm
Nanoparticles	compact particles, $D < 10$ nm
Nanopowder	the same, $D < 100$ nm
Nanodots	crystals with sizes up to 100 nm
Nanowhiskers	needle-like structures with a length of several millimetres and a base thickness of < 100 nm
Nanoribbons	structures as planar ribbons with a thickness of up to 100 nm and a width larger than the thickness
Nanocolumns	nanostructures with $D \leqslant 100$ nm, $L > D$
Nanocable	structures with a morphology of a coaxial cable, $D \leqslant 100$ nm
Nanobridges	structures with a morphology analogous to a bridge construction with a length of tens of micrometers containing 'details' with a diameter of up to 100 nm
Nanonails	nail-like structures, $D \leqslant 100$ nm
4(6)-Fold nanorotors	nanostructures as four(six)-blade rotors; the constituent diameter is up to 100 nm
Tetrapod nanostructure	nanostructures consisting of four nanorods ($D \leqslant 100$ nm) sharing a centre
Nanocomposite	material consisting of particles of different compounds with sizes up to 100 nm

[a] D is the diameter, L is the length.

Modern investigations of nanotubular oxides and related materials are aimed at developing and improving particular synthetic schemes and extending the range of oxides, whose nanotube forms can be prepared. In most original publications, procedures for the preparation of nanotubes of a particular oxide and their selected characteristics (generally, the elemental composition, the morphology and the structural parameters) were reported. Experimental data accumulated in this new field do not allow one to reveal general regularities of the formation of particular nanostructures and decide which methods for their synthesis are most efficient and universal. Hence, in the present review, we summarise methods for the preparation of nanotubular oxides and related quasi-one-dimensional forms. A comparison and critical analysis of these methods are beyond the scope of this review.

Modern methods for the preparation of nanosized forms of simple and complex oxides can be classified into two main groups, *viz*., chemical and template methods. The chemical synthesis involves the spontaneous formation of nanostructures in reactions of the starting reagents existing in different states (aqueous or aqueous-organic media, solid or vapour phases, during thermolysis of salts, *etc*.). The template method is based on the formation of nanostructures on the surfaces of solid materials (organic and inorganic), which dictate the size and morphology of the reaction products. In particular, organic molecules can serve as templates. Such molecules are inserted into layered structures of oxides, thus making it possible to change the form of nanotubes in their synthesis. Among these methods, vapour condensation of oxides and their electrochemical deposition also hold promise.

Below we consider methods for the synthesis and properties of three main groups of 1D nanostructures formed by first-, second- and third-row transition metal oxides. Main data on their compositions and morphology are given in Table 2.

1. Nanostructures of 3d4s-metal oxides

a. Titanium oxides

Nanosized forms of titanium dioxide can be prepared by both chemical and template methods. Well-crystallised nanotube forms of TiO_2 can be synthesised by hydrothermal reactions of titanium dioxide (anatase or rutile) powder with an aqueous NaOH solution.[128–134] For various tubes, the O : Ti atomic ratio differs from those observed in crystalline anatase or rutile.[128] Generally, multilayer tubes with an interlayer distance of ~ 0.75 nm and an average diameter (D) of ~ 9 nm are produced.[129] The mechanism of their formation involves the rolling-up of the (100) plane of $H_2Ti_3O_7$ about the [001] direction. The ends of the tubes are open and their walls are corrugated.[134] The morphology of the tubes depends on the size and structure of the starting TiO_2 nanoparticles.[130]

Ultradispersed rutile with an average particle size of 7.2 nm gives longer nanotubes compared to those formed by anatase or large rutile particles. Nanotubes with $D \approx 8-10$ nm and a length (L) of ~ 100 nm were synthesised [131] by keeping TiO_2 with a specific surface area of 50 $m^2\ g^{-1}$ in a 10 M NaOH solution at 110 °C for 20 h. The morphology of the resulting samples depends on the TiO_2 structure type, and their properties depend on subsequent acid and thermal treatment.[132, 133] For example, after treatment with a H_2SO_4 solution followed by annealing at 300 °C, TiO_2 nanotubes show high catalytic activity in esterification of cyclohexanol with acetic acid,[132] whereas the starting anatase is inactive in this catalytic process.

Hydrothermal treatment of TiO_2 powders (4.0–18.5 nm) in a NaOH solution at 110 °C for 20 h followed by washing with dilute HNO_3 affords multilayer anatase nanotubes 500 nm in length.[133] The use of HNO_3 instead of HCl results in the formation of more

Table 2. Main methods of synthesis and morphology of nanostructured transition metal oxides.

Oxide	Method of synthesis	Morphology	Oxide	Method of synthesis	Morphology
TiO_2	chemical	tubes with $D = 9-12$ nm	Co_3O_4	chemical	tubes with $D = 200-400$ nm
	"	rods with $D =$ $(4-6)-(50-100)$ nm		template	fibres
			$CoFe_2O_4$	"	wire with $D = 50$ nm
	"	wire with $D = 20-200$ nm	NiO	"	ribbon with a width of 4 nm
	"	ribbon with a width of 20–200 nm		"	wire with $D = 4$ nm
			CuO	chemical	rods with $D = 8$ nm
	"	needles and whiskers with $D = 5-8$ nm		template	tubes with $D = 20-90$ nm
				electrochemical	fibres and whiskers with $D = 2-10$ nm
	template	tubes with $D = 2-70$ nm			
	"	hollow fibres with $D = 20-50$ nm	ZnO	chemical	rods with $D = 5-300$ nm
				"	tubes
	"	rods with $D = 20-30$ nm		"	chiral rods with $D = 500$ nm
	electrochemical	tubes with $D = 25-120$ nm		vapour phase	wire with $D = 15-80$ nm
		wire with $D = 40$ nm		"	rods with $D = 15-45$ nm
$H_2Ti_3O_7$	chemical	rods with $D = 9$ nm		"	whiskers with $D = 50-500$ nm
$K_2Ti_8O_{17}$	"	ribbons		"	belts
$Na_2Ti_4O_9$	"	belts with a width of 100–500 nm		"	bridges
$SrTiO_3$ }	"	tubes with $D = 8-15$ nm		"	nails
$BaTiO_3$ }		rods with $D = 5-60$ nm		"	tadpoles
Composite TiO_2/poly-pyrrole (poly-aniline)	"	tubes with $D = 90-130$ nm		vapour phase combined with template synthesis	wire with $D = 30-200$ nm
				electrochemical	wire with $D = 50$ nm
TiO_2/SiO_2	"	tubes with $D = 13$ nm	composite Zn/ZnO	pyrolysis	cable with $D = 60$ nm
Composite Au/TiO_2	template	wire with $D = 210$ nm			
			composite $Ga/Ga_2O_3/ZnO$	"	cable
$VO_x(C_nH_{2n+4}N)_y$	chemical	tubes with $D = 15-150$ nm			
VO_x	template	tubes with $D = 20-55$ nm	Y_2O_3	template	tubes
$V_{0.99}Mo_{0.01}O_{2.49} \cdot (C_{16}H_{36}N)_{0.27}$	chemical	tubes with $D = 30-100$ nm	ZrO_2	"	tubes with $D = 40-50$ nm
				"	tubes with $D = 1.3-5.9$ μm
γ-LiV_2O_5	"	rods with $D = 30-40$ nm	Nb_2O_5	"	tubes with $D = 1.3-5.9$ μm
NaV_2O_5	"	rods	MoO_3	chemical	fibres with $D = 20-280$ nm
β-$Na_xV_2O_5$	vapour condensation	wire with $D = 20-200$ nm		template	tubes with $D = 50-300$ nm
			CdO	electrochemical	wire with $D = 40-60$ nm
$Na_{0.26}VO_x$	ion exchange	tubes with $D = 60-100$ nm	Ta_2O_5	template	tubes
$K_{0.27}VO_x$	"	tubes with $D = 60-100$ nm	$Sr_{0.8}Bi_{2.2}Ta_2O_{9+y}$	"	tubes with $D < 2$ μm
$Cu_{0.12}VO_x$	"	tubes with $D = 60-100$ nm	WO_x	vapour phase	needles and whiskers with $D = 50-500$ nm
Fe-VO_x	"	tubes with $D = 60-100$ nm			
$Mn_{0.1}VO_{2.5+\delta} \cdot n\,H_2O$	"	tubes with $D = 60-100$ nm	$WO_{2.9}$	"	rods with $D = 20$ nm
			WO_3	template	fibres with $D = 20$ nm
CrO_3	template	tubes			
α-MnO_2	"	fibres			
α-Fe_2O_3	chemical	hollow fibres with $D = 4-10$ nm			

dispersed NT powder. Titanium dioxide nanotubes prepared by the chemical method consist of 2–5 monolayers and have an inner diameter of 4.2–5.9 nm.[135] Such materials with a specific surface area of 379 $m^2\ g^{-1}$ hold promise in photocatalysis.

Films of oriented TiO_2 NT were prepared by the hydrochemical method (titanium foil, which contained TiO_2 nanoparticles deposited from an aqueous suspension, was subjected to hydrothermal treatment in 10 M NaOH at 95–160 °C).[136] Most of these nanotubes are open and consist of several layers. The outer and inner diameters of NT are 12 and 3.7 nm, respectively. The distance between the layers is 0.78 nm. The nanotubes are characterised by the monoclinic unit cell of $H_2Ti_3O_7$ with the unit cell parameters $a = 16.03$, $b = 3.75$, $c = 9.19$ Å, $\beta = 101.45°$. The most probable[137] composition of these nanotubes is $Na_2Ti_3O_7$; the Na^+ ions are removed by acid treatment. The distance between the layers in these nanotubes is independent of the number of layers and the inner and outer diameters of TiO_2 NT and is determined by OH^- groups. Taking into account the Ti—OH bond lengths and the van der Waals radius of the O atom, the interlayer distance should be equal to 0.63 nm, but it increases to 0.8 nm due to repulsion between the OH^- groups. The sodium cations play a decisive role in structure stabilisation.[138] Unmodified TiO_2 nanotubes exist only in an amorphous state[139] and are destroyed during crystallisation.

Anatase nanotubes prepared under hydrothermal conditions have a high capacity for lithium cations in electrochemical intercalation.[140] The insertion of Li^+ into TiO_2 NT occurs at a voltage of lower than 2.2 V. At a voltage of about 1.7 V, voltammetric curves have a plateau, which indicates that the electrochemical resistance reaches a minimum. These nanostructures were proposed as light-sensitive materials for solar batteries.[141]

Nanosized rods of rutile TiO_2 ($D = 4-6$ nm, $L = 50-150$ nm) were prepared[142] in air under atmospheric pressure by the reaction of 15 M HNO_3 with an aqueous $TiCl_4$ solution (3 mol $litre^{-1}$) with stirring (100–250 °C, 6–24 h). The sizes of nanorods are independent of the temperature and time of hydrolysis. These nanorods belong to the rutile modification and are characterised by the [110] growth direction. Mixing of $TiCl_4$ and HNO_3 solutions leads to oxolation of the $[TiO(OH_2)_5]^{2+}$

complex ion and isolation of rutile as brushes. The anisotropic growth was accounted for by selective absorption of Cl^- and NO_3^- anions and $[TiO(OH_2)_5]^{2+}$ cations on the (110) and (111) surfaces, respectively.

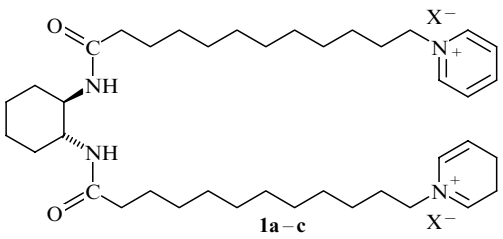
Thermolysis of titanium tetraisopropoxide $[Ti(OPr^i)_4]$ vapour in the presence and in the absence of NH_3 at 500 °C affords TiO_2 nanowires (D = 50–100 nm, L = 0.5–2 μm) on the WC substrate.[143] Thermolysis at 600 and 400 °C gives nanoparticles and thin films, respectively, of the anatase modification. In the presence of NH_3, thinner and longer nanorods are produced. The formation of 1D structures of TiO_2 is catalysed by cobalt admixtures.

A crystalline TiO_2 nanowire was prepared[144] by annealing TiS_2 in the presence of a flux (NaCl) and in the absence of a flux under an atmosphere of NH_3. In the former case, titanium disulfide was mixed with NaCl powder in a mass ratio of 1 : 3.5 and heated at 820 °C for 2.5 h. In the latter case, TiS_2 was heated at 820 and 970 °C. The precipitates were washed with an HCl solution, water and ethanol and dried at 85 °C. Samples prepared in the presence of the flux crystallised in the anatase modification with the unit cell parameters a = 3.782, c = 9.502 Å, whereas samples synthesised in the absence of the flux crystallised in the rutile modification (a = 4.953, c = 2.958 Å). Titanium dioxide nanoparticles are predominantly produced in the absence of NaCl. Anatase nanowires (smooth and straight) have a diameter of 20–200 nm and an L/D ratio of $\approx$ 500. Rutile nanowires with D = 150 nm and a length of several micrometres were prepared at 970 °C. The formation of TiO_2 nanostructures also occurs through the intermediate Na_2TiO_3 phase during its exchange interaction with HCl.

An amorphous TiO_2 gel prepared by hydrolysis of $Ti(OPr^i)_4$ in an ethanolic solution was used as a precursor for the preparation of interconnected structured nanosized fibres.[145] The precursor (0.1–0.3 g) was mixed with a 5–15 M NaOH solution (20 ml) and subjected to hydrothermal treatment at 100–180 °C for 48 h. The powder that precipitated was filtered off, washed with water and 0.1 M HCl to pH < 7 and dried *in vacuo* at 100 °C for no less than 10 h. The resulting twisted fibres with a thickness of 5–30 nm and a length from tens to hundreds of micrometres, which are wrapped together to form superstructured materials, have a layered structure with an interlayer distance of 0.7 nm and contain defects and dislocations. Alkaline treatment of the precursor (at a temperature higher than 180 °C) afforded thin ribbon structures 30–200 nm in width and from a few to tens of micrometres in length. A change in the NaOH concentration has no effect on the morphology of the product. The specific surface area of the nanofibres was 267, 354 and 375 $m^2\ g^{-1}$ at the synthesis temperatures of 100, 130 and 150 °C, respectively.

In the synthesis by the chemical method, TiO_2 nanotubes are formed at the instant crystalline TiO_2 reacts with a NaOH solution and transforms to the amorphous state. The reaction of an amorphous TiO_2 gel with NaOH produces well-interconnected fibres, in which the Ti atoms are octahedrally coordinated by two types of oxygen atoms, *viz*., the bridging μ_2-O atoms, through which the Ti atoms of the adjacent octahedra are linked to each other, and the OH^- groups. The presence of hydroxyl groups is a distinguishing feature of the 'TiO_2' gel. The reaction of the latter with NaOH is accompanied by cleavage of some Ti—OH and Ti—O—Ti bonds, with the result that the TiO_6 octahedra are linked into chains with long-range order, and the latter are partially transformed into layered structures. After lithium ion intercalation into nanofibres, the latter can be used as an electrode material in lithium cells and as atmospheric oxygen and nitrogen separators.

The template method has gained wide acceptance in the synthesis of TiO_2 nanotubes.[146, 147] Chiral organic compounds **1a**–**c** can be used as templates.[148, 149]



1a–**c**

X^- = PF_6^-, (1*R*,2*R*) (**a**); ClO_4^-: (1*R*,2*R*) (**b**), (1*S*,2*S*) (**c**).

In alternative methods, a 25% aqueous NH_4OH solution or 2 M HCl was added to a solution of $Ti(OPr^i)_4$ and compound **1a** in ethanol.[148] The resulting mixture was heated at 80 °C, homogenised, cooled to 25 °C, dried in air for 10 days and warmed at 50 °C *in vacuo* for 5 h. The dry sample was kept at 200 °C or 450 °C for 2 h. In the course of the sol–gel synthesis, template **1a** is self-organised to form a three-dimensional network of helical fibres (D = 50–300 nm) stabilised by hydrogen bonds involving NH_2^+ groups. The fibre structure was absent after heating of samples, which were pre-treated with an acid, at 450 °C. However, hollow fibres with an outer diameter of 150–600 nm and a length of up to 200 μm are retained upon alkaline treatment. The inner diameter of TiO_2 fibres (50–300 nm) is, apparently, dictated by the sizes of the template network.

The sol–gel synthesis with the use of chiral molecules **1b** and **1c** as templates produced chiral helical-like TiO_2 NT (Fig. 1).[149] Derivatives of *trans*-(1*R*,2*R*)- and *trans*-(1*S*,2*S*)-1,2-diaminocyclohexane give left- and right-handed helical fibres stabilised by intramolecular hydrogen bonds between the amino groups. The synthesis was carried out by stirring a mixture of solutions of enantiomers (1 mol $litre^{-1}$), $Ti(OPr^i)_4$ (5 mol $litre^{-1}$), H_2O (2.5 mol $litre^{-1}$) and NH_4OH (0.4 mol $litre^{-1}$) in ethanol at 0 °C followed by heating to 80 °C. The resulting transparent solution was slowly cooled to 25 °C and the resulting gel was dried

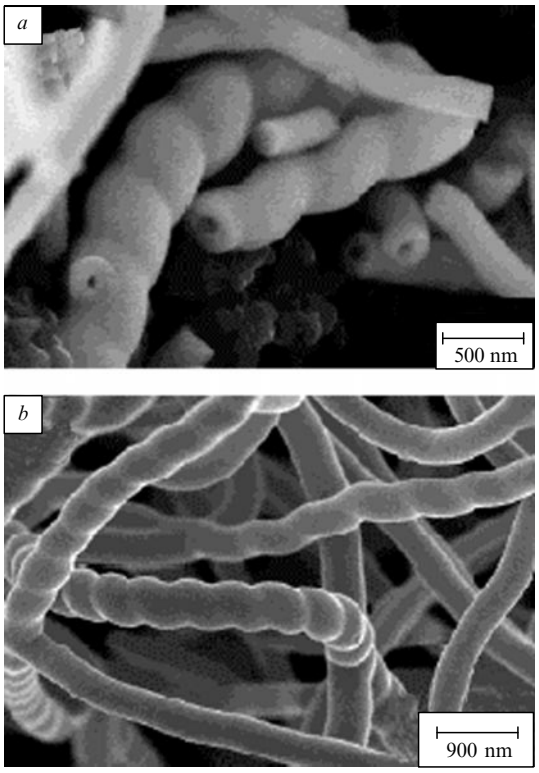


Figure 1. The SEM images of TiO_2 fibres prepared from enantiomers **1b** (*a*) and **1c** (*b*).[149]
Hereinafter, SEM is scanning electron microscopy.

at 25 °C for 10 days and then kept at 50 °C *in vacuo* for 5 h. To remove the templates, the xerogel was washed with acetone and calcined at 200 °C for 2 h and at 450 °C for 24 h. The resulting fibres have an outer diameter of 100–600 nm, an inner diameter of 30–180 nm and a length of up to 30 μm. This method was used also to synthesise chiral vanadium and tantalum oxide nanotubes.

Well-ordered helical-like ribbons and nanotubes were prepared [150] by sol–gel polymerisation of $Ti(OPr^i)_4$ in template gels of neutral dibenzo-30-crown-10 bound to cholesterol. The synthesis successively produces TiO_2 ribbons, twisted ribbons and open nanotubes with helical (right-handed) chirality ($D \approx 500$ nm). After removal of the template by annealing under a nitrogen atmosphere at 500 °C for 4 h, hollow helical ribbons and hollow nanotubes with a distance of 8–9 nm between the walls were obtained. Apparently, oligomeric TiO_2 particles are adsorbed on both sides of the corresponding structures from the template gel with a thickness of 8–9 nm and, consequently, the resulting tubes contain micro- and macropores. The mechanism of formation of helical ribbons and nanotubes involves adsorption of 'oligomeric' titanium dioxide particles on a tubular structure of an organic gel and their further growth through sol–gel polymerisation.

The use of laurylamine hydrochloride as a template and $Ti(OBu^n)_4$ as a precursor made it possible to prepare TiO_2 microtubes with mesoporous walls.[151] The outer diameter of the tubes was 2–8 μm. Their walls (0.2–2 μm in thickness) consist of cylindrical channels with the same diameter of 3.2 nm. These microtubes are thermally stable up to 773 K, have a specific surface area of 390 $m^2\ g^{-1}$ and consist of anatase with a low degree of crystallinity. The pore volume is 0.586 ml g^{-1}.

Ultrathin nanosized titanium dioxide layers were synthesised with the use of carboxylate latex and tobacco mosaic virus (TMV) particles as templates.[152] The latex and TMV particles on a substrate were coated with ultrathin TiO_2 layers by the sol–gel method and subjected to plasma treatment. The resulting hollow titanium spheres were linked to form nanotubes. After oxidative removal of the template, a rod-like TiO_2 structure with $D = 20–30$ nm was obtained. It is preferable to use oxygen plasma to retain the tubular structure after removal of the template.

Anatase nanoparticles prepared by gradual hydrolysis of a TiF_4 solution (0.04 mol $litre^{-1}$, pH 2) after the addition of NH_4OH (0.1 mol) were deposited on the surface of various templates,[153, 154] such as organic (cotton, silk or wool) or polymeric [155] fibres, aluminium porous membranes, plant fibres, *etc*. After immersion of the template into a solution and storage at 60 °C for 1–48 h, the hydrolysis product undergoes dehydration, and an anatase layer appears on the surface. Organic compounds were removed by annealing in air at 500 °C, and aluminium metal was dissolved in ammonia water (pH 12). Traces of fluorine were removed by calcination in air at a temperature higher than 300 °C. The use of cotton threads as a template results in the formation of hollow TiO_2 fibres consisting of anatase particles with a diameter of 20–50 nm; their inner diameter corresponds to the thread size. The wall thickness of TiO_2 depends on the deposition time. The hollow structure is destroyed at sizes greater than 500 nm. The specific surface area of these nanotubes is 50–70 $m^2\ g^{-1}$, and their walls contain microscopic pores.

Studies of the photocatalytic activity of anatase as films and nanotubes formed on wool in oxidation reactions of NO demonstrated that the activity on nanotubes increases by a factor of almost nine. Anatase nanotubes with an inner diameter of 50–150 nm were prepared on an aluminium membrane with a channel diameter of ~200 nm. The specific surface area of the material is 100–140 $m^2\ g^{-1}$. The use of leaf fibres as a template gives rise to a honeycomb structure consisting of TiO_2 nanotubes.

Nanosized crystalline anatase is generally prepared by the non-hydrolytic sol–gel method.[156] In a conventional method, $TiCl_4$ is added with stirring to benzyl alcohol at room temperature, and then the mixture is warmed to 40 °C and subjected to aging for 7–14 days. The resulting suspension is centrifuged and the precipitate consisting of TiO_2 particles with a diameter of 4–5 nm is washed with ethanol and dried.

An anodised porous aluminium plate was used [157] as a template to prepare compact open anatase nanotubes with an inner diameter of 50–70 nm and a wall thickness of 3–10 nm. The pores of the Al_2O_3 surface layer (70 nm in diameter and 10–12 μm in depth) were filled with liquid $Ti(OPr^i)_4$ and heated at 500 °C for 1 h under a stream of O_2. Decomposition of $Ti(OPr^i)_4$ on the surface of Al_2O_3 afforded a TiO_2 layer. Then anodised aluminium was partially and completely dissolved in a mixture of phosphoric (6 mass%) and chromic (1.5 mass%) acids. Etching at 80 °C for 15 min, as a rule, completely removed the template without destruction of TiO_2 nanotubes.

Hydrolysis of TiF_4 in an HCl + NH_4OH solution with pH 1.6 at 60 °C produced [158] single-crystalline TiO_2 nanotubes on an anodised aluminium membrane with a pore diameter of 100 nm and a length of 60 μm. The product was washed with water and dried at 60 °C for 24 h. Nonuniformly distributed irregularly shaped columnar crystals of TiO_2 containing straight TiO_2 nanotubes with a cavity extended in the axial direction grew on the upper surface of the membrane. The outer and inner diameters of the nanotubes were 20–40 and 4–5 nm, respectively. The interlayer distances in the walls (3.6 ± 0.1 Å) corresponded to the interplanar distance d_{101} of anatase. Larger isolated tetragonal crystals of anatase appeared on the lower surface of the membrane.

Titanium dioxide nanotubes of the anatase modification were also prepared in nanosized channels of a porous aluminium membrane, which was stored in a TiF_4 solution (0.04 mol $litre^{-1}$, pH 2) at 60 °C for 24 h.[159] The template was dissolved in an aqueous ammonia solution (pH 12) at room temperature. The inner diameter of the nanotubes (Fig. 2) is 50–150 nm, the walls consist of TiO_2 particles with a size of 10–20 nm and the pore diameter is smaller than 10 nm. The size of the inner channels in the tubes depends on the time of deposition of TiO_2. If the deposition time is longer than 12 h, compact rods grow. The morphology of the nanotubes is retained because they are prepared without calcination. This material is of interest for photocatalytic gas reactions and liquid filtration. The photoelectrochemical characteristics of TiO_2 nanotubes and nanorods were studied,[160] and the dependence of the photocurrent on the potential was demonstrated to be analogous to that observed for nanocrystalline films.

The mechanism of formation and the microstructure of TiO_2 nanotubes prepared according to the above-considered procedure [159] were investigated.[161] The outer and inner diameters of the

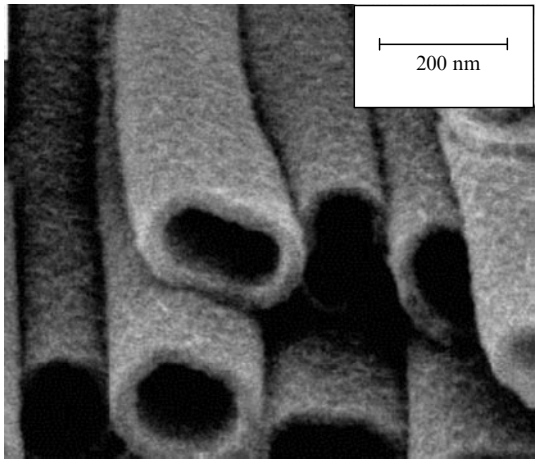


Figure 2. The SEM image of TiO_2 nanotubes synthesised on anodised aluminium as a template.[159]

samples were 9 and 5 nm, respectively. These nanotubes with an interlayer distance of ~7.1 Å, which is twice as large as the analogous distance along the [101] direction in anatase ($a = b = 3.78$, $c = 9.52$ Å), are structurally similar to carbon nanotubes and are formed by rolled-up planar TiO_2 layers. Taking into account the crystallographic parameters of anatase and rutile ($a = b = 0.459$, $c = 0.295$ nm), it can be concluded that the anatase modification is more favourable for the formation of TiO_2 nanotubes. This conclusion is supported by the fact that the surface energy of anatase is lower than that of rutile.[161]

The model of TiO_2 nanotube formation can be represented by the $3D \rightarrow 2D \rightarrow 1D$ scheme. A three-dimensional (3D) anatase crystal reacts with a NaOH solution to form a laminar two-dimensional (2D) structure, which is bent so as to bind unsaturated bonds of the terminal atoms. Further rolling-up results in the formation of a tubular structure. There are two possible $2D \rightarrow 1D$ transformations giving rise to concentric and non-concentric structures. Only non-concentric structures were experimentally observed.[161]

An ethanolic solution of $Ti(OPr^i)_4$, to which an HCl solution in ethanol is added at 15 °C, can be used as a precursor in the synthesis of TiO_2 nanotubes.[162] An aluminium membrane was placed in the resulting sol for 5–60 s. Then the membrane was dried and annealed at 400 °C for 6 h. Immersion of the membrane into the sol for 5 and 60 s affords nanotubes and nanofibres, respectively. In the case of an intermediate immersion time (25 s), nanotubes with thick walls grow. The sol temperature and the time of membrane immersion also influenced the morphology of nanostructures and the wall thickness of TiO_2 nanotubes. In membrane pores with a size of 22 nm, bundles of 2–4, 10 or a larger number of fibres grow as long prismatic crystals with the rare and metastable anatase-like orientation of the (001) plane with the [110] direction. After irradiation with sunlight, fibrillar TiO_2 exhibits high catalytic activity in decomposition of salicylic acid, which is associated with its larger specific surface area. This method can also be used to prepare photocatalytically active TiO_2 nanowires.[163]

In the synthesis of TiO_2 NT by colloidal heterocoagulation, carbon nanotubes (C-NT) were used as a template. A TiO_2 gel with an admixture of NaOH was added dropwise to an aqueous suspension of carbon nanotubes, which were pre-treated with ammonia, and polyethyleneamine $(CH_2CH_2NH)_n$ at pH 8. The negatively charged TiO_2 particles were deposited on the walls of the carbon nanotubes and cover them uniformly. The resulting composite contained ~1.5 mass% C-NT, had a low specific gravity, was easily separated from the reaction mixture and possessed photocatalytic properties.[164–166]

Nanoparticles of anatase TiO_2 were prepared on carbon nanotubes[167] in water by hydrolysis of dihydroxy titanium bis(ammonium lactate) $[MeCH(O^-)CO_2NH_4]_2Ti(OH)_2$ and dispersion of C-NT (90–100 °C, 20 h). Carbon nanotubes coated with titanium dioxide and ultradispersed TiO_2 were separated by centrifugation and dried *in vacuo*; the size of the resulting particles was in a range of 2–10 nm.

The TiO_2–SiO_2 nanotube composite with a coaxial structure was synthesised on anodised aluminium.[168] In the first step, SiO_2 nanotubes were obtained in pores (with a size of 200–250 nm) of anodised aluminium. Then TiO_2 nanotubes grew on their inner shell. The formation of this nanotube composite depends on the presence of Ti—O—Si bonds and the amorphous character of the SiO_2 layer. This method allows one to prepare tubes with the more complex TiO_2–SiO_2–TeO_2 composition.[169]

Silicon-containing titanium dioxide nanotubes can be prepared by the sol–gel method in the absence of a template.[170] For this purpose, butanediol, $Si(OEt)_4$ and $Ti(OPr^i)_4$ in ratios of 2 : (0 at.% – 10 at.% Si) : 1 were stirred at room temperature and kept for several days until a dry gel was obtained. The dry gel, which was pre-heated with a rate of 5 K min^{-1}, was crystallised at 400–600 °C for 1 h to form nanotubes and nanoparticles (for pure TiO_2 and TiO_2 + 10 at.% Si, only nanoparticles were prepared). The inner and outer diameters of TiO_2 NT containing 5 at.% Si were 3 and 13 nm, respectively. The amount of silicon plays an important role in the nanotube formation. The specific surface area of the samples prepared at 600 °C increases with increasing amount of silicon from 1.6 (TiO_2) to 110.66 $m^2\ g^{-1}$ (TiO_2 + 10 at.% Si). In this case, the pore size decreases, which is associated with suppression of growth of TiO_2 nanoparticles in the presence of silicon.

Iron-doped TiO_2 nanotubes with a diameter of up to 10 nm and a length of 200 nm were synthesised[171] by the hydrothermal method in an alkaline medium. Iron-containing anatase and rutile powders with a particle size of 30 and 42 nm, respectively, were used as precursors. A procedure was developed[172] for the synthesis of a nanocomposite in the form of Au/TiO_2 nanowires 60 μm long. These nanowires contain the smooth surface formed by anatase and the gold core ($D = 210$ nm, which corresponds to the pore diameter of an aluminium membrane). The thickness of the shell consisting of TiO_2 particles with sizes 10–15 nm is 40 nm. The ordered structure of the composite was achieved by layer-by-layer deposition of cationic polyelectrolytes and a titanium-containing precursor on gold nanowires.

A semiconductor/metal nanocomposite was prepared[173] from semiconducting TiO_2 nanotubes filled with polypyrrole nanowires (the latter were grown by chemical polymerisation[174]). This nanocomposite is as an efficient photocatalyst, because it has a large specific surface area and the conducting core.

A composite consisting of polyaniline (PAni) nanotubes ($D = 90$–130 nm) filled with TiO_2 nanoparticles (~10 nm) was synthesised in the presence of β-naphthalenesulfonic acid (β-NSA) as an admixture.[175] Titanium dioxide powder was added to a β-NSA solution (10^{-3} mol $litre^{-1}$), the mixture was treated ultrasonically until a homogeneous suspension was prepared, an aniline and water mixture (10^{-3} mol $litre^{-1}$) was added, and oxidative polymerisation was carried out by adding $(NH_4)_2S_2O_8$ (2×10^{-3} mol). The precipitate of the PAni–β-NSA–TiO_2 nanotube composite that formed was filtered off, washed with water and ethanol and dried *in vacuo* at 20 °C. The morphology, size, conductivity and hydrophobicity of the composite are determined by the amount of TiO_2 nanoparticles in the tubes. At a TiO_2 concentration lower than 0.08 mol $litre^{-1}$, the resulting amorphous composite consisted of hollow fibres. In the concentration range of 0.04–0.06 mol $litre^{-1}$, the composite consisted of nanotubes. At a concentration of 0.12 mol $litre^{-1}$, the composite contained granules. X-ray powder diffraction study revealed an impurity of crystalline TiO_2.

The conductivity of the composite depends on its morphology and the percentage of TiO_2. The conductivity is 4.4×10^{-3} and 1.2×10^{-1} S cm^{-1} for granules and nanotubulenes, respectively. The conductivity decreases with increasing TiO_2 concentration. The temperature dependence of the conductivity of the composite in the range of 300–77 K is typical of semiconductors with the hopping charge-transfer mechanism. The hydrophilicity of the composite can be varied by varying the TiO_2 content in the composite.

Nanowires of the anatase/poly(vinylpyrrolidine) (PVP) composite with a porous structure were prepared[176] by electrocentrifugation.[177] Titanium tetraisopropoxide was mixed with acetic acid and ethanol, PVP was added, and the mixture was homogenised for 1 h. Then the mixture was placed in a centrifuge and nanofibres were collected on an aluminium foil at 30 kV. Traces of PVP were removed from the nanofibres by heating them in air at 500 °C for 3 h, which led to a decrease in the diameter of nanofibres from 78 ± 9 to 53 ± 8 nm.

The fibre thickness of the TiO_2/PVP composite and anatase nanofibres can be varied in the ranges of (52 ± 11)–(374 ± 66) and (33 ± 6)–(192 ± 69) nm, respectively. Their sizes depend on the parameters of electrocentrifugation, the $Ti(OPr^i)_4$ concentration and the rate at which PVP is added in the course of preparation of the precursor. Titanium dioxide nanoparticles are involved in the formation of composite fibres with a size of ~10 nm. The surface

porosity of TiO_2 nanofibres can be varied as desired by changing the rate of hydrolysis of $Ti(OPr^i)_4$ in fibres through changes in atmospheric humidity. Composite fibres up to several centimetres in length are prone to form a nonwoven structure, which can be used as a sensor after deposition on a substrate. When annealed, this structure is transformed into a ceramic membrane without deterioration of porosity. In this case, fibres can partially melt, which enhances the mechanical strength of the membrane.

Noteworthy is the electrochemical method for the preparation of TiO_2 nanotubes by anodic oxidation of titanium metal strips in an aqueous electrolyte containing 0.5 mass % – 3.5 mass % HF.[178] A porous TiO_2 layer that appeared on the metal surface represents a high-density homogeneous lattice consisting of parallel tubes. The upper ends of the tubes are open, whereas the lower ends are closed. The average diameter of the tubes (25 – 65 nm) increases with increasing voltage of anodic oxidation, but the length of the tubes is determined by the thickness of the oxide layer and is independent of the electrolysis time.

Amorphous TiO_2 nanotubes can be prepared by anodic oxidation of a titanium foil in 0.5% HF at a potential of 12 – 20 V using a platinum cathode.[179] The length of nanotubes is ~400 nm, D = 46 – 76 nm, and the wall thickness is 17 – 27 nm. Annelation of these nanotubes at 500 °C under an oxygen stream affords the anatase and rutile modifications. The former modification is concentrated on the walls of nanotubes, whereas the second modification is concentrated on the barrier layer. The nanotubes are stable up to 600 °C and are of interest as materials for resistive hydrogen sensors.[180, 181] A TiO_2-NT-based sensor has the highest sensitivity for hydrogen at 375 °C, which increases with decreasing diameter of the tubes. The hydrogen sensor is completely reversible, its response time is 150 s, the hysteresis is absent, and the sensitivity threshold is 10^{-4}. The sensor is highly selective for hydrogen compared to CO, CO_2 and NH_3, but is responsive also to O_2 at the high concentration of the latter.

Electrochemical oxidation of a TiN layer on a silicon substrate with the use of a nanoporous anodised Al_2O_3 film as a template afforded nanosized TiO_x crystallites[182] with $D \approx 60$ nm belonging to the hexagonal system. This method is suitable also for the preparation of nanocrystallites of other semiconducting oxides.

Titanium dioxide nanoparticles were synthesised in mesopores of Al_2O_3 with the use of a new precursor, *viz*., bis(toluene)-titanium, which served as a molecular source of Ti^0.[183] Insertion of the precursor into mesopores of an aluminium template leads to elimination of titanium metal, which is oxidised to TiO_2 (anatase) with a particle size of ~2 nm. This material readily adsorbs UV radiation.

Various geometric structures can be prepared from TiO_2 nanoparticles.[184 – 189] A simple chemical method for the synthesis of needle-like samples[184] consists in mixing $Ti(OPr^i)_4$ and $Si(OEt)_4$ solutions in ethanol with admixtures of HCl and H_2O to prepare a composite with the molar ratio $TiO_2 : SiO_2 = 4 : 1$. Hydrolysis and gel formation in moist (70%) air at 40°C for 5 days followed by annealing at 600 °C (2 h) and storage of anatase that formed in an autoclave in an aqueous NaOH solution (a Teflon vessel) at 20, 60 or 110 °C for 20 h afforded well-crystallised TiO_2 with a specific surface area of 400 $m^2\ g^{-1}$. After washing with 0.1 M HCl and water, the product exhibited high photocatalytic activity. The synthesis with the use of 10 M NaOH at 60 – 110 °C for 20 h produced 'needles' with a tubular structure ($D \approx 8$ nm, $L \approx 100$ nm). Analogous anatase samples were also prepared without the addition of SiO_2 to the starting reaction mixture.

Ultrasonic treatment allows one to prepare nanotube forms of TiO_2 not only as nanotubes but also as whiskers.[185] Particles ($D \approx 20$ nm) prepared by thermal treatment of titanium hydroxide at 650 °C for 1 h (17% of anatase and 83% of rutile) serve as a precursor. To produce whiskers, a sample was placed in a 10 M NaOH solution, heated to 80 °C and subjected to ultrasonic treatment at an output power of 560 W for 80 min (treatment at an output power of 280 W for 60 min gave nanotubes). The precipitate that formed was washed with 0.1 M HNO_3 and water, kept at 110 °C for 4 h on an oil bath, washed once again and dried *in vacuo* (12 h). The sizes and composition of the whiskers depend on the time of washing with water in the first step. After 6 h, $L \approx 1$ μm, $D \approx 60$ nm, and the composition is $H_2Ti_3O_7 \cdot 0.5\,H_2O$. An increase in the washing time to 8 h leads to a decrease in the diameter of whiskers to 5 nm and the TiO_2 composition (the so-called B modification).[186] Storage of a sample at 110 °C for 4 h followed by washing with 0.1 M HNO_3 for 2 h and with water for 14 h results in the formation of open sodium-free nanotubes with $D \approx 5$ nm, $L \approx 200 – 300$ nm and the ratio $Ti : O = 1 : 2$.

Titanium dioxide whiskers cannot be prepared without ultrasonic treatment. Treatment of a TiO_2-containing NaOH solution affords sodium titanate consisting of layers of TiO_6 octahedra, between which alkali metal cations are located. In an HNO_3 solution, ion exchange occurs to give $H_2Ti_3O_7 \cdot 0.5\,H_2O$. Ultrasonic treatment not only accelerates the reaction between the starting components but also facilitates a particular orientational growth of titanate layers. After washing of the sample with water, the resulting TiO_2 layers increase in size and roll up into nanotubes.

Titanium dioxide whiskers can also be prepared by treating a $TiOCl_2$ precipitate, which is prepared by the reaction of $TiCl_4$ with a 5 M aqueous ammonia solution, in an autoclave.[187] To prepare anatase and rutile whiskers, titanium oxochloride is pre-calcinated at 450 and 800 °C, respectively. Whiskers ($D < 20$ nm) as bundles are produced under hydrothermal conditions at 100 °C for 12 h along with TiO_2 nanotubes 60 – 100 nm in length and 10 – 30 nm in diameter. An increase in the temperature leads to an increase in the amount of nanotubes in the samples, their length becomes as large as 150 nm, and the diameter is 15 – 20 nm. At 200 °C, the amount of tubes is larger than the amount of spherical particles (which are always present in samples), their length increases to 200 – 500 nm, and the inner diameter is 7 – 8 nm. An increase in the temperature leads to an increase in the size of the tubes, but the rate of their formation decreases. This is associated with the predominant formation of less soluble spherical particles (TiO_2 crystal nuclei). Since the lattice parameter of anatase $c \gg a$, its powder more easily forms nanotubes, which is attributed to the anisotropy of growth of TiO_2 particles during the autoclave treatment.

Nanosized TiO_2 ribbons with a length from a few to tens of micrometres, a thickness of several nanometres and a width of 30 – 200 nm were prepared by the hydrothermal method from titanium dioxide powder in a NaOH solution.[188] A TiO_2 gel, crystalline anatase or an anatase and rutile mixture were used as the starting titanium compound. The precursor (0.3 g) was mixed with a NaOH (5 – 15 M) solution (20 ml) and subjected to hydrothermal treatment at 180 – 240 °C for 1 – 2 days, and the products were washed with water and 0.1 M HCl. It was found that the temperature and the alkali concentration have no effect on the morphology of ribbons, which can roll up about the [00l] direction. The corrugated surface of such ribbons results from cluster condensation. These thin ($\leqslant 5$ nm) ribbons can be doped with various elements, which is of considerable importance in the synthesis of functional materials.

The sol – gel method is most widely used in the synthesis of nanotube forms of TiO_2 with different geometry. The drawbacks of this method as applied to the preparation of nanorods are that the template pores are difficult to fill with a high-concentration gel and that the use of dilute gels leads to the formation of cracks and defects. The template pores can be filled using electrophoresis of sol – gel nanocomposites. However, this procedure is unsuitable for the preparation of nanorods with $D < 20 – 50$ nm.

The synthesis of single-crystalline TiO_2 nanorods by the sol – gel method was performed under cathodically induced conditions.[189] The electrolyte was prepared by dissolving titanium metal powder in H_2O_2 and ammonia, the resulting yellow gel was dissolved in 4 M H_2SO_4, and then KNO_3 was added to the

solution to pH 2–3. The pores (12–50 nm) of an anodised aluminium membrane were filled using the electrochemical method at room temperature at potentials (V) from -0.9 to -1.2 V. At $V < -0.9$ V, electroreduction of nitrate ions occurred at the cathode

$$NO_3^- + 6H_2O + 8e^- \longrightarrow NH_3 + 9OH^-$$

which was accompanied by the formation of titanium hydroxide sol and gel

$$TiO^{2+} + 2OH^- \longrightarrow TiO(OH)_2,$$

$$TiO(OH)_2 \xrightarrow[-xH_2O]{} TiO_{1+x}(OH)_{2-2x}.$$

Annelation of a sample (450 °C, 24 h) gave TiO_2 nanowires of the anatase modification with $D \approx 40$ nm and a length of 2–10 μm depending on the electrolysis time (0.5–3 h). A high gel density in template pores prevents the formation of defects and cracks during heating.

Electrochemical deposition of a titanium hydroxide gel in pores of poly(methyl methacrylate) using gold electrodes afforded TiO_2 nanotubes.[190] An electrolyte with pH 2.5 was prepared under nitrogen from $NaHCO_3$ and a $TiCl_3$ solution in hydrochloric acid. The electrochemical reaction

$$nTiOH^{2+} + mH_2O \longrightarrow [Ti^{4+}O_x(OH)_{4-2x}]_n + 3nH^+ + ne^-$$

was carried out at an anode potential of +0.5 V. Amorphous TiO_2 nanotubes were prepared by removing the polymer using dissolution in acetone at 40 °C. Heating of these nanotubes at 450 °C for 1 h afforded intergrown anatase nanotubes with an outer diameter of 120 nm and a wall thickness of 25 nm. At short distances between the pores of the polymer, a compact porous TiO_2 film was obtained.[190]

The influence of the molar ratio of the starting components on the morphology of TiO_2 nanorods and nanotubes, which were synthesised from a sol by the template method on anodised aluminium, was studied.[191] The sol was prepared by adding a $Ti(OPr^i)_4$ solution in ethanol to an ethanol, water and acetylacetone mixture. The amount of perfect nanorods (D = 200–250 nm) formed by particles with a size of ~20 nm can be increased by increasing the percentage of ethanol in the sol. This can be achieved with the use of the starting molar ratio $Ti(OPr^i)_4$: acetylacetone : H_2O : EtOH = 1 : 1 : 3 : (20–40). An increase in the percentage of acetylacetone in the TiO_2 sol (1 : 2 : 3 : 20) results in the formation of TiO_2 nanotubes with thin walls (15–20 nm), which are easily broken and cracked.

Titanium dioxide nanowires were synthesised by deposition of a precursor on the corrugated surface of a polymeric template (based on azobenzene-functionalised epoxide resin) or silicon dioxide followed by calcination at 500 °C in air for 3 h.[192] The precursor was prepared as a sol by hydrolysis of a $Ti(OPr^i)_4$ solution in isopropanol in a moist air atmosphere. Nanowires grow on a polymer template but do not grow on SiO_2. An increase in the isopropanol concentration in the sol results in the formation of cracks parallel to grooves in the template.

Considerable progress was made in the synthesis of nanostructures of complex titanium oxides.[193–198] For example, nanorods of titanic acid $H_2Ti_3O_7$ were synthesised by the hydrothermal method[193] involving mixing of anatase with 10 M NaOH and heating at 130 °C for 72 h. The precipitate that formed was washed with water to prepare tubular particles 9 nm in diameter and hundreds of nanometres in length. Alkaline treatment of TiO_2 gives rise to Ti–O–Na bonds, which are cleaved in water due to the replacement of Na^+ ions with H^+ ions. This results in the formation and subsequent rolling-up of laminar particles. In an acidic medium, the formation of nanotubes is not accelerated, but the resulting nanotubes contain numerous defects.

The formation of a disordered intermediate phase containing sodium ions is an important step in the formation of these nanotubes. The synthesis with the use of amorphous TiO_2 as a precursor does not afford nanotubes, because TiO_2 is recrystallised into needle-like brookite. The use of KOH or LiOH instead of NaOH leads to the formation of nanorods and platelets or nanoparticles, respectively. Therefore, a high concentration of Na^+ cations and a strongly alkaline medium are essential conditions for the nanotube formation. All $H_2Ti_3O_7$ nanotubes are open and are formed by rolling up TiO_2 layers with an interlayer distance of ~7.8 Å.

The $H_2Ti_3O_7$ phase belongs to the monoclinic system with the unit cell parameters a = 16.03, b = 3.75, c = 9.19 Å and β = 101.45°. The formula of this weak acid is generally represented as hydroxide $Ti_3(OH)_2O_5$ stable in an alkaline medium. Its monolayer is formed by corrugated ribbons consisting of TiO_6 octahedra sharing edges (three octahedra in width), which form stepwise planes separated by H^+ ions. In the polymeric titanate ion $(Ti_3O_7^{2-})_n$, the atomic layers roll up about the [001] direction of the crystal structure of $H_2Ti_3O_7$. An interesting feature of these nanotubes is the simultaneous presence of an interlayer space and a quasi-one-dimensional inner channel. Titanate $H_2Ti_3O_7$ is a potential protonic electrolyte for fuel cells. In a concentrated NaOH solution, the nanotube material $Na_2Ti_2O_4(OH)_2$ was produced from polycrystalline TiO_2 at 110 °C for 20 h.[194] Treatment of this material with an HCl solution at pH 1 gives rise to the orthorhombic tubular structure of $H_2Ti_2O_4(OH)_2$.

The reaction of nanodispersed TiO_2 (4 nm) with a 4–10 M KOH solution in an autoclave at 160–180 °C for 48 h affords the monoclinic $K_2Ti_8O_{17}$ phase.[195] This phase consists of nanostructures analogous to twisted and bent ribbons (a few micrometres in length and tens of nanometres in width and thickness) extended along the [010] direction. The synthesis by this method in a NaOH solution produced nanosized belts of titanate $Na_2Ti_4O_9$ with a width of 100–500 nm and a thickness of 30 nm. In these structures, the Na^+ ions can be replaced by most cations. Potassium titanate shows chemoluminescence at 270 °C, which is 140 °C lower compared to that observed for TiO_2 nanopowders. For this phase, photoluminescence at an excitation wavelength of 401 nm and an emission wavelength of 612 nm was observed for the first time.

The low-temperature hydrochemical method afforded $SrTiO_3$ and $BaTiO_3$ nanotubes with an outer diameter of 8–15 nm, an inner diameter of 4–7 nm and a length of 50–500 nm.[196] They have a cubic perovskite structure with the unit cell parameter a of 3.889 and 3.975 Å for $SrTiO_3$ and $BaTiO_3$, respectively. The samples contain impurities of an amorphous product, the starting reagents and carbonates. The synthesis was carried out by stirring $SrCl_2$ or $Ba(OH)_2$ and TiO_2 NT solutions under argon or nitrogen for 6–20 h. Then pH of the suspension was brought to 12 and 10 by the addition of NaOH or HCl, respectively, and the precipitate was separated by decantation, washed with water and dried. Crystalline $SrTiO_3$ and $BaTiO_3$ nanorods (the unit cell parameter a is 3.90 and 4.03 Å, respectively) can also be prepared by thermolysis of $Sr(OPr^i)_2$ and $Ba(OPr^i)_2$ in the presence of oleic acid at 280 °C for 6 h.[197] Isolated nanorods have a diameter of 5–60 nm and a length of 10 μm. These materials can be used as nanosized ferroelectrics and memory elements.[198]

b. Vanadium oxides

The first vanadium(V) oxide nanotubes have been synthesised only recently.[199] The sol–gel method giving rise to xerogels with a pronounced quasi-one-dimensional structure proved to be efficient in the synthesis of such nanotubes.[200] A combination of the sol–gel process with hydrothermal treatment at 180 °C for 5 h produced nanowires of composition $V_2O_5 \cdot nH_2O$ ($0.3 \leqslant n \leqslant 1.7$) with the [010] growth axis.[201, 202]

Extensive experimental data[203] on the chemistry of intercalates based on the $V_2O_5 \cdot nH_2O$ xerogel provided the basis for developing new procedures for the synthesis of nanotube forms of vanadium oxide.[204] Evidently, the layered structure of a xerogel, in which the distances between the V–O layers are controlled by organic molecules, plays the key role in the design of vanadium

oxide nanotubes. Organic guest molecules serve as templates, thus determining the structure of a multilayer nanotube composite.

Primary amines $C_nH_{2n+1}NH_2$ ($4 \leqslant n \leqslant 22$) and α,ω-diamines $H_2N(CH_2)_nNH_2$ ($14 \leqslant n \leqslant 20$) were proposed as templates for these syntheses.[204–208] An ethanolic solution of vanadium(V) triisopropoxide $VO(OPr^i)_3$ and amine in a molar ratio of 2 : 1 was stirred for 1 h under an inert atmosphere and then subjected to hydrolysis. After 12–96-h aging of the system, an orange composite was obtained, which was subjected to hydrothermal treatment in an autoclave at 180 °C for 2–7 days to prepare a black product, *viz*., single-phase nanotubes with a length of up to 15 μm, an outer diameter of 15–150 nm and an inner diameter of 5–50 nm. The walls of these tubes consisted of 2–30 layers of crystalline vanadium oxide, between which intercalated amine and diamine molecules are located. The distance between the layers (1.7–3.8 nm) is proportional to the length of the guest molecule. The general formula of such nanotubes can be represented as $VO_xO_{y/2}(C_nH_{2n+4}N)_y$ or $VO_x(C_nH_{2n+4}N)_y$, where $2.30 \leqslant x \leqslant 2.47$ and $0.25 \leqslant y \leqslant 0.30$, respectively. In the case of diamines, the tubes have thicker walls and a smaller inner diameter.

Vanadium–oxygen layers of the nanotubes under consideration consist of VO_4 tetrahedra and VO_5 tetragonal pyramids. The vanadium oxide tubes are stable after removal of amines but decompose at a temperature above 250 °C. Unlike mesoporous metal oxides with a laminar structure, these composites are characterised by a tubular morphology and well-structured walls. It is believed [201] that twisted layers of vanadium oxides are very flexible, and they can be stretched and involved in numerous exchange reactions.

In the above-described procedure for the synthesis of nanotubes, vanadium(V) oxochloride and oxide are also used as precursors.[209] In the first step, $VOCl_3$ or V_2O_5 is mixed with primary amine $C_nH_{2n+1}NH_2$ under an inert atmosphere, and the mixture is hydrolysed with an acetate buffer (pH 7) or water. The next step involves hydrothermal treatment at 180 °C for 7 days. Elemental analysis demonstrated that the composition of the nanotubes synthesised from $VOCl_3$ corresponded to the formula $VO_{2.45\pm0.05}(C_nH_{2n+4}N)_{0.27\pm0.01}$ ($11 \leqslant n \leqslant 16$). The tubes prepared from V_2O_5 had the composition $VO_{2.43\pm0.03}\cdot(C_nH_{2n+4}N)_{0.27\pm0.01}$ ($11 \leqslant n \leqslant 20$).

The morphological characteristics of vanadium oxide nanotubulenes depending on the type of the precursor and the nature of the template are given in Table 3. The multilayer walls of these well-crystallised open tubes consist of rolled-up vanadium–oxygen layers built from VO_4 squares with the unit cell parameter $a = 6.1$ Å.[210] The tubes composed of ideal cylindrical layers are rarely produced (< 1%), and these tubes contain no more than six layers. Nanotubes of VO_x are more often composed of rolled-up layers and are characterised by the roll morphology.

The majority of vanadium oxide tubes contain various defects. An isolated layer forms an inner part of the tube, whereas its outer surface is generally transformed into a roll of two layers between which amine molecules are located. These tubes are characterised by the formation of bundles and intergrowths. A roll of one VO_x layer can go to the adjacent tube with a change in the direction of rolling. This pair of tubes sharing layers is often observed in VO_x nanotubes with intercalated diamines after ion exchange. Aromatic amines can also be used as templates in the synthesis of VO_x nanotubes.[211] For example, the reaction of $VO(OPr^i)_3$ with 3-phenylpropylamine followed by hydrolysis and hydrothermal treatment of the product affords nanotubes containing defects in the structure of the walls.

The structural characteristics of nanotubes can be varied as desired by changing the pH of the V_2O_5 gel through the addition of ammonia.[212] In a neutral or weakly acidic medium, nanotubes with an interlayer distance proportional to the length of the $(CH_2)_n$ chain are produced. The nanotubes synthesised at pH 9–10 have a unique structure of the walls, which consist of VO_x layers regularly alternating with intercalated amine and ammonia molecules (interlayer distances are 20 and 9 Å, respectively). The tubes formed in the presence of ammonia have a much larger outer diameter (larger than 250 nm) and smaller length (2–5 μm) compared to the nanotubes prepared at pH 4–8 (Fig. 3). The general formula of these nanotubes can be represented as $[(NH_4)_yVO_x][(RNH_3)_xVO_x]$ (R is a hydrocarbon fragment).

Derivatives of *trans*-(1*R*,2*R*)- and *trans*-(1*S*,2*S*)-1,2-diaminocyclohexane were proposed [49] as templates for the synthesis of the helical chiral structure of VO_x NT. The *R*,*R*- and *S*,*S*-enantiomers always give the left- and right-handed helices, respectively.

The synthesis of VO_x nanotubes from a $V_2O_5\cdot nH_2O$ gel ($n \approx 300$), which was prepared by dissolution of vanadium(V) oxide in hydrogen peroxide, was documented.[213,214] A solution of hexadecylamine (0.45 g ml^{-1}) in acetone (the molar ratio V : amine = 2 : 1) was added to this gel, the mixture was stirred at room temperature for 16 h, and the composite was subjected to hydrothermal treatment at 150 or 180 °C for 2–10 days. The resulting black powder was washed with ethanol and cyclohexane and dried *in vacuo* at 80 °C for 5 h. The interlayer distance in VO_x NT decreases from 37 to 32 Å with increasing temperature and time of the hydrothermal process.

The X-ray powder diffraction patterns of the resulting nanotubes are typical of layered compounds. They contain intense 00*l* reflections (reflections from atomic planes) and weak *hk*0 reflections determined by a two-dimensional structure of the layer. The alkylamine molecule is perpendicular to the planes of VO_x, because the interlayer distance is close to the chain length of the amine (33 Å). Water molecules located between the layers along

Table 3. Morphological characteristics of V–O nanotubulenes ($C_nH_{2n+1}NH_2$ template).[209]

Precursor	*n*	Outer diameter of NT /nm	Inner diameter of NT /nm	Number of layers	Length of NT /μm
$VO(OPr^i)_3$	$4 \leqslant n \leqslant 22$	15–150	5–50	2–30	1–15
$VOCl_3$	11	50–100	15–35	10–20	1.5–5
	16	80–100	20–35	11–14	0.8–1.5
V_2O_5	11	70–140	20–35	9–13	2–12
	12	50–90	15–35	7–13	1–3
	16	70–100	20–45	6–13	1–2
	20	60–90	20–45	6–10	1–3

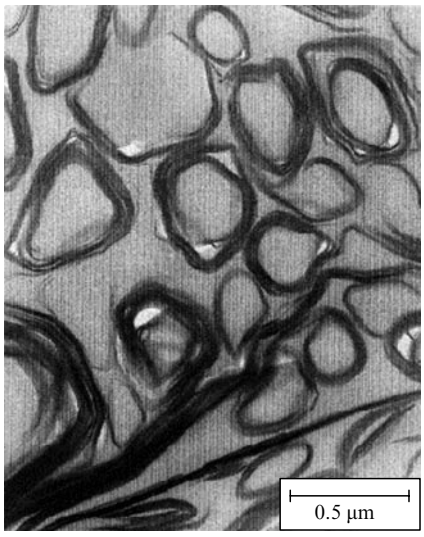


Figure 3. The TEM image of cross-sections of VO_x NT.[212] Hereinafter, TEM is transmission electron microscopy.

with protonated amines increase this distance to 37 Å. The inner and outer diameters of the nanotubes are 30–40 and 50–130 nm, respectively, the length is 1–10 μm, and the number of the layers varies from 5 to 25.

Vanadium(V) oxide powder can be used as a precursor in the synthesis of VO_x nanotubes.[215–217] In this case, V_2O_5 and hexadecylamine are mixed in water, the mixture is heated in an autoclave at 140 or 180 °C for 24 h or 3 days, respectively, and the resulting black product is washed with water and dried at 70 °C. The product consists of nanotubes with a length of 1–10 μm and a diameter of 30–100 nm depending on the conditions of the synthesis, the template type, the precursor concentration and the reaction time. The walls of these nanotubes are formed by 3–10 VO_x layers with interlayer distances of 35.3 Å. The ESR spectra of these samples contain a single line without hyperfine structure, which is typical of interacting V^{4+} ions. This is indicative of the close arrangement of paramagnetic centres ($d < 0.7$ nm) and the occurrence of spin–spin coupling interaction. The g factor (1.961) is equal to that of the $VO(H_2O)_5^{2+}$ ion (1.962).

Hydrothermal treatment of a V_2O_5, MoO_3 and hexadecylamine mixture (180 °C) for one week afforded $V_{0.99}Mo_{0.01}O_{2.45}(C_{16}H_{36}N)_{0.27}$ nanotubes with a diameter 30–10 nm and a length of 2–8 μm.[217] The interlayer distance in these nanotubes determined by X-ray and electron diffraction is 34 and 29.3 Å, respectively. The unit cell parameter a of the two-dimensional tetragonal unit cell in the layer is 6.23 Å.

Manganese-containing VO_x nanotubes of composition $Mn_{0.1}VO_{2.5+\delta}\cdot n\,H_2O$ were synthesised by the ion exchange method from the layered $V_2O_{5+\delta}(C_{12}H_{25}NH_3^+)$ precursor.[218] Their largest diameter is 100 nm and the length is 1.3 μm. The nanotubes contain defects as partially broken zigzag layers with a tetragonal structure ($a = 6.157(3)$ and $c = 10.52(3)$ Å). This compound with a tubular morphology was tested as a cathode material for electrochemical lithium intercalation. At a potential of ~2 V, 0.5 mol of Li per mole of V_2O_5 are reversibly inserted into VO_x nanotubes. The cell capacity is 140 A h kg^{-1}.

Reaction products of multilayer VO_x nanotubes, which contain α-monoamines with a chain length of 4–22 carbon atoms between the layers (for example, C_{12}-VO_x contains alkylamine with 12 carbon atoms), with salt solutions were studied.[219] This process was demonstrated to be accompanied by intercalation of alkali (Na^+, K^+), alkaline earth (Mg^{2+}, Ca^{2+}, Sr^{2+}) and transition metal (Fe^{2+}, Co^{2+}, Ni^{2+}, Cu^{2+}, Sm^{3+}, Tb^{3+}) cations with a decrease in the interlayer distance in the tubes to 0.9–1.2 nm. The intercalated K^+ cations bound to crown ether can be partially replaced with dodecylamine with the result that the initial interlayer distance is restored. The reactions with RbCl, CsCl, $AgNO_3$, $SrCl_2$ and $BaCl_2$ solutions lead to destruction of nanotubes, whereas $ZnCl_2$ and Pb^{2+} salts are not intercalated. The largest atomic cation : V ratio in the insertion compounds is as high as 0.27.

Nanotubes intercalated with Na^+, K^+ and Cu^{2+} ions were prepared by the ion exchange method at the molar ratio $VO_x : MCl_n = 1 : 4$.[220] These cations in the samples account for 0.26, 0.27 and 0.12, respectively. The unit cell parameters for the intercalated tubes are as follows (the parameters of the starting nanotubes are given for comparison):

	a/Å	c/Å
C_{12}-VO_x	6.12(1)	27.1(2)
$Na_{0.26}VO_x$	6.05(1)	9.2(1)
$K_{0.27}VO_x$	6.11(1)	9.6(1)
$Cu_{0.12}VO_x$	6.08(2)	10.6(2)

The Raman spectra of VO_x nanotubes show a broad low-intensity band at 995 cm^{-1} (V=O) and two broad bands at 800–600 and 500–200 cm^{-1} (V–O–V). These broad bands are associated with high disorder of the atomic structure of the tubes.[220] Galvanostatic studies of these materials provided evidence that the redox process is reversible (more then 100 cycles) in current sources with a lithium anode. The discharge capacity is 120–150 A h g^{-1} and the maximum lithium content is 0.5 Li^+ per vanadium atom.

Multilayer Cu–VO_x and Fe–VO_x nanotubes were prepared[221] by stirring (20 h) a dodecylamine–VO_x NT suspension in aqueous-alcoholic $CuCl_2$ and $FeCl_3$ solutions followed by filtration, washing and drying in air at 60 °C. The starting nanotubes (primarily, open) have an outer diameter of 60–100 nm, an inner diameter of 15–40 nm and a length of 1–3 μm. Their walls consisted of 6–12 rolled-up layers of vanadium oxides with cracks and dislocations; the average interlayer distance (~30.2 Å) is indicative of the perpendicular arrangement of the dodecylamine molecules. The starting dodecylamine–VO_x nanotubes are characterised by the tetragonal unit cell ($a = 6.12$, $c = 33.71$ Å). The Cu- and Fe-containing nanotubes have the same structure, the interlayer distances are 10.9 and 10.5 Å, respectively, the inner diameter varies in the range of 40–65 nm and the outer diameter varies in the range of 60–80 nm.

The structural changes resulting from the transformation of a dodecylamine–VO_x xerogel into nanotubes followed by intercalation with Cu^{n+} and Fe^{n+} cations were studied by IR spectroscopy. The main absorption bands for the dodecylamine–VO_x composite are observed at 998, 957, 733, 531 and 838, 809, 635 cm^{-1}, and the main absorption bands for the dodecylamine–VO_x nanotubes are observed at 1001, 792, 721, 573 and 487 cm^{-1}. The spectra of the nanotubes also show the shift of the N–H stretching band from 3049 to 3127 cm^{-1} and changes in the 1600–1500 cm^{-1} region of bending vibrations associated with the difference in the environment about the NH_3^+ groups. After ion exchange (Cu–VO_x NT), new bands appear at 3571, 3440 and 1615 cm^{-1}, which correspond to O–H stretching vibrations and H–O–H bending vibrations. In the region of V–O bonds, two new bands at 755 and 526 cm^{-1} (a shoulder at 590 cm^{-1}) correspond to V–O–V and V–O–Cu bending vibrations, and the V=O band is shifted from 1001 to 1007 cm^{-1}. For the Fe–VO_x nanotubes, the shifts of the bands are insignificant (997, 576, 495 cm^{-1} and 3384, 3203 and 1614 cm^{-1}). This indicates that the Fe^{n+} cations are bound to the VO_x layers.

X-ray photoelectron spectroscopy demonstrated[221] that intercalated nanotubes contain a large amount of tetravalent vanadium. Copper atoms exist primarily in the monovalent state, and Cu^{2+} cations and copper clusters are also present in small amounts. In Fe–VO_x nanotubes, iron atoms exist in the Fe^0, Fe^{2+} and Fe^{3+} states. Analysis of the N1s band shows that trace amounts of amines are present in the samples. The compositions of NT were represented as $VO_{2.3}(C_{12}H_{25}NH_3)_{0.38}$, $VO_{1.53<x<2.1}(C_{12}H_{25}NH_3)_{0.21}Cu_{0.08}(H_2O)_{<0.56}$ and $VO_{2.08<x<2.68}(C_{12}H_{25}NH_3)_{0.13}Fe_{0.19}(H_2O)_{<0.33}$. The chlorine content in the intercalates was lower than 0.01 mol.

Upon heating in air to 180 °C, Cu–VO_x NT remain unchanged. The weight loss (~9%) occurs due to elimination of water coordinated to copper cations. At about 350 °C, the weight loss is 17%, residual water and organic molecules are eliminated, and the tubular structure is destroyed to form the unstructured V_2O_{5-x}/CuO composite. Under nitrogen, the weight loss in Cu–VO_x NT occurs in the temperature range of 180–650 °C, and thermolysis affords Cu and V_2O_3. The process gives rise to V_2O_3 nanotubes consisting of V_2O_3 crystallites with a size of 3–5 nm. These nanotubes are thermally stable under nitrogen up to 650 °C, and copper metal nanoparticles are present inside the nanotubes. The Cu–VO_x nanotubes are catalytically active in decomposition of HCN giving rise to $Cu(CN)_2$. Additional data on copper-containing VO_x nanotubes were reported in the study.[222]

The VO_x nanotubes are structurally related to $BaV_7O_{16}\cdot n\,H_2O$[223] and (en)V_7O_{16}.[224] The $(V_7O_{16})_n$ layers form a framework of the tube, whereas the amine molecules are inserted between the layers. These isotropic layers formed by the equivalent planes, which are composed of VO_5 square pyramids on

both sides of the layer, roll up to compensate free bonds of the terminal atoms giving rise to a tubular morphology.

The (en)V_7O_{16} compound is an example of structures characterised by strong electrostatic interactions between the negatively charged VO_x layers and the ethylenediamine cations. This compound crystallises in the triclinic system with the unit cell parameters $a = 6.161(2)$, $b = 6.170(2)$, $c = 19.111(7)$ Å, $\alpha = 96.138(9)$, $\beta = 92.819(9)$, $\gamma = 90.067(9)^\circ$. (In an independent electron diffraction study, the following unit cell parameters were determined: $a \approx b \approx 6.15$, $c \approx 18.5$ Å, $\alpha \approx 98$, $\beta \approx 93$, $\gamma \approx 90^\circ$.) Each V_7O_{16} layer consists of two planar sheets, which, in turn, are composed of VO_5 square pyramids linked *via* VO_4 tetrahedra. However, (en)V_7O_{16} was not prepared in pure form, and the NH_2 groups in this compound are protonated. The model of intercalated vanadium oxide nanotubes can be derived from the (en)V_7O_{16} structure. The unit cell parameters for C_{12}-VO_x nanotubes are $a = 6.152$, $c = 54.80$ Å, the space group is $P4_2/m$. The nanotube formation is favoured by a large interlayer distance (larger than 1.6 nm), as well as by the presence of amines and diamines containing long alkyl chains, which are inserted in the nanotubes.

Nanostructured vanadium oxide was synthesised using carbon nanotubes as a template.[225,226] The procedure involves coating of carbon NT with a V_2O_5 gel followed by removal of carbon by calcination in air at 700 °C. To create acid centres on the surface of C-NT, the pre-treatment with boiling HNO_3 was carried out for 24 h. The diameter of the nanotubes thus prepared was 20–55 nm and the length was 2–3 μm. The orthorhombic system and the unit cell parameters $a = 11.44$, $b = 3.54$, $c = 4.35$ Å were determined by electron diffraction.

Oxide γ-V_2O_5 forms a layered orthorhombic structure with the unit cell parameters $a = 9.946$, $b = 3.585$, $c = 10.042$ Å. The shortest interatomic distances (in Å) in the VO_5 pyramids of vanadium oxides are as follows:

Oxide	V=O	V–O(–V)	O···O
γ-V_2O_5 (V_1)	1.547	1.726	1.891, 1.986
γ-V_2O_5 (V_2)	1.581	1.848	1.898, 1.967
α-V_2O_5	1.576	1.778	1.878, 2.018

Nanorods and nanowires of γ-V_2O_5 were synthesised[227] under mild conditions using the micelle method. The average lengths of the nanorods and nanowires were 90 nm and 1 μm, respectively. The sizes of these nanostructures depend on the time during which particles are kept in a micellar solution. The syntheses were carried out in a colloidal sodium bis(ethyl-2-hexyl)sulfosuccinate–isooctane–H_2O solution, where the first component served as a stabilising surfactant, to which a solution of $VO(OPr^i)_3$ in isooctane (5×10^{-3} mol litre^{-1}) was added at 20 °C for 24 h and 100 days, respectively. Well-crystallised nanorods, whose axes are parallel to the [101] direction, and nanowires extended along the [100] direction were synthesised.

The IR spectra of the nanorods are similar to those of the nanowires. The 1750–1000 cm^{-1} region shows bands assigned to surfactants and bending vibrations of water molecules (1630 cm^{-1}). The V–O stretching vibrations are observed at 1022, 1000, 963, 745 and 537 cm^{-1}. X-ray photoelectron spectroscopy demonstrated that vanadium in these nanostructures exists in the pentavalent state; the bond energies of the 2p doublet are 518.8 and 525 eV.

Nanorods of γ-LiV_2O_5, which crystallise in the orthorhombic system and have a diameter of 30–40 nm and a length of 0.4–2 μm, were synthesised by the solvatothermal method[228] with the use of ethanol as the solvent, which served simultaneously as a reducing agent:

$$2\,LiOH + 2\,V_2O_5 + EtOH \longrightarrow 2\,\gamma\text{-}LiV_2O_5 + MeCHO + 2\,H_2O.$$

A 1:1 LiOH and V_2O_5 mixture in ethanol was kept in an autoclave at 160 °C for 24 h, and the precipitate was filtered off, washed with ethanol and dried at 100 °C. The nanorods thus prepared were tested as a cathode material in a cell with a lithium anode. In the potential range of 1.5–4.2 V, the discharge capacity of the cell was 259 mA h g^{-1}. In the first five charge–discharge cycles, the discharge capacity rapidly decreased and then remained constant (199 mA h g^{-1} after 20 cycles).

Nanosized crystalline mixed-oxidation-state vanadium oxide was prepared by the addition of $VOCl_3$ to benzyl alcohol at room temperature and heating of a solution to 120 °C.[156] After aging, the precipitate was separated by centrifugation, washed with ethanol and dried.

Nanorods of NaV_2O_5 (the orthorhombic system, the unit cell parameters $a = 11.293$, $b = 3.606$, $c = 4.798$ Å) were produced by the hydrothermal method.[229] Their geometric parameters are determined primarily by pH and the concentration of the reducing agent (NH_2OH). The magnetic properties of the samples were determined in the temperature range from 2 K to room temperature.

Single-crystalline samples of tubes with composition $Na_2V_3O_7$ were grown *in vacuo* from a $Na_{1.9}V_2O_5$ melt as black fibres several millimetres in length.[230,231] Fibre bundles can be easily separated into individual crystalline fibres with $D < 100$ μm. The crystals belong to the trigonal system, $a = 10.886$, $c = 9.538$ Å, $Z = 6$, and consist of VO_5 square pyramids sharing edges and vertices to form parallel tubes with an inner diameter of ~0.5 nm. The Na ions are located along the axis of the tube and between the tubes. This material should have an unusual ionic conductivity and properties of a low-dimensional quantum magnet and can be involved in ion-exchange reactions. The electronic and vibrational characteristics of $Na_2V_3O_7$ NT were studied.[231] The electronic structure of $Na_2V_3O_7$ is similar to that of nanotubular vanadates. The optical absorption spectrum shows a band at ~1.2 eV, which was assigned to V(d → d) transitions, and bands at 3.3 and 3.9 eV assigned to O2p → V3d transitions.

Chemical vapour deposition from a β-diketonate complex and vanadyl acetylacetonate mixture on a glass substrate afforded nanowires of the β phase of $Na_xV_2O_5$ with $D = 20–200$ nm and $L = 10–30$ nm.[232] A single-phase sample of β-$Na_xV_2O_5$, in which the growth orientation along the [*h*0*l*] direction prevails, was prepared only at 550 °C. A decrease in the temperature to 540 °C results in the appearance of an impurity as V_2O_5 platelets.

Complex manganese vanadium oxide $Mn_{7-2/3x}(OH)_3.(VO_4)_{4-2x}(V_2O_7)_x$, where $x = 0.2$, with a hexagonal structure also exhibits a tubular morphology (Fig. 4).[233] This oxide was synthesised by hydrothermal treatment of an alkaline solution (pH 10.2) containing V_2O_5, $MnSO_4$ and tetrabutylammonium cations (the template) in a molar ratio of 1 : 1 : 4 at 165 °C for 72 h.

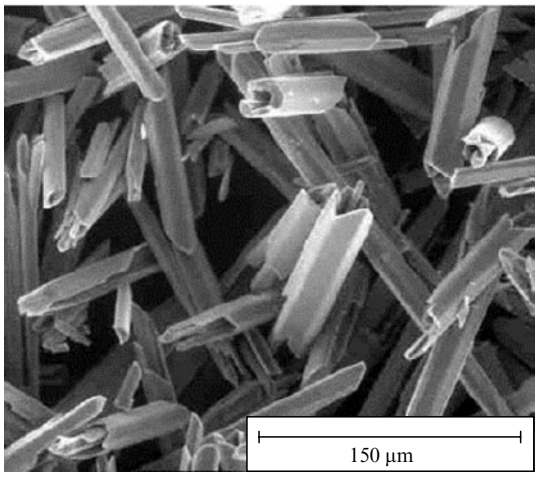


Figure 4. The SEM image of $(Mn,V)O_x$ NT.[232]

Nowadays, most studies of VO_x nanotubes are aimed at developing procedures for the synthesis and investigating the morphology of samples. Data on their physicochemical properties are scarce.[234] The prospects of the use of vanadium oxide tubulenes as cathode materials for lithium cells,[235–238] semiconductors for the production of FET transistors [239] and catalysts for oxidation [227] were estimated. Studies of the cathode properties of VO_x nanotubes in chemical current sources with a lithium anode demonstrated that vanadium (which initially consisted of 60% of V^{5+} and 40% of V^{4+}) is reduced to the tetra- and trivalent states.[240] The theoretical cathode capacitance is 240 mA h g^{-1} and the experimental capacitance is 210 mA h g^{-1}. During the first twenty discharge cycles (5 h), the discharge capacity increased.

At a potential below 2 V, the cathode material contains V^{5+}, V^{4+} and V^{3+} derivatives. Consequently, vanadium can be reduced further, which accounts for the observed increase in the discharge capacity. When charging the current source, the charge is localised in the V(3d) band.[241] The C-NT/aerogel/V_2O_5 nanocomposite exhibits good cathode properties at a high discharge rate.[242] At a current density of 112 mA g^{-1}, the discharge capacity of this cathode is higher than 560 mA h g^{-1}. For the graphite/aerogel/V_2O_5 composite, the discharge capacity is 450 mA h g^{-1}. The resistance of electrodes composed of the C-NT/aerogel/V_2O_5 composite is four times lower, which is primarily responsible for the improvement of their characteristics.

Nanosized oxide tubes and rods are promising modules for nanotechnologies.[243] Nanowires prepared on a Si/SiO_2 substrate have a symmetric nonlinear voltammetric parameter and high resistance.[244] Measurements performed in the temperature range of 100–300 K provided evidence for the hopping mechanism of conductivity. Small-radius polarons migrate between V^{4+} and V^{5+} with an activation energy of 0.11 eV. The electrical characteristics of V_2O_5 nanowires with a ribbon structure formed on a Si/SiO_2 substrate were studied [240, 244, 245] (the length of the ribbons is a few micrometres, the width is 10 nm and the thickness is 1.5 nm). The conductivity of the fibres from such ribbons is 20.5 S cm^{-1} and the contact resistance between the fibres is 62 MΩ. In strong electric fields ($E > 10^5$ V cm^{-1}), the conductivity depends nonlinearly on the length of nanofibres. An analogous dependence has been observed earlier for V_2O_5 films. In the region adjacent to the electrodes ($L < 300$ nm), non-Ohmic transport can occur.

c. Chromium oxides

A composite consisting of carbon nanotubes filled with chromium oxide CrO_3 was synthesised in air at room temperature.[246] For this purpose, C-NT were treated with a paste consisting of CrO_3 and HCl (12 M) in a molar ratio of 2 : 1. The tubes were filled over a period of time from 3 h to 2 days. The material is formed by the following reaction of CrO_3 with HCl:

$$CrO_3 + 2\,HCl \longrightarrow CrO_2Cl_2 + H_2O.$$

Initially, chromium oxochloride and unconsumed CrO_3 are inserted between bundles of carbon nanotubes to form intercalation compounds. The CrO_2Cl_2 compound is sensitive to light, gradually decomposes, releases chlorine and oxidises carbon:

$$2\,CrO_2Cl_2 + Cl_2 + 2\,C \longrightarrow 2\,CrCl_3 + 2\,CO_2.$$

Oxidation of carbon atoms is induced by defects and impurities on the surface of C-NT, due to which the tubes contain pores. As a result, concentrated CrO_3 solutions can penetrate into their inner cavity. The latter reaction competes with filling of the tubes. The structure of C-NT remains intact upon mild oxidation of carbon. Chromium trichloride was washed with water. The resulting composite is stable *in vacuo* under ion bombardment, as well as in air and in polar solvents, such as water, ethanol and acetone.

d. Manganese oxides

Nanoribbons of complex manganese magnesium oxide of composition $Mg_{2.11}Mn_{5.46}O_{12} \cdot x\,H_2O$, with a length varying from a few to tens of micrometres, a width of 20–100 nm and a specific surface area of 81 m^2 g^{-1} were synthesised.[247] The compound crystallises in the pseudoorthorhombic (monoclinic) system with the unit cell parameters $a = 9.7$, $b = 2.9$ Å, $\beta = 90°$; the parameter c was not determined. The average oxidation state of Mn is +3.62. The nanosized crystalline ribbons contain tunnels with equal diameter extended along the a axis, which are arranged in an ordered fashion about the b axis. The size of the framework of the tunnel structure is 6.9×6.9 Å. The synthesis was carried out in an autoclave at 120, 150 and 200 °C using layered microporous MgO and a $(Et_4N)_xMnO_y$ gel as precursors. Heating of the nanoribbons at 40–130 °C was accompanied by elimination of physically adsorbed water (5%). Water located in the tunnels was removed (~11%) in the temperature range of 130–420°C, and destruction accompanied by elimination of coordinated water and oxygen occurred at 420–560 °C. Relatively active oxygen chemosorbed in tunnels was eliminated at 480 °C, and oxygen involved in the crystal structure was eliminated at 550 °C. The catalytic activity of the nanoribbons in oxidation of benzyl alcohol to benzaldehyde was studied; the degree of conversion was as high as 45%.

Nanofibres of nanostructured α-MnO_2 were synthesised [248] by the template method. An aluminium membrane was placed in a sol (which was prepared by stirring fumaric acid, $KMnO_4$ and a H_2SO_4 solution for 10 min) for 10 s. Then the membrane was dried and heated in air at 500 °C for 24 h. The resulting manganese dioxide layers were separated and treated with a 6 M NaOH solution to remove the residual aluminium template.

e. Iron oxides

Macroscopic hollow fibres of hematite (α-Fe_2O_3) with a diameter of 4–10 μm, a wall thickness of 1–2 μm and a length of up to 20 cm were synthesised.[249] Reduction of hematite with hydrogen affords hollow fibres of α-Fe. Iron alkoxide $Fe(OEt)_3$, which was dissolved in ethanol and mixed with 2-methoxyethanol (MOE) in the molar ratio Fe^{3+} : MOE = 1 : 3, was used as a precursor in the synthesis. Within 2 h after dissolution of the red precipitate in acetic acid (Fe^{III} : AcOH = 1 : 10), a sol appeared. The sol was transformed into green fibres of the gel at 40 °C during several days. After removal of organic components at 200 °C, amorphous fibres were obtained. At 300 and 400 °C, the fibres were transformed into β-Fe_2O_3 and α-Fe_2O_3, respectively. Final thermal treatment of the fibres was carried out at 500–700 °C.

The mechanism of formation of hollow fibres can be represented by the following sequence of transformations:

$$Fe(OEt)_3 + x\,ROH \rightleftharpoons Fe(OEt)_{3-x}(OR)_x + x\,EtOH,$$

$$Fe(OEt)_{3-x}(OR)_x + 3\,AcOH \longrightarrow$$

$$\longrightarrow Fe(OAc)_3 + x\,ROH + (3-x)\,EtOH.$$

The ROH (MOE) molecules form hydrogen bonds with the polymeric $Fe(OAc)_3$ units, resulting in the formation of an ethanol sol. Further polymerisation affords fibres containing large amounts of ethanol and acetate anions. Heating of the composite leads to diffusion of sol particles, evaporation of organic compounds and formation of tubes, which are transformed into hollow polycrystalline fibres by thermal decomposition of acetate with elimination of CO_2 and H_2O. Hollow fibres were observed also after storage of gels in air for one month.

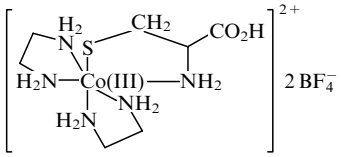
Nanoparticles of α-Fe_2O_3 with a size of smaller than 100 nm were deposited [250] as round-shaped particles with a size of ~1 μm on the (001) crystallographic face of silicon from a ferrocene, xylene and water vapour mixture at 1000 °C. In the absence of water vapour, carbon nanotubes are produced. Water vapour reacts with silicon of the substrate giving rise to round-shaped templates to which Fe_2O_3 nanoparticles are bound as a result of selective etching and oxidation of Fe^0 with H_2O vapour. It was also found [251] that γ-Fe_2O_3 nanoparticles (~5 nm) prepared by

hydrolysis of $FeCl_3$ in the presence of n-octylamine undergo aggregation. Highly crystalline α-Fe_2O_3 nanotubes were prepared [252] by hydrothermal treatment of $Fe(NO_3)_3$ in cavities of C-NT and in a NaOH solution.

Nanowires of cobalt ferrite $CoFe_2O_4$ with an average diameter of 50 nm and a length of up to a few micrometres were synthesised under mild conditions inside C-NT.[253] Carbon nanotubes with an outer diameter of 120 nm and an inner diameter of 60 nm were filled with aqueous $Co(NO_3)_2$ and $Fe(NO_3)_2$ solutions in a molar ratio of 1 : 2 and heated in air at 100 °C. The amount of cobalt and iron salts recalculated for the metals accounts for 30% of the mass of C-NT. Thermal treatment of long-fibre $CoFe_2O_4$ nanowires (with a diameter of ~60 nm, which is equal to the inner diameter of the template tube) at 450 °C afforded cobalt ferrite nanoparticles as capsules 10 nm in size. Biological macromolecules, for example, hollow protein tubes of tobacco mosaic virus, can also be used as a template for the preparation of iron oxide nanotubes.[254]

f. Cobalt oxides

It was found [255] that the trivalent cobalt complex $CoL(en)_2(BF_4)_2$



[where L = $NH_2CH(CO_2H)CH_2S$] can be readily inserted into polyelectrolyte (PE) layers of colloidal particles, is deposited on these particles and serves as a precursor of CoO NT. The starting composite was prepared by the addition of poly(diallyldimethylammonium chloride) (PDADMAC) to an aqueous suspension of polystyrene particles (PS) with stirring followed by centrifugation to remove an excess of PDADMAC and layer-by-layer deposition of poly(sodium 4-styrenesulfonate) (PSS) and $CoL(en)_2(BF_4)_2$ onto PS particles. After drying at room temperature in air, spherical particles of modified PS form a necklace-like structure (Fig. 5). [In the absence of the cobalt(III) complex, this structure is not formed, because hydrogen bonds of the cobalt-containing precursor in the composite play the key role.] The use of Co complexes, which are not involved in hydrogen bonding, led to the formation of hollow spheres. Calcination of modified PS particles at 385 °C under nitrogen and oxygen for 2 and 6 h, respectively, afforded Co_3O_4 tubulenes with $D = 200-400$ nm and $L = 3-4$ μm.

The necessary condition for the nanotube formation is the presence of ten alternating PDADMAC and PSS layers on PS particles. If the number of layers is smaller than six, nanotubes are not produced. The amount of the precursor in multilayer polyelectrolyte particles and the time of their heating under a stream of nitrogen and oxygen play an important role in the synthesis of Co_3O_4 nanotubes. The morphology of nanostructures also depends substantially on the type of hydrogen-containing Co^{3+} complexes inserted into a multilayer polyelectrolyte on the surface of colloidal particles.[256] Cobalt complexes with strong intermolecular hydrogen bonds form one-dimensional Co_3O_4 nanotube structures. Complexes, in which hydrogen bonds are weak, if at all present, give rise to short defect-containing nanotubes and destroyed balls.

Nanostructures of Co_3O_4 with a large specific surface area are of practical interest, because this Co^{2+}- and Co^{3+}-containing oxide with the spinel structure serves as a good catalyst for oxidation of CO. Nanosized Co_3O_4 fibres can be prepared by the template sol–gel method.[248] An aqueous solution of $Co(NO_3)_2$ (0.3 mmol litre^{-1}) and citric acid (0.05 mmol litre^{-1}) was subjected to hydrolysis for 1 h, the resulting sol was incorporated into an aluminium template membrane for 10 s, and the membrane was dried in air and annealed at 500 °C for 24 h. Then the membrane was dissolved in alkali to prepare individual Co_3O_4 fibres.

g. Nickel oxides

Nickel-containing tubulenes can be synthesised by the template method.[257] For example, nickel nanowires were grown starting from C-NT, which were prepared by decomposition of propene on an anodised aluminium membrane.[257] The tubes were filled with nickel metal by decomposition of nickelocene under a stream of hydrogen at 105 °C. Then the aluminium membrane was removed by dissolution in 10 M NaOH at 150 °C in an autoclave. The length of the nickel nanowires thus prepared varies from tens to hundreds of nanometres, the diameter is 4 nm, and the inner size of C-NT is 20 nm, which is uncharacteristic of the template method. The latter usually gives nanowires with a length that coincides with the inner diameter of the channels in the template. The growth of nanowires occurs predominantly along the (111) plane of the crystal structure of nickel metal. The formation of the latter in the vicinity of the open ends of C-NT was not observed. Nickel nanowires are produced inside C-NT by vacuum evaporation of nickelocene.[258]

Decomposition of nickelocene at 275 °C under a water vapour atmosphere followed by deposition of nickel on a carbon film afforded a Ni–C composite.[257] Treatment of the latter with 10 M NaOH at 150 °C in an autoclave produced C-NT with inclusions, which are analogous to nanosized NiO ribbons 4 nm in width and 10–800 nm in length, and nickel metal particles (larger than 10 nm, Fig. 6). The upper and lateral surfaces of the nanoribbons are parallel to the (111) and (202) crystallographic planes, respectively, of NiO, if its axis is oriented along the [211] direction.

The formation of NiO results from oxidation of nickel with atmospheric oxygen, which occur during alkaline treatment of the composite in an autoclave. In the cavity of C-NT with an inner diameter of 20 nm, NiO crystals grow along the tube axis. In

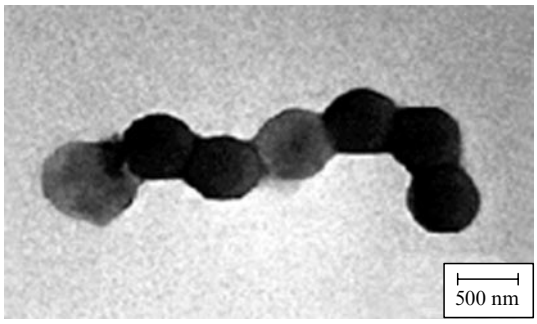


Figure 5. The TEM image of CoO_x NT.[255]

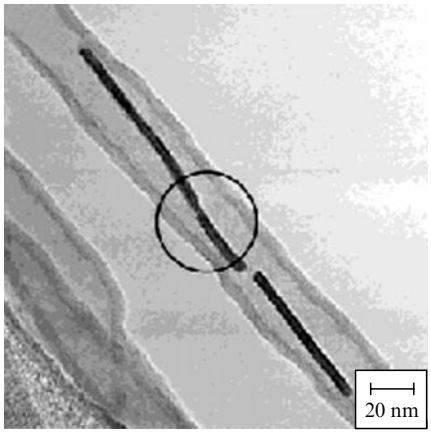


Figure 6. The TEM image of a NiO nanoribbon intercalated into a carbon nanotube.[257]

C-NT with $D > 20$ nm, platelets with sizes (in the plane) of hundreds of nanometres can be produced. The complete filling of the cavities in C-NT with NiO crystals is needed for the synthesis of nanowires or nanorods. However, this does not occur due to the growth of a thin crystalline NiO plate along the tube axis. The NiO–C-NT nanocomposite can also be prepared by filling carbon nanotubes, which are pre-treated with nitric acid followed by annealation under a stream of argon at 450 °C for 5 h, with nickel nitrate.[259] In this case, nickel oxide completely fills the inner cavity of the tube ($\sim 3-6$ nm in diameter) to form elongated nanoparticles (10–40 nm in length). This composite can be used as a catalyst in organic synthesis.

h. Copper oxides

Nanosized CuO rods were synthesised[260] according to a rather simple procedure by stirring $CuCl_2 \cdot 2H_2O$ and NaOH in the presence of polyethylene glycol (PEG). Then the composite was washed with water and EtOH and dried in air at 60 °C for 3 h. The final product consisted of identical CuO nanorods 8 nm in diameter and 40 nm in length. The type of the nanostructures is determined by PEG, which forms chain aggregates in water. The synthesis of bamboo-like CuO nanoparticles ($D = 20-90$ nm, $L = 250-700$ nm) was documented.[261] Templates of multilayer C-NT were treated with boiling HNO_3 (68%) for 24 h, stirred with a $Cu(NO_3)_2$ solution for 48 h, filtered, washed with water and dried at 60 °C for 12 h. Heating under a stream of argon at 450 °C (5 h) followed by burning up of C-NT in air (750 °C, 1 h) afforded copper oxide with the parameters of the monoclinic unit cell $a = 4.697$, $b = 3.425$, $c = 5.130$ Å, $\beta = 99.67°$. The average size of the crystallites was 37 nm (calculated from the width of the (110) reflection), and the crystallites are oriented predominantly along the [101] direction. It should be noted that the sizes of the CuO nanoparticles are much larger than those of the template, which is attributable to the tendency of the system to decrease the surface energy and to the intergrowth of the adjacent CuO nanostructures upon burning up of carbon tubes.

One-dimensional well-ordered CuO nanofibres are produced during autocatalytic growth.[262] Copper nuclei with sizes equal to the pore diameter of the membrane (50–60 and 100–150 nm) were deposited on a copper plate having a polycarbonate (PC) membrane as a template from a $CuSO_4$ solution in the electric field of 15 V cm^{-1}. Heating of Cu crystallites under an oxygen atmosphere results in their transformation into nanocrystalline CuO fibres with an average length of 2 μm and a packing density of 10^7-10^8 cm^{-2}. The diameter of nanofibres corresponds to the average size of copper particles. The solid-phase synthesis of nanosized whiskers ($D = 2-10$ nm, $L > 100$ nm) in the presence of the non-ionic surfactant polyethylene glycol (PEG-400) was also documented.[263]

The CuO/C-NT composite with the mass ratio CuO : C = 3 : 2, which was prepared by oxidation of Cu/C-NT by heating to 160 °C in air for 12 h, was studied as a cathode material in current sources with a lithium anode.[264] Lithium (1.88 g-at of Li per 6 g-at of C) was inserted into C-NT by the electrochemical method. This amount of lithium corresponds to the capacity of 700 mA h g^{-1}. For CuO/C-NT layers, the capacity is 268 mA h g^{-1}. Lithium is inserted into the CuO structure at a potential of 1.7–1.0 V and is eliminated at 2.3–2.5 V. The stable operating time of the CuO/C-NT cathode material during cycling is determined by stability of the intercalation compound Li_xCuO, which decomposes into Cu, Cu_2O and Li_2O. In this case, the microstructure of C-NT is of considerable importance. Intercalation and deintercalation of lithium causes destruction of C-NT.

k. Zinc oxides

Nanostructured ZnO has attracted considerable attention,[265] because materials based on this compound are widely used in electronics, optoelectronics, optics, solar batteries and sensors and also serve as photocatalysts. Zinc oxide nanorods and nanofibres were prepared by the hydrothermal method.[266–269] The simplest microemulsion method is the reverse of the micelle formation.[266] Cetyltrimethylammonium bromide (CTAB) was used as a microemulsifying agent. Sodium hydroxide was added to a solution of zinc acetate in n-hexanol and n-heptane to pH 14. The mixture was stirred until a $Zn(OH)_4^{2-}$ emulsion was formed and then heated in an autoclave at 140 °C for 13 h. The white precipitate that formed was washed and dried *in vacuo* at 60–70 °C. The product consisted of nanowires of hexagonal ZnO ($D = 30-150$ nm, L to 3 μm) with the growth direction along the ZnO (110) crystallographic plane. Single-crystalline ZnO nanowires ($D = 80-100$ nm, $L \approx 10$ μm, the $[0\bar{1}10]$ growth direction) were also synthesised by hydrothermal treatment of $Zn_4CO_3(OH)_6 \cdot H_2O$.[269]

Hydrothermal oxidation of zinc metal in the presence of CTAB (180 °C, 20 h) affords ZnO nanorods.[268] Surfactants, such as CTAB and n-hexanol, play an important role in the formation of ZnO nanowires. These surfactants facilitate the orientational growth of ZnO. In the synthesis with the use of zinc metal as a precursor, the surfactants promote erosion of ZnO. Ultrasonic pre-treatment of the reaction mixture before hydrothermal treatment facilitates nucleation and gives rise to a unified morphology of ZnO nanorods in an alkaline solution in the ratio $Zn^{2+} : OH^- = 1 : 20$ in the presence of ethanol and ethylenediamine.[267] Intergrowths of ZnO rods with a diameter 30–40 nm, a length of 1.5 μm were prepared (the unit cell parameters $a = 3.25$, $c = 5.21$ Å). These rods exhibit photoluminescence at 385 and 485 nm under excitation with a He–Cd laser at a wavelength of 325 nm.[266]

A zinc oxide tubular material with an outer diameter 450 nm, an inner diameter of 250 nm and an average length of 4 μm was synthesised[270] under hydrothermal conditions (180 °C, 13 h) from an ethanolic solution containing $Zn(NH_3)_4^{2+}$ cations by the reaction

$$Zn(NH_3)_4^{2+} + 2OH^- \longrightarrow ZnO + 4NH_3 + H_2O.$$

Ammonia that is eliminated plays an important role in the formation of the tubular morphology of ZnO. The reaction performed at a temperature below 180 °C with the use of methanol or propanol instead of ethanol produces the final product consisting only of ZnO nanoparticles.

Zinc oxide nanorods can be prepared by simple thermal decomposition of hydrated zinc acetylacetonate $Zn(acac)_2 \cdot nH_2O$ in an atmosphere of a N_2 and O_2 mixture at a pressure of 5×10^{-3} mm Hg and at 130–140 °C on silicon [(100) plane] and sapphire substrates.[271] The ordered ZnO structure ($D = 60-80$ nm, $L = 450-500$ nm) is prepared on the silicon (100) plane, whereas ZnO nanorods, which are oriented along the c axis and arranged in an ordered fashion along the a axis, were grown only on the sapphire (110) plane. Zinc oxide nanorods were grown also on an amorphous SiO_x layer of a Si(100) plate heated to 500 °C. These rods show emission and absorption in the UV region at 386 nm and are characterised by a low concentration of oxygen vacancies. The synthesis of high-quality well-oriented nanorods with a controlled diameter (45, 60 or 90 nm) was carried out by varying the vapour temperature (135–138 °C), the flow rate of a N_2/O_2 mixture and the substrate temperature. The synthesis at 130–200 °C from $Zn(acac)_2$ vapour and products of its partial decomposition [for example, Zn(acac)] affords zinc metal, which is oxidised on the substrate surface followed by the growth of nanostructured ZnO.

Zinc oxide nanowires and nanorods can also be prepared in aqueous solutions of zinc salts.[272,273] The oppositely charged $Zn(NH_3)_4^{2+}$ and $Zn(OH)_4^{2-}$ micelles act as microreactors, resulting in the anisotropic growth of ZnO during a simple solvatothermal process.

Nanostructured ZnO was synthesised[274] at room temperature by adding 0.02 M NaOH to a mixture of solutions of $Zn(OAc)_2 \cdot 2H_2O$ (0.01 mol litre^{-1}) and triethanolamine (TEA) (0.07 mol litre^{-1}), which was used as a surfactant, and stirring for

30 min. The composite was washed with water and ethanol using ultrasonic treatment and dried at 80 °C. The final product consisted of hexagonal nanorods (the hexagonal system, $a = 3.249$, $c = 5.209$ Å) with a diameter of 20 nm and a length of up to 200 nm. In the absence of TEA, ZnO nanoparticles were prepared. The optimum $TEA : Zn^{2+}$ ratio is smaller than $(0.1-1):1$.

The solid-phase synthesis of hexagonal ZnO nanorods ($a = 3.250$, $c = 5.207$ Å; $D = 40-120$ nm, L is up to several micrometres)[275] was carried out with the use of a $ZnCl_2$, Na_2CO_3 and KCl mixture, which was prepared with poly(oxyethylene)-5-nonylphenol or poly(oxyethylene)-9-nonylphenol ether in cyclohexane, as a precursor. The latter gave a precipitate, which was washed with acetone, separated by centrifugation, dried, annealed in air (770 °C, 3 h) and washed with water. The use of NaCl instead of KCl (as a flux), an increase in the temperature to 820 °C or an increase in the annealing time led to the formation of larger nanorods.

The growth of perfect individual ZnO nanorods with $D = 150 \pm 10$ nm and $L = 2.17 \pm 0.13$ μm was observed upon decomposition of amorphous tubular $Zn(OH)_2$ as a precursor.[276] Good reproducibility of the sizes was achieved with the use of sodium dodecylbenzenesulfonate (DBS) as a modifying and protecting agent.

Zinc oxide nanorods with a diameter of 5–300 nm and a length of up to several hundreds of micrometres can be synthesised by the reaction

$$Zn + H_2O \longrightarrow ZnO + H_2$$

in the gas phase at 730–1000 °C.[277–280] The growth of ZnO occurs along the c axis (the [001] direction). For nanostructures synthesised at 1000 °C under argon for 30 min, the following three luminescence bands are observed:[280] a strong band in the UV region (379 nm), a blue band (466 nm with a shoulder at ~452 nm) and a weak yellow band (612 nm). The UV emission is induced by direct exciton recombination, and the blue band appears due to the imperfect ZnO structure. After annealing under oxygen at 500 °C, the blue and yellow luminescence bands are substantially weakened due to a decrease in the concentration of O and Zn defects.

A modification of the chemical vapour-phase synthesis of ZnO nanowires is based on the reaction

$$Zn(g) + SiO(g) \longrightarrow ZnO(sol) + Si(sol)$$

at 900 °C under a stream of argon.[281] Oxidation of zinc vapour in the temperature range of 850–925 °C affords high-quality ZnO nanostructures as intergrowths of four nanorods (Fig. 7).[282] The morphology of the particles depends on the conditions of the process.[283] Tetrahedral intergrown T-ZnO nanorods are produced in air (see Table 1), whereas individual nanorods are formed under wet argon and nitrogen. The T-ZnO structure consists of tetrahedrally shaped intergrowths with four 'legs' 2–3 μm in length and the central core with a size of 70–200 nm.[284]

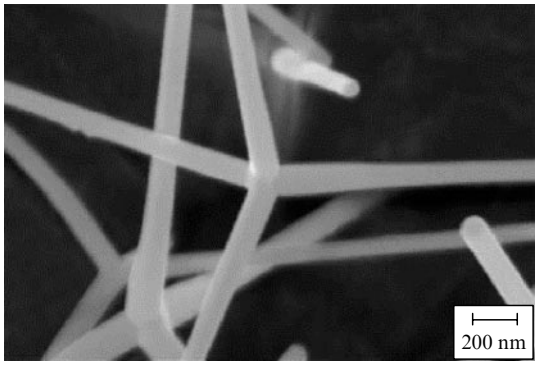


Figure 7. The SEM image of an intergrowth of T-ZnO nanorods.[282]

Oxidation of an aluminium-based melt containing 6% Si, 2% Zn and 0.8% Fe (mass %) produced relatively linear ZnO whiskers 50–500 nm in diameter.[285] The process was carried out at 1100 °C for 1 h under oxygen. The melt was oxidised to form Al_2O_3 microchannels on the surface. These channels were filled with a liquid alloy, and zinc metal was oxidised to ZnO on the surface of the alloy, resulting in the growth of nanowhiskers tens of micrometres in length. In this example, iron serves as a catalyst, and silicon acts as a promoter of growth of ZnO nanowhiskers.

Zinc oxalate, which was prepared in cyclohexane in the presence of a surfactant, was used as a precursor to prepare ZnO nanowires.[286] Zinc oxalate with an admixture of a flux (NaCl) was heated at 920 °C under a stream of argon. Thermolysis of ZnC_2O_4 afforded ZnO, which was reduced with carbon of the surfactant to Zn, and the latter went to the gas phase. Zinc and zinc oxide vapours were deposited on the walls of the reactor to form zinc oxide nuclei containing defects in the oxygen sites. Zinc oxide nanowires ($a = 3.249$, $c = 5.206$ Å, $D = 15-80$ nm) were grown when air was passed through the mixture. Depending on the flow rate of argon, either nanowires or nanowhiskers grow on the (101) surface. The addition of a NaCl flux facilitates the formation and nucleation of nanostructured ZnO, hinders particle agglomeration and promotes evaporation of Zn and ZnO.

Crystalline nanowhiskers of hexagonal ZnO were prepared by reduction of ZnS with hydrogen (5% H_2 under argon) at 1300 °C to give Zn followed by oxidation to ZnO in an Ar + 5% O_2 gas mixture.[287,288] The process is autocatalytic and occurs by the vapour–liquid–solid mechanism. The growth of ZnO occurs along the [0001] direction. The outer diameter, the length and the wall thickness of the whiskers range up to 400 nm, 15 μm and 100–150 nm, respectively.[288] The photoluminescence spectrum of the whiskers shows a strong emission band in the UV region (381 nm) and a broad band at 583 nm (green luminescence).

Zinc oxide forms unusually extended and oriented chiral nanostructures.[289] Such nanorods and nanocolumns grow in the presence of citrate ions that control the crystal growth due to adsorption on the (002) surface. The synthesis was carried out with the use of oriented ZnO nanorods, which were grown on a glass substrate in a solution of $Zn(NO_3)_2$ (0.03 mol litre^{-1}) and hexamethylenetetramine (HMT) (0.03 mol litre^{-1}) at 60 °C for 3 days. To grow helical ZnO nanostructures, the substrate was placed in a solution containing $Zn(NO_3)_2$ (0.03 mol litre^{-1}), HMT (0.01 mol litre^{-1}) and sodium citrate (0.001 mol litre^{-1}) and the mixture was kept at 95 °C for 1 day. The process was repeated by adding small amounts of sodium citrate. Chiral nanorods 1 μm in length were prepared. The base and top diameters were 500 and 30 nm, respectively. The nanorods were composed of helically arranged platelets with a step height of ~15 nm.

The microwave-induced plasma method was used[290,291] to synthesise ZnO structures with different morphologies (nanowires, nanocables, nanotubes) and specified sizes. Zinc or zinc oxide powder was placed in a quartz tube furnace, through which hydrogen was passed. Microwave heating of the precursor (400 W, 2.45 MHz) up to the plasma formation (1000 °C) led to condensation of Zn vapour in the furnace region with a temperature 500 °C. After evaporation for 30 min, hydrogen flow was terminated, and zinc was oxidised by passing a 1 : 50 oxygen and argon mixture for 15–30 min. Zinc nanowires formed under hydrogen served as a template in the synthesis of nanosized Zn/ZnO cables involving partial oxidation of zinc with oxygen followed by the formation of ZnO NT. The wall thickness of the tubes depends on the time of oxidation occurring along the [001] direction. The average outer and inner diameters of nanotubes were 40 and 10 nm, respectively, and the length was 1 μm. The sizes of the tubes can be varied depending on the conditions of the microwave-induced plasma process, the flow rate of hydrogen and the oxidation time. The microwave-induced plasma method

combined with heating in a furnace allows one to prepare also nanostructured ZnO as aggregates consisting of four nanorods with a diameter of 10–25 nm and a length of up to 160 nm.[291] Cathode luminescence of such structures is characterised by strong UV radiation at 385 nm.

Nanosized whiskers of oxalate $ZnC_2O_4 \cdot 2H_2O$ can be prepared by a chemical method.[292] For this purpose, the $Zn(OAc)_2 \cdot 2H_2O$ precursor was dispersed in xylene with an admixture of sodium DBS as a template. An ethanolic solution of $H_2C_2O_4 \cdot 2H_2O$ was added to the resulting suspension, and the white precipitate consisting of nanosized whiskers (D = 200–300 nm, L up to 20 μm) was separated by centrifugation, washed and dried *in vacuo* at 60 °C. Some whiskers were obtained as tubes with a wall thickness of ~30 nm. Heating of these nanostructures at 180 and 427 °C was accompanied by elimination of H_2O and CO_2, respectively. The resulting nanosized ZnO powder (50–60 nm) was stable up to 1280 °C. At a temperature below 280 °C, $ZnC_2O_4 \cdot 2H_2O$ was transformed into β-ZnC_2O_4 nanowhiskers. The $ZnC_2O_4 \cdot 2H_2O$ nanoparticles prepared from an aqueous solution had a size and shape, which were determined by a microreactor composed of the surfactant (DBS).

Considerable progress was made in the synthesis of nanostructured ZnO by evaporation of zinc metal and its compounds. Zinc oxide nanowires (D < 50 nm and up to tens of micrometres in length) were prepared by heating Zn under a stream of nitrogen or argon in the absence of a catalyst (zinc metal serves as the catalyst, which is then oxidised to ZnO).[293] Heating of a zinc plate at 900 °C affords ZnO nanostructures exhibiting a tetrahedral morphology (see Fig. 7).[294] Evaporation of Zn powder at 800 °C under argon gives rise to the hexagonal phase of ZnO as wires with a diameter of 0.2–0.4 μm and a length of several tens of micrometres.[295] This material exhibits strong green luminescence at 520 nm and relatively weak UV luminescence near 370 nm. The former appears due to electron–hole recombination with the involvement of electrons of the charged oxygen vacancies in the ZnO structure. Zinc oxide nanowires (30–60 nm in diameter and tens of micrometres in length), which were prepared by heating Zn powder in the presence of Au nanoparticles as the catalyst at 900 °C, also show a strong green emission.[296]

Evaporation of zinc oxide at 1380 °C under a stream of argon or *in vacuo* [297–299] affords single-crystalline ZnO nanowires (D = 15–60 nm, L = 10–70 μm) with the [110] growth direction.[298] Samples synthesised *in vacuo* hold promise as materials for short-wavelength nanolasers.[299] Condensation of ZnO vapour in the temperature range of 900–1030 °C gave a mixture of nanosized rods and belts of nanometre to micrometre diameter (width).[300] In the temperature range of 650–700 °C, rods and belts with D = 70–300 nm were grown. More homogeneous materials were produced at 350–450 °C as wires 15–40 nm in diameter and 10–70 μm in length. The growth direction of ZnO crystals is perpendicular to the $(01\bar{1}0)$, (0001) and $(11\bar{2}0)$ planes for the belts, rods and wires, respectively. Crystalline ZnO nanobelts, which were prepared [301] by thermal evaporation of ZnO in pores of an aluminium membrane, had a length of 10–100 μm, a width of 30–300 nm and a thickness of 6–30 nm and contained a smaller number of oxygen defects than powders synthesised under analogous conditions.

Additives of oxides [302] or low-melting point metals [303] in the synthesis of nanostructures from ZnO vapour increase the evaporation rate of the latter and influence the morphology of the final product. Nanosized bridges and nails can be prepared from ZnO on a graphite, silicon or $SrTiO_3$ substrate by varying the conditions of the synthesis. Nanobridges are produced by the addition of In_2O_3 to zinc oxide at 1000 °C and an air pressure of 2 Torr, and nanonails grow at 950–970°C and 0.5–1.0 Torr. A typical bridge (Fig. 8) is tens of micrometres in length and up to several micrometres in height and width;[302] it consists of a ZnO belt and nanorods (50–200 nm in diameter and up to 2 μm in length) located at the edges of the belt. Each nanorod belonging to the hexagonal system grows epitaxially along the [0001] or $[000\bar{1}]$ direction. The rows of nanorods are parallel to the $[0\bar{1}10]$ direction of the belt, which forms a ring in the centre of the bridge (Fig. 8 *a*). Two belts can be linked together perpendicular to each other (Fig. 8 *b*). The epitaxial growth of ZnO nails along the *c* axis occurs on a graphite substrate (Fig. 9). These structures are

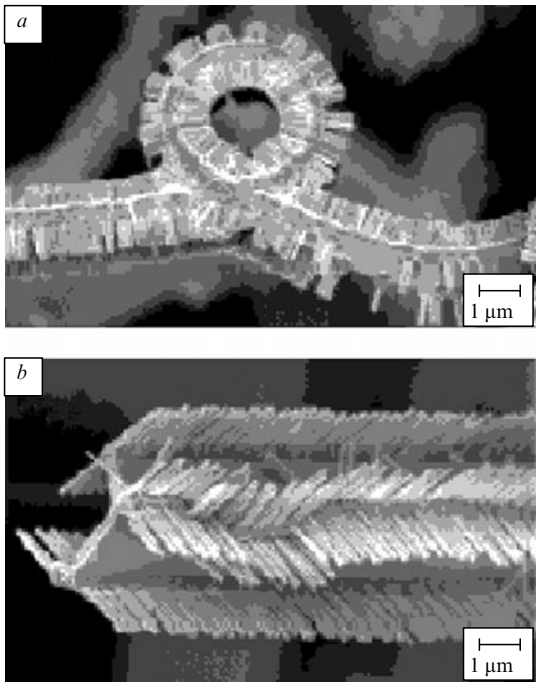


Figure 8. The SEM images of different types of ZnO bridges; (*a*) coiled; (*b*) doubled.

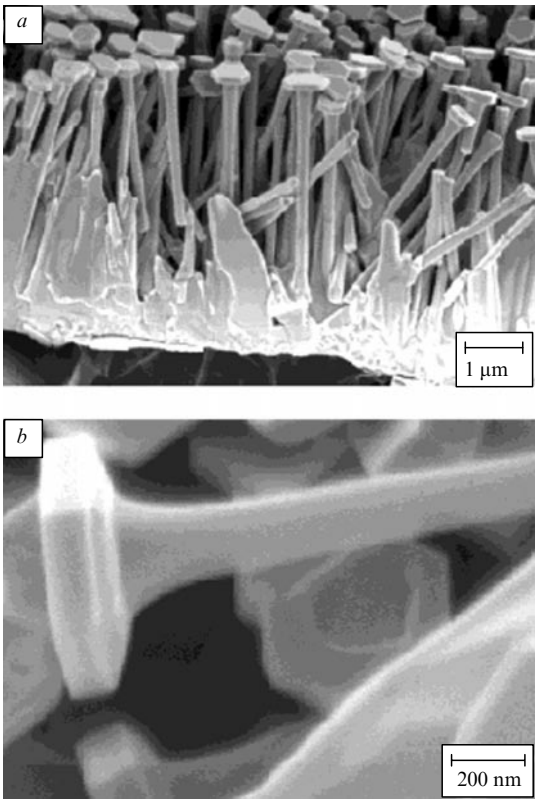


Figure 9. The SEM images of ZnO nanonails.[302]

several micrometres in length, the diameters of the rods are in a range of 150–200 nm, and the diameter and thickness of the hexagonal nail-heads are ~1 μm and 50–100 nm, respectively.

The characteristic feature of ZnO nanostructures formed in the presence of low-melting point elements is the growth of attached branches of various shapes. In this case, the surface segregation of low-melting point elements plays an important role due to enrichment of the tops of nanostructures in these elements. A three-dimensional self-organised nanosized ZnO-based heterostructure doped with In or Sn was synthesised by condensation from a vapour phase on a graphite substrate.[303] A ZnO, In_2O_3 (or SnO_2) and graphite mixture was heated at 1000 °C and condensed at 850 °C by oxidation with atmospheric oxygen to form nanosized In- or Sn-doped ZnO ribbons. Indium-containing comb-shaped heterostructures have a core composed of nanowires (D = 10–15 nm) grown along the $[01\bar{1}0]$ direction. The $\pm(2\bar{1}\bar{1}0)$ faces of the core are covered with nanoribbons located perpendicular to this face. The chemical composition of the core is described by the formula $(ZnO)_{11}In_2O_3$. At a higher percentage of indium in the starting mixture, an additional growth of ZnO nanorods with a length of 100–3000 nm on both sides of the nanowires (perpendicular to the ribbon plane) is observed. These nanorods form a straight row. Therefore, the nanorods and nanoribbons grow epitaxially on the core formed by nanowires.

A further increase in the percentage of indium in the starting mixture leads to the formation of nanostructures as four- or six-blade rotors (Fig. 10). The length of such rotors along the central axis is equal to tens of micrometres, and the length of the nanorods forming the blades varies from 200 nm to several micrometres. The terminal blades of the nanorods are ordered in a line and are hexagonal in shape. The core of the rotors consists of In_2O_3 belonging to the cubic system with the unit cell parameters a = 10.118 Å. If the growth of the core occurs along the [001] direction, there are four equivalent (100) planes, on which ZnO nanorods grow to form a four-blade rotor. If the In_2O_3 core grows along the [111] direction, the resulting nanorotor has six symmetrical blades corresponding to six equivalent (110) planes.

The growth of nanoribbons with a length of 1–20 μm and a width of ~1 μm, which cover the core of the nanostructure, occurs also in the presence of tin. The core of the structure consists primarily of ZnO and grows in the $[01\bar{1}0]$ direction, while the ribbons grow in the $[2\bar{1}\bar{1}0]$ direction. The Sn : Zn ratio increases from the centre to the ends of the structure, where it is ~8%.

The self-organised type of the structural configuration of ZnO nanowires and nanoribbons butt-joined together was obtained [304] by thermal evaporation of a ZnO and SnO_2 mixture in a mass ratio of 1 : 1 at 1300 °C under a stream of argon (300–400 Torr). Nanostructured oxide ZnO is produced in a furnace in the upper part of the alundum tube at 700–800 °C. Tin particles reduced from SnO_2 serve as the catalyst for this process. The morphology of the resulting structures appears like a liana: Sn balls are attached to the axial ZnO nanowire ($D \approx$ 30 nm) by nanoribbons (Fig. 11). The junctions of the ribbons with the axial nanowire are tens of nanometres at size, the width of the ribbons varies from 100 to 200 nm, and the ribbons are arranged about the axial nanowire at approximately 60 degree intervals. In the first step of formation of this configuration, the axial ZnO nanowire rapidly grows along the [0001] direction under the catalytic action of tin. Then particles of tin melt on the surface of the nanowire and initiate nucleation and epitaxial growth of nanoribbons. In this slower step, tin particles at the ends of the nanoribbons grow in size to form a tadpole-shaped structure (Fig. 11 *b*). The growth of ZnO nanoribbons along six directions, $\pm[10\bar{1}0]$, $\pm[01\bar{1}0]$ and $\pm[\bar{1}100]$, give rise to six symmetrically arranged tadpoles with an angle between the adjacent tadpoles of ~60°.

Semiconducting single-crystalline ZnO wires were synthesised by thermal evaporation of ZnS on a Si(100) substrate in the presence of Au as the catalyst [305] at 1223 K under argon (150 Torr) according to the reactions

$$ZnS(sol) \longrightarrow ZnS(g),$$

$$ZnS(g) + O_2(g) \longrightarrow ZnO(sol) + SO_2(g).$$

The nanowires 20–60 nm in diameter and tens of micrometres in length grow along the [001] direction and contain a high density of structural defects. Evaporation of a ZnS and $Fe(NO_3)_3$ mixture in

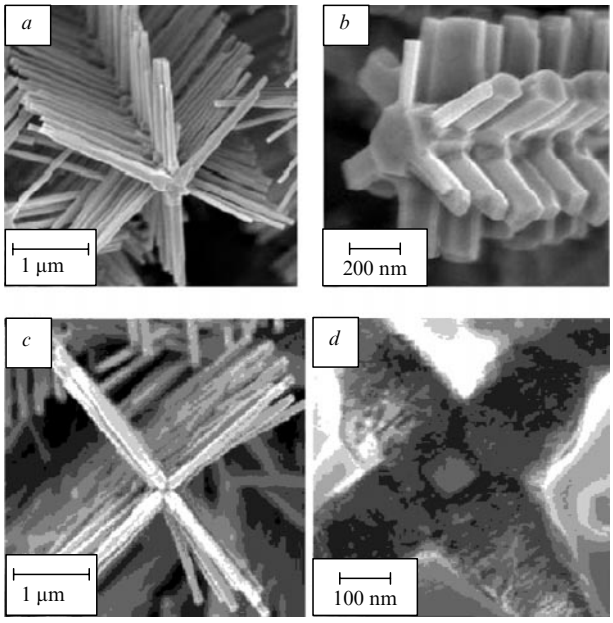


Figure 10. The SEM (*a* and *c*) and TEM images (*b* and *d*) of ZnO nanorotors with six (*a* and *b*) and four (*c* and *d*) blades.[303]

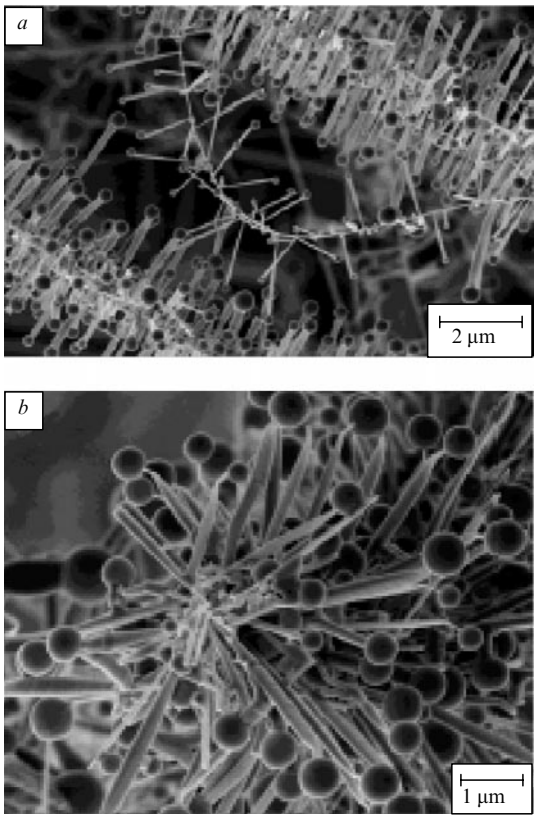


Figure 11. The SEM images of nanosized liana-shaped (*a*) and tadpole-shaped (*b*) ZnO heterostructures.

a molar ratio of 1 : 2 (1300 °C, 12 h) under argon containing 5% H_2 (350 Torr) affords whiskers with a diameter of 200 – 500 nm and tens of micrometres in length.[306] Zinc oxide whiskers do not grow under pure argon or nitrogen. In oxygen, micronic-size ZnO particles are produced by the reactions

$$4\,Fe(NO_3)_3 \longrightarrow 2\,Fe_2O_3 + 12\,NO_2 + 3\,O_2,$$

$$ZnS + H_2 \longrightarrow Zn + H_2S,$$

$$6\,Fe_2O_3 \longrightarrow 4\,Fe_3O_4 + O_2,$$

$$2\,Zn + O_2 \longrightarrow 2\,ZnO.$$

Thermolysis of Fe_2O_3 occurs very slowly, due to which a low O_2 concentration in the gas phase leads to the formation of nanosized ZnO nuclei and growth of oxygen-defect whiskers. Zinc oxide nanobelts, which grew along the $[01\bar{1}0]$ direction and were bounded by the $\pm(0002)$ and $\pm(01\bar{1}0)$ planes, were synthesised by evaporation of $ZnCl_2$ in an Ar and O_2 gas mixture in a ratio of 10 : 1 at 700 °C.[307] The resulting material is intended for use in light-emitting and laser diodes.

In the Et_2Zn and N_2O vapour phase (1 : 3 ratio, 200 Torr), high-quality ZnO nanorods and layered structures were grown epitaxially.[308] Nanorods with a diameter of 10 – 50 nm and a height of 0.5 – 1 μm grow on a sapphire substrate at 500 °C, whereas ZnO layers of identical shape grow at 800 °C. Three-dimensional structures are generally synthesised when the temperature of a sapphire[308] or silicon[309,310] substrate is lower than 700 °C, whereas two-dimensional layered structures grow at higher temperatures.

Evaporation of $Zn(acac)_2 \cdot n\,H_2O$ at 130 – 140 °C under an atmosphere of an N_2 and O_2 mixture (in a ratio of 1 : 1, 200 Torr)[311] and with the use of a Si(001) substrate heated to 450 °C produced nanorods with $D = 45$ nm and $L = 200$ nm. The diameter of the nanorods increased with increasing temperature. The epitaxial growth of ZnO nanorods from an organometallic phase occurs also on an $Al_2O_3(001)$ substrate at 400 °C.[312] Nanorods of equal length and density and with $D \approx 25$ nm grow perpendicular to the substrate along the c axis of the ZnO lattice.

The growth of nanosized ZnO wires, rods and whiskers on a sapphire substrate by evaporation of zinc oxide was documented.[313 – 316] Analogous structures were also grown on a silicon substrate.[317 – 322] A substrate imperfection influences the selectivity of the initial growth of nanowires.[318] On an imperfect Si(100) face consisting of terraces separated by steps, nuclei of ZnO nanowires appear at the edges of the steps along the $[01\bar{1}]$ direction and grow perpendicular to the support. Zinc oxide nanowires virtually do not grow on a defect-free Si(100) substrate. Twinned ZnO nanowires, in which the boundary between single-crystalline domains is parallel to the growth axis, grow on a Si substrate during evaporation of Zn under an atmosphere with a low oxygen content.[319] The components of the twin, which have no dislocations and amorphous regions, are parallel to the $(0\bar{1}14)$ plane and grow along the $[0\bar{1}1\bar{1}]$ direction and the $(2\bar{1}\bar{1}0)$ plane. The distance between the adjacent planes of the crystal lattice (2.60 ± 0.05 Å) corresponds to the distance between the (0002) planes. This unusual structure serves as a model for studying the electrical charge transport and mass transfer along a single planar defect.

Single-crystalline ZnO nanobelts were prepared[320] on a Si substrate by infrared heating of a Cu – Zn melt under moderate vacuum. Nanostructures grow along the [0001] direction, and their length is twice as large as their width. Long ZnO nanowires can be prepared catalytically on a Si substrate partially covered with gold under an atmosphere of an Ar and H_2S mixture at a low partial pressure of hydrogen sulfide.[321] A vapour phase was prepared by carbon thermal reduction of ZnO. Nanowires grown under these conditions show blue-green luminescence, whose intensity increases with increasing H_2S partial pressure in the synthesis of this material.

A substrate and a template composed of anodised aluminium are widely used to grow ZnO nanostructures with different morphologies.[322 – 325] Polycrystalline ZnO nanowires were prepared on anodised aluminium by vacuum evaporation of ZnO.[322] Nanosized tower-shaped ZnO columns were produced by pyrolysis and oxidation of ZnS.[323] Apparently, these columns grow by layering nanocrystalline zinc oxide. Zinc oxide nanowires ($D = 40 – 200$ nm) containing a low concentration of oxygen vacancies were also grown on an aluminium substrate by heating a 1 : 1 mixture of ZnO and Zn powders to 500 °C in the presence of water vapour as an oxidiser.[324]

The synthesis of ZnO nanowires with a high degree of crystallinity was carried out on an aluminium substrate in the presence of the NiO catalyst.[325] Zinc metal was evaporated at 450 – 950 °C under argon. The samples thus prepared have a hexagonal structure, a diameter of 55 nm and a length of 2.6 μm (Fig. 12). At a growth temperature of 500 °C, the nanowires are characterised by the perfect hexagonal morphology. All ends of nanowires are well-formed and can serve as mirror planes for a laser matrix.

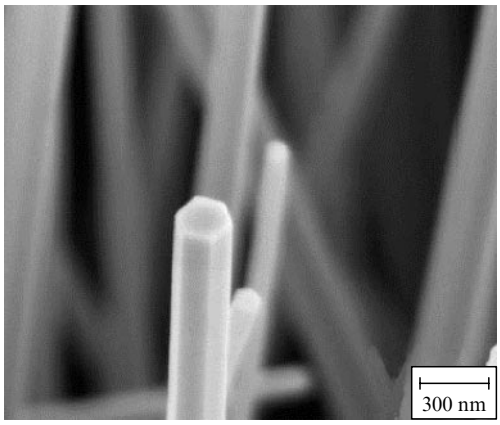


Figure 12. The SEM image of ZnO nanowires prepared on an aluminium membrane.[325]

Electrochemical deposition using an anodised aluminium template membrane also allows one to prepare ZnO nanomaterials with different morphologies.[326 – 328] Zinc oxide nanowires consisting of individual crystalline particles were prepared in hexagonal channels of the membrane by electrochemical deposition in a 0.1 M $Zn(NO_3)_2$ solution at a voltage of 1 V using a zinc electrode.[327] The composite can be used in optical, electrical and sensor nanodevices. Well-ordered high-density ZnO nanowires with constant dimensions were prepared by electrochemical deposition on a Si substrate using a template composed of anodised aluminium.[329] Electrolysis was carried out in an aqueous $Zn(NO_3)_2$ solution, and the membrane pores were filled with the sol that formed upon its hydrolysis.[330] Then the template was successively annealed at 200 °C (1 h) and 400 °C (2 h) and dissolved in 1 M NaOH at 60 °C using ultrasonic stirring to prepare well-crystallised nanowires. The X-ray diffraction pattern of the latter has the (100), (002) and (101) reflections corresponding to the interplanar distances of 2.8, 2.6 and 2.5 Å, respectively.

Treatment of multilayer C-NT with zinc vapour on outer graphite layers afforded ZnO ultrathin films, nanocrystallites (quantum dots), nanowires and nanorods.[331] Nanowires with an average diameter of 30 nm and a length of up to 1.5 μm were grown at 600 °C on the surface of a carbon tube in the absence of a catalyst. Zinc oxide nanorods with a diameter of 80 – 150 nm and a length of 0.5 – 1 μm were produced at 800 °C.

Considerable progress was made in the synthesis of composite heterostructured nanomaterials of applied importance. The synthesis of metal – semiconductor heterostructures as nanorods and

nanocables was documented.[332–335] Evaporation followed by condensation of zinc metal vapour on vertically arranged ZnO nanorods afforded a Zn/ZnO composite.[332] In this case, Zn is localised primarily at the tips of nanorods. Gold-coated heterostructured ZnO nanorods had the pronounced Au/ZnO interface.

Pyrolysis of zinc acetylacetonate produced a Zn/ZnO coaxial cable ($D \approx 30$ nm) with a zinc core and a ZnO shell.[333] The latter has a crystal structure and is transformed into ZnO nanotubes with a wall thickness of 4 nm, which appear due to evaporation of Zn from the cable core. Zinc oxide nanotubes and Zn/ZnO coaxial nanocables were also prepared by thermal reduction of ZnS (1300 °C) under a stream of an $Ar + H_2$ gas mixture at 300 Torr.[334] The nanocables are several micrometres in length, the core diameter is ~50 nm, and the thickness of the outer shell is 5 nm. Hollow ZnO samples with an outer diameter ~ 60 nm and a wall thickness of ~10 nm were also synthesised. There is a good epitaxial relationship between the zinc core and the ZnO shell. However, dislocations occur at the Zn/ZnO interface due to incommensurability in the crystal structures of the components. The use of ZnO nanobelts as templates made it possible to synthesise ZnO/ZnS nanocables by a chemical method.[335]

Coaxial structures of more complex composition were prepared [336] by the thermal reaction combined with physical evaporation. A three-layer coaxial nanocable had a gallium core, a Ga_2O_3 inner layer and an outer shell composed of ZnO. The mechanism of formation and the luminescent properties of this composite were studied. It was suggested that an Al_2O_3 coating be used to protect ZnO nanorods against contamination and corrosion.[337] The coating was prepared with the use of water vapour and $AlMe_3$ as a precursor. The reagents were fed into a furnace containing ZnO nanotubes grown on silicon (300 °C, 250–280 Torr) under a stream of argon. The resulting nanotubes have a shell composed of amorphous oxide Al_2O_3 46 nm in thickness.

Doping of Zn/ZnO nanocables with copper [338] using $CuSO_4$ (0.01–0.5 mol litre^{-1}) and $Cu(NH_3)_4^{2+}$ (0.1 mol litre^{-1}) solutions occurs according to the reaction

$$Cu^{2+} + Zn \longrightarrow Zn^{2+} + Cu.$$

Depending on the concentration of the solution, copper-containing clusters are produced, which can form larger structural networks. In the presence of the complex cations $Cu(NH_3)_4^{2+}$, copper nanorods grow on the surface of cables. This redox reaction occurs both on the damaged surface of Zn/ZnO nanocables and on its ZnO shell.

Considerable progress was made in the practical application of zinc-containing nanostructures.[339–354] It was suggested that well-crystallised ZnO nanowires be used in planar displays.[339] The emission current density of the material is as high as 1 mA cm^{-2} at an electric field strength of 11 V μm^{-1}, which provides sufficient brightness of FET emitters based on this material. The turn-on voltage of glow of these wires is 6 V μm^{-1} at a current density of 0.1 μA cm^{-2}. For nanosized ZnO needles with tips several nanometres in diameter, the emission current density is as high as 2.4 A cm^{-2} at an electric field strength of 7 V μm^{-1}.[340] Due to a very stable emission current density and a low turn-on field (2.4 V μm^{-1}), this nanomaterial holds considerable promise for the construction of field emission displays.

Zinc oxide nanowires with a diameter of 60 nm are highly sensitive to UV radiation, due to which they can be used in optical switching devices.[341] Samples of ZnO nanorods synthesised from an organozinc vapour phase in the absence of a catalyst are characterised by high optical quality.[342] Poly(vinylpyrrolidone)-capped ZnO nanorods are of interest as an optical material.[343] Luminescence of this nanocomposite is observed at a temperature below 50 K.

A nanosized field-effect transistor (FET) was constructed based on ZnO nanobelts 10–30 nm in thickness with gold electrodes.[344] At a threshold input voltage of 15 V, the ratio of the turn-on current to the turn-off current is ~100, and the maximum conductivity is 1.25×10^{-3} S cm^{-1}. Comparative characteristics of diodes composed of ZnO nanorods and Au/ZnO heterostructures were given in the study.[345] Both diodes have nonlinear and asymmetric voltammetric characteristics. However, the Au/ZnO heterostructure is characterised by a higher puncture potential (8 V) compared to that of ZnO nanorods (3 V). Zinc oxide nanowires are of interest as a material for frequency converters in optical chains and logical components in nanosized optoelectronic devices.[346]

A procedure for the design of the nanosized Au(MEA)/(ZnO/PSS)$_{19}$ZnO/Ag device [MEA is mercaptoethylamine and PSS is poly(sodium 4-styrenesulfonate)], which can rectify the current, and its electronic properties were described, and the mechanism of current rectification was proposed.[347] Single ZnO nanobelts can be used as resonators, whose mechanical resonance is induced by an alternating electric field.[348] It was suggested [349] that the Rh–ZnO/C-NT nanocomposite be used as a highly active catalyst for the methanol synthesis (the yield of MeOH with respect to the catalyst is 411.4 mg g^{-1} h^{-1}, the selectivity is 96.7% at 250 °C). The activity of this material is higher than that of the known Cu–ZnO/Al_2O_3 catalyst (for the latter, the yield of MeOH is 213.6 mg g^{-1} h^{-1}). The multilayer structure of a C-NT substrate facilitates rapid transport and proton and electron binding. Zinc oxide nanowires with a large specific surface area is of importance for photocatalysis.[350] The ZnO nanoparticles–acrylic resin composite prepared by ultrasonic stirring of tetrahedral and usual ZnO nanoparticles in a surfactant-containing solution possesses antistatic and antibacterial properties.[351]

2. Nanostructures of 4d-metal oxides

a. Yttrium oxides

Yttrium oxide was prepared [258] as the Y_2O_3/C-NT nanocomposite. Carbon nanotubes, which were pre-treated with nitric acid, were filled with yttrium nitrate and heated at 450 °C for 5 h under a stream of argon. X-ray diffraction study of bulky samples determined $d = 2.65$ Å for the Y_2O_3 (400) planes.

b. Zirconium oxides

Hollow zirconium dioxide nanotubes were synthesised [355] using C-NT as a template. Carbon tubes were treated with a 16 M HNO_3 solution, mixed with $Zr(OPr^i)_4$ under argon, subjected to ultrasonic treatment for 2 min, washed and dried. Annealing at 450 °C in air afforded the ZrO_2/C-NT composite. Carbon was removed by heating the product at 700 °C. Zirconium dioxide nanotubes thus prepared had a diameter of 40 nm and a wall thickness of 6 nm (Fig. 13). Electron diffraction study demonstrated that these nanotubes consisted of a 1:1 mixture of the monoclinic and tetragonal phases. Heating of the samples led to their destruction. The problem of the preparation of single-phase nanotubes was resolved by preparing yttrium-stabilised ZrO_2 nanotubes ($0.92\,ZrO_2 \cdot 0.08\,Y_2O_3$). The latter were synthesised as follows: NH_4OH was added to a mixed $ZrOCl_2$ and $Y(NO_3)_3$ solution to pH 9, and the resulting gel was mixed with C-NT, dried in air and annealed successively at 450 °C (12 h) and 700 °C (48 h). This method was used to synthesise hollow nanotubes belonging to the cubic system ($a = 5.116$ Å) with an outer diameter of 40–50 nm and a wall thickness of 6 nm.

Hollow tubes of amorphous ZrO_2 with a length of 40–200 μm, a wall thickness of 0.2–0.7 μm and an outer diameter of 1.3–5.9 μm were prepared with the use of needle-like crystals of ammonium tartrate as a template.[356] Zirconium dioxide was deposited on the surface of these crystals from an ethanolic solution upon the addition of zirconium alkoxide. The template was removed by dissolving in water. The specific surface areas and the pore size of these tubes depend on the alkoxide used, the conditions of deposition of ZrO_2 and the amount of water. Both open and closed composite BN nanotubes, which were filled with nanorods composed of monoclinic ZrO_2, were synthesised.[357] The diameter of the latter (20–40 nm) corresponds to the inner diameter of BN nanotubes.

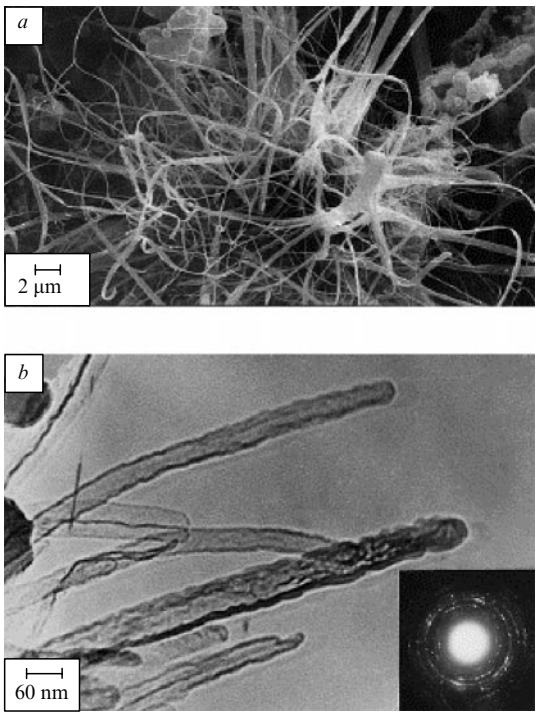


Figure 13. Images of a hollow ZrO_2 nanotube;[355]
(*a*) SEM, (*b*) TEM. The electron diffraction pattern of the sample is shown in the inset.

c. Niobium oxides

Hollow amorphous rectangular-shaped Nb_2O_5 tubes were prepared analogously to ZrO_2 tubes using ammonium tartrate as a template.[356] The length and width of the tubes varied in ranges of 40–200 and 1.3–5.9 μm, respectively, the channel size was 1.0–4.9 μm, and the wall thickness was 0.2–0.7 μm. The specific surface area and the pore size of the tubes depend on the composition of niobium alkoxide, and the microporous structure depends on the conditions of its hydrolytic polycondensation.

d. Molybdenum oxides

Molybdenum trioxide has attracted interest because of its catalytic, photochromic and electrochromic properties. The composite consisting of carbon nanotubes filled with MoO_3 single crystals was prepared[358] by heating the corresponding mixture in a quartz tube at 800 °C (3 h). The yield of the target product was ~50%. Infrared heating of a molybdenum foil under moderate vacuum (950–1000 °C, 5 Torr, 1 h) on a tantalum substrate afforded a pale-blue film consisting of quasi-linear MoO_3 tubes (the orthorhombic system, $a = 3.95$, $b = 13.88$, $c = 3.70$ Å) with a length of 5–8 μm, an outer diameter of 50–300 nm and an inner diameter of 20–150 nm. Compared to crystalline MoO_3, the unit cell parameter a is smaller by 0.3%, whereas the unit cell parameters b and c are larger by 0.16 and 0.1%, respectively, due to the influence of a tubular structure. The nanotubes grow predominantly along the [100] direction. Disturbance of the ordered arrangement of the tubes along the [010] direction due to weak interactions between the oxide (020) planes gives rise to a three-dimensional structure. Nucleation and growth of MoO_3 nanotubes rather than nanorods or nanobelts was associated with a layered structure and a low concentration of molybdenum trioxide vapour.

Nanosized MoO_3 fibres were synthesised[358, 359] by the sol–gel method in three steps. The reaction of molybdic acid $H_2MoO_4 \cdot H_2O$ with amine $C_nH_{2n+1}NH_2$ (in a molar ratio of 2 : 1) in ethanol followed by the addition of water produced the MoO_3/amine composite, which was subjected to hydrothermal treatment in an autoclave at 120 °C for 3–5 days. The product was filtered off, washed with ethanol and diethyl ether and stirred in 33% HNO_3 at 20 °C for 48 h to prepare fibrous molybdenum trioxide. The MoO_3/amine composite $(C_{12}H_{28}N)_{0.5}MoO_{3.25}$ was prepared using components in a ratio of 3 : 1. This composite has a laminar structure and contains template molecules between the layers. The morphology of the product is independent of the reaction time (1–14 days) at 100–120 °C, but it strongly depends on the reaction time at 150 °C. Hydrothermal treatment at 180 °C for 7 days led to destruction of the laminar structure and the formation of a black crystalline powder. The template was removed by treatment of the composite with HNO_3, which was accompanied by the transformation of the laminar structure into quasi-one-dimensional MoO_3, *viz.*, planar-needle- or cylinder-shaped fibres (with a diameter 20–280 nm and a length varying from 350 nm to 15 μm) formed by threads with $D = 20$–50 nm. The morphology of the MoO_3 fibres remained unchanged upon annealing at 400 °C in air for several hours, and these fibres are of interest as catalysts for oxidation of ethanol and methane.

Calcination of $MoO_3(4,4'\text{-bipy})_{0.5}$ single crystals with a layered structure ($d = 11.2$ Å) in the temperature range of 300–450 °C afforded molybdenum trioxide plates (60–100 nm).[360] In the temperature range of 320–350 °C, the metastable β-MoO_3 phase was prepared. At 380 °C, the latter was transformed into the orthorhombic α-MoO_3 phase. Nanoplates of these oxides were packed in stacks 50–250 μm in height.

e. Cadmium oxides

Cadmium oxide is an n-type semiconductor, which is of interest in the fabrication of light-emitting diodes, diode lasers and field emission displays. Cadmium oxide nanowires were prepared by electrochemical deposition of cadmium metal from the aqueous electrolyte $CdCl_2$ (40 g litre^{-1}) and H_3BO_3 (30 g litre^{-1}) on an anodised aluminium membrane at a current density of 1 mA cm^{-2} followed by oxidation of Cd in air at 400 °C and dissolution of the membrane in a NaOH solution.[361] Cadmium oxide nanowires had an ordered structure. The diameter of the nanowires was equal to the channel size of the membrane (~60 nm).

Single-crystalline CdO nanowires several micrometres in length (the cubic system, $a = 4.569$ Å, $D = 40$–60 nm) were prepared by oxidation of a mixed Cd (70%) and Te (30%) film electrochemically deposited on an aluminium substrate from a $CdCl_2$ and TeO_2 solution (0.1 and 0.2 mol litre^{-1}, respectively, pH 10, 0.2 mA), at 450 °C under an atmosphere of O_2 and Ar (1 : 9).[362] Tellurium served as a flux, which facilitates growth of CdO nanowires. Nanostructured oxide CdO was grown as needles by vapour deposition.[363] Single needles with high conductivity were proposed as a material for highly sensitive IR photoprotectors and NO_2 gas sensors. Semiconducting CdO nanowires hold promise for electronics, optics, sensors and optoelectronic nanodevices.[364]

3. Nanostructures of 5d-metal oxides

a. Tantalum oxides

Tubulenes of Ta_2O_5 were synthesised analogously to Nb_2O_5 nanotubes.[356] Nanotubes of complex oxide of composition $Sr_{0.8}Bi_{2.2}Ta_2O_{9+y}$ were also prepared by the template method.[365] A protonated silicon membrane with hexagonal pores having diameters of 2 μm and 800 nm and a depth of 100 μm was used as a template. The precursor was deposited on the template from a solution of Sr, Bi or Ta ethylhexanoate (0.1 mol litre^{-1}) in toluene. After two-step pyrolysis of the composite at 100 and 300 °C, the membrane was subjected to thermal treatment in air at 850 °C for 30 min and then the template was removed by dissolving in a HF and HNO_3 mixture (15 mol.% and 50 mol.%, respectively). Nanotubes of identical shape with a wall thickness smaller than 100 nm, a diameter of up to 2 μm and a length of 100 μm were prepared. Partial removal of the template gives rise to a periodic structure consisting of isolated

nanotubes. Such nanotubes exhibiting both ferroelectric and piezoelectric properties can be used in memory elements.

b. Tungsten oxides

Heating of a tungsten foil, which contained a SiO_2 plate on its surface, at 1600 °C under argon (p_{Ar} = 100 Torr) afforded a nanostructured WO_x material ($x = 0-3$).[366] Ultrasonic treatment of the latter led to its decomposition to give needles (5–50 nm in thickness and 20–200 nm in length) and planar polyhedral nanoparticles (10–50 nm in cross-section). The nanoneedles consisted primarily of oxide $W_{18}O_{49}$, and nanoparticles contained primarily WO_3. The process of their formation can be described by the reactions

$$W + x\,SiO_2 \longrightarrow WO_x + x\,SiO,$$

$$(4+x)W + 2x\,SiO_2 \longrightarrow 4\,WO_x + x\,WSi_2.$$

The epitaxial growth of monoclinic oxides WO_x (WO_3, $W_{18}O_{49}$ and W_3O) occurs from the gas phase at the W (foil)–SiO_2 plate interface along the [010] crystallographic axis.

Hollow fibres of crystalline oxide $W_{18}O_{49}$ forming a pine-needle-shaped structure were synthesised[367] by heating WS_2 powder on a tungsten foil at 1300–1400 °C under an atmosphere of argon and oxygen ($p_{Ar} = 490 \pm 90$, p_{O_2} = 10 Torr). The outer diameter of the fibres is 3–10 μm and the length is 0.1–2 mm. The fibres consist of thin whiskers 50–500 nm in diameter (Fig. 14). The formation of hollow $W_{18}O_{49}$ fibres is attributed to their single-crystalline axial growth, which provides efficient scattering of released heat.

The synthesis of $W_{18}O_{49}$ nanorods and their optical properties were documented.[368] The starting compounds [$W(CO)_6$, $Me_3NO \cdot 2H_2O$ and oleylamine] were stirred and heated to 270 °C for 2 h. After aging for 24 h, the mixture became viscous and turned bright-blue. This composite was dissolved in toluene, ethanol was added, and a blue precipitate was separated by centrifugation and purified by reprecipitation with ethanol from toluene. The final powder consisted of nanorods 4 ± 1 nm in diameter and 75 ± 20 nm in length. The electron diffraction pattern of the sample has two intense rings corresponding to d = 3.78 and 1.89 Å, which is indicative of the predominant growth of nanorods in one direction. X-ray diffraction study demonstrated that these nanorods have a structure of $W_{18}O_{49}$ with the [010] growth direction. The length of the nanorods depends on the temperature of the synthesis (25 ± 6 nm at 250 °C and 130 ± 30 nm at 270 °C). At temperatures below 250 °C, nanorods do not grow.

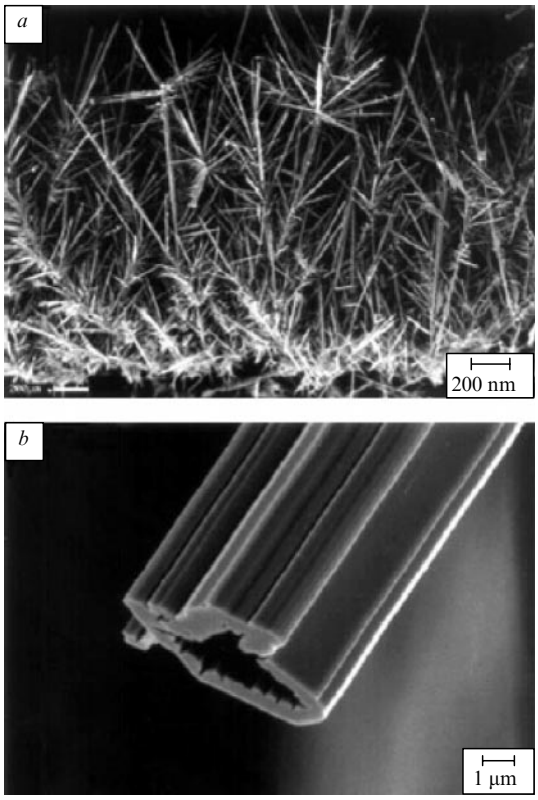


Figure 14. The SEM images of crystalline (*a*) and hollow (*b*) $W_{18}O_{49}$ fibres with a pine texture.[367]

Thermal oxidation of tungsten[369] produced $WO_{2.9}$ nanorods on Si(001), Si(111) and SiO_2/Si plates and silver-coated glasses. A tungsten coil was heated to 600–2000 °C by passing current *in vacuo* (3×10^{-2} Torr). Tungsten oxide vapour was condensed on plates, whose temperature was lower than 200 °C. Single-crystalline $WO_{2.9}$ nanorods with a diameter of 20 nm and a length of 400 nm were arranged in an ordered fashion on substrates. For the majority of nanorods, the $WO_{2.9}$ [010] crystallographic axes are almost parallel and coincide with their growth direction. There are orientational relationships not only between the nanorods but also between the nanorods and the substrate. Thus, the $WO_{2.9}$ [010] axis is parallel to the Si (001) plane. At the tungsten coil temperature of 850 °C, $WO_{2.9}$ nanorods were deposited. At a temperature above 1100 °C, WO_2 nanorods began to grow, and these nanorods prevailed at 1450 °C. These results are attributed to the difference in the degree of oxidation of the coil under an atmosphere with a constant concentration of oxygen.

The template method was used to grow WO_3 fibres with a diameter of 20 nm and a length of 50 μm inside the pores of an anodised aluminium membrane.[162] Tungsten hexachloride was dissolved in ethanol and an aqueous pentane-2,4-dione solution was added. Then the membrane was immersed in this mixture for 1 min, dried in air and annealed at 550 °C for 6 h. Hydrated oxide $WO_3 \cdot H_2O$ was prepared as two-dimensional plates with an average size of 30–100 nm using benzyl alcohol as a template.[156] A WCl_6 and $C_6H_5CH_2OH$ mixture was heated at 100 °C for 48 h, and the precipitate of $WO_3 \cdot H_2O$ nanoplates that formed was separated by centrifugation, washed with ethanol and dried.

III. Computer design of structures and electronic properties of oxide nanotubes

1. Structural models of inorganic nanotubes

Most of the known inorganic nanotubes were prepared (or predicted) for layered substances and compounds with layered (graphite-like) structures,[31–38] due to which the models of their atomic structures can be constructed and their geometry can be described using approaches and the classification developed for carbon tubes.[2–7]

Models of ideal carbon nanotubes can be built by wrapping atomic ribbons, which are cut out from a hexagonal graphite sheet (the so-called graphene sheet), and cross-linking the broken bonds of the terminal atoms in such a way as to form a cylinder. Depending on the mode of wrapping (the type of graphene-like ribbons), two main types of tubes (chiral and achiral) are constructed. In turn, the latter are divided into the so-called zigzag and armchair NT.

The modes of construction of NT are illustrated in Fig. 15. The $\boldsymbol{a}_1$ and $\boldsymbol{a}_2$ basis vectors of the hexagonal graphene network specify the chiral vector $\boldsymbol{C}_h = n\boldsymbol{a}_1 + m\boldsymbol{a}_2$, which lies in the plane of the network and links two crystallographically equivalent positions. The scalar of vector $\boldsymbol{C}_h$ is equal to the cylinder perimeter (the tube cross-section). The diameter (D) and the chiral angle (α) between the $\boldsymbol{C}_h$ and $\boldsymbol{a}_1$ vectors, which is uniquely related to the $\boldsymbol{a}_1$ and $\boldsymbol{a}_2$ vectors by the n and m indices, respectively, are the main geometric characteristics of the tubes. The notations (n,m)-NT are used in the classification of nanotubes. According to this classification, all (n,m)-NT with $n \neq m \neq 0$ belong to chiral (helical) nanotubes with $0 < \alpha < 30°$. Achiral (n,0)-NT (zigzag) and (n,n)-

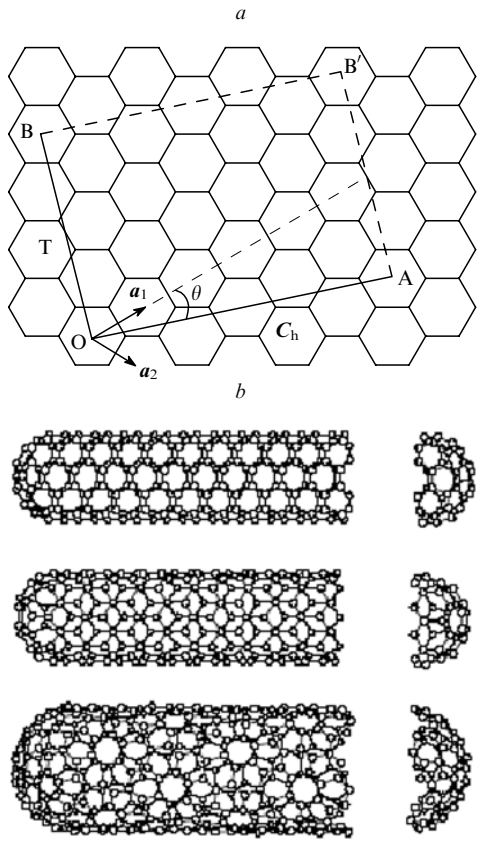


Figure 15. Models of the construction (*a*) and types of carbon nanotubes (*b*) formed by wrapping a graphene sheet into a cylinder.
Terminal structures of achiral armchair, achiral zigzag and chiral nanotubes.

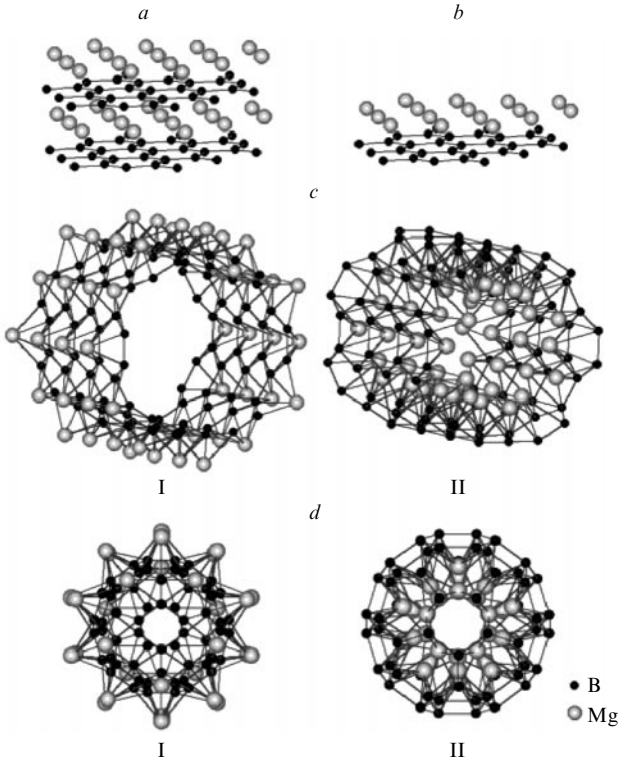


Figure 16. Fragments of a crystal (*a*), a bilayer (*b*) and atomic models of single-layer tubes (*c*) and fullerene-like molecules (*d*) based on metal diborides AlB_2.[107]
Two types are shown: a cylinder consisting of metal atoms (a polyhedral shell of the molecule) outside (I) or inside (II) the tube (shell) formed by boron atoms.

NT (armchair) have $\alpha = 30$ or $\alpha = 0°$, respectively. These tubes are called in accordance with the structure of their cross-sections (zigzag or armchair; see Fig. 15).

This approach can be applied to the construction of atomic structures of nanotubes for typical representatives of layered inorganic compounds. Both homo- and heteroatomic networks (for example, Si or BN) and molecular layers consisting of two (metal diborides), three (d-element dichalcogenides, $NiCl_2$) or more (Bi_2S_3) atomic networks can serve as monolayers of the starting crystalline phases, which form NT. A network or a molecular layer can be either planar (BC_x, CN_x, $B_xC_yN_z$, *etc.*) or corrugated (for example, a network of black phosphorus).[36–38]

Tubes of the layered modifications of carbon nitride (CN_x), boron nitride (BN) or boron carbonitrides ($B_xC_yN_z$) isostructural with graphite are the simplest analogues of carbon NT.[31, 369–375] Their atomic structures (taking into account the differences in the interatomic distances in graphite and the above-mentioned B–C–N phases) are analogous to those of C-NT, and the distinguishing features depend on the structural type, the ratio of the elements and the mutual arrangement of their atoms in the cell, *i.e.*, the atomic ordering in the walls of the tubes.

Tubes of hexagonal metal diborides MB_2 are structurally more complex. Their structures (AlB_2, space group $P6/mmm$) consist of the alternating hexagonal networks of metal M and graphite-like boron networks.[106–110, 376] The atomic models of single-layer tubes with formal stoichiometry MB_2 are derived by wrapping the atomic bilayer $(MB_2)_\infty$ of the crystal. These models consist of two coaxial cylinders formed by a planar hexagonal metal network and a planar graphite-like boron network linked to each other. Chiral and achiral MB_2 NT can be constructed analogously to carbon tubes. In addition, two other configuration types of such tubes can in principle, exist. In these tubes, a 'metallic' cylinder is located outside (I) or inside (II) the cylinder composed of boron atoms (Fig. 16). This figure also shows models of polyhedral (fullerene-like) $(MB_2)_n$ molecules.[107] The hemispheres of these molecules can serve as caps of closed diboride tubes. Like tubes, the $(MB_2)_n$ molecules consisting of the concentric spherical M_n and B_{2n} shells can have two configurations with an M_n shell outside (I) or inside (II) the polyhedron composed of boron atoms.

Layered metal dichalcogenides MX_2 (X = S, Se or Te) contain the three-atom $(X-M-X)_\infty$ layers. These 'molecular monolayers' were wrapped to construct[377–382] models of MX_2 NT consisting of three coaxial cylinders. The outer and inner cylinders are formed by chalcogen atoms and the central cylinder consists of the metal atoms. Theoretical electron diffraction patterns calculated from these structural models[377] agree well with the experimental patterns. Recently, models for more complex nanotubes of layered metal halide nitrides β-MNX (M = Zr or Hf; X = Cl or Br) have been proposed.[113] These hypothetical nanostructures (for examples, based on β-ZrNCl, in which the [Cl–{ZrN}–{ZrN}–Cl] 'molecular layers' include six atomic networks) consist of six concentric atomic cylinders (Cl–Zr–N–Zr–N–Cl, Fig. 17).

Models of single-layer nanotubes as ideal infinite cylinders, which are wrapped up from mono- or polyatomic basis molecular layers, are widely used to describe their electronic properties in terms of the band theory.[6, 28, 31, 33–38]

It is known that the ends of nanotubes can be open or closed. Various terminal structures can have hemispherical, conical or more complex structures. Multilayer nanotubes can consist of a set (up to several tens) of concentric cylinders or exhibit a roll-like, papier-mache or more complex (combined) morphology.[2–38] Nanotubes can be prepared in the isolated form or give various aggregates (bundles, intergrowths, *etc.*). Unique symbiosis nano-

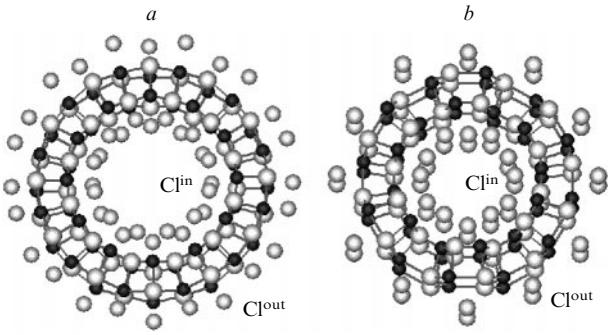


Figure 17. Structures of zigzag (12,0) (*a*) and armchair (12,12) (*b*) ZrNCl nanotubes.[113]
The positions of the chlorine atoms in the inner and outer cylinders are labelled by Cl^{in} and Cl^{out}, respectively.

structures, *viz*., regular chains of fullerenes (including endohedral fullerenes) encapsulated into nanotubes, have been synthesised and extensively studied.[383–401] These nanostructures are called peapods.

Nowadays, studies on modelling of multilayer tubes and caps of closed NT are extended to nanotubular structures of boron nitride and d-metal disulfides.[33–38, 377–382] Attempts were made[402, 403] to design atomic models of more complex systems, *viz*., nanotube composites. The structural model of composite silicon oxide nanotubes prepared with the use of a C-NT template is shown in Fig. 18.[402]

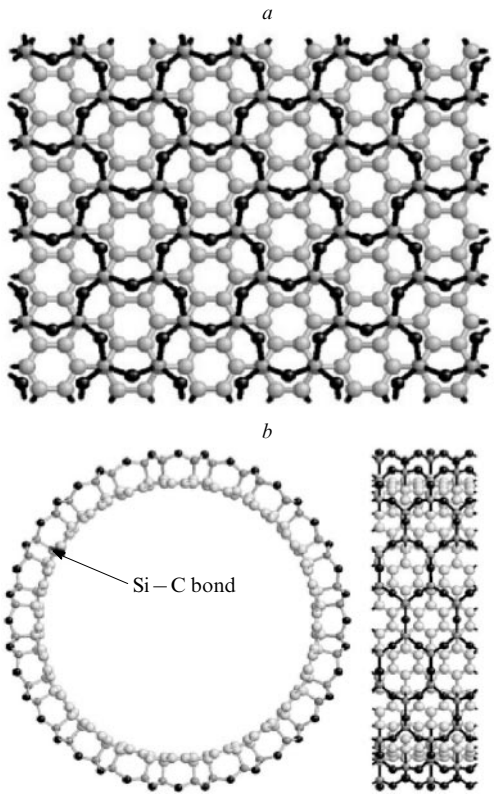


Figure 18. Model of the composite C/SiO_x layer (*a*) and a nanotube constructed from this layer (*b*).[403]

2. Structural models and electronic structures of titanium, vanadium and molybdenum oxide nanotubes

Let us consider atomic models of Ti, V and M oxide nanotubes constructed by the above-described method and the results of theoretical studies of their electronic structures.

a. Titanium oxide

Structural models of titanium dioxide nanotubes were constructed, their electronic structures and chemical bond parameters were studied, and these materials were compared with hypothetical VO_2 tubes.[404, 405] Models of TiO_2 NT were constructed using the anatase (101) layers, which, like graphene sheets, were wrapped into cylinders to form three-layer (O–Ti–O) tubes of armchair (*n*,*n*) and zigzag (*n*,0) types (Fig. 19). Models of tubes based on rutile-type VO_2 (space group $P4_2/mnm$, $a = b = 0.4555$, $c = 0.2851$ nm) were constructed analogously.[406] The electron bands were calculated by the strong-bond method[405] for (*n*,0)- and (*n*,*n*)-like TiO_2 NT and for VO_2 in the (8,0)–(15,0) and (4,4)–(15,15) series, which corresponds to the ~0.6–2.3 nm range of the nanotube diameters.

The densities of states (DOS) of (*n*,*n*)- and (*n*,0)-like TiO_2 NT are similar for all nanotubes and show a general resemblance to DOS of crystalline titanium dioxide (anatase).[407] The valence band is formed by the Ti3d and O2p states, and the lower conduction band edge is formed predominantly by the Ti3d states. The forbidden band gap ΔE depends most substantially on the type of the atomic configuration and the tube diameter. For nanotubes with the largest diameters, ΔE are ~3.34 and ~3.01 eV for armchair (15,15)- and zigzag (15,0)-NT, respectively, which is comparable with the theoretical (~2.0 eV)[407] and experimental (~3.4 eV)[408] forbidden band gap for anatase. The

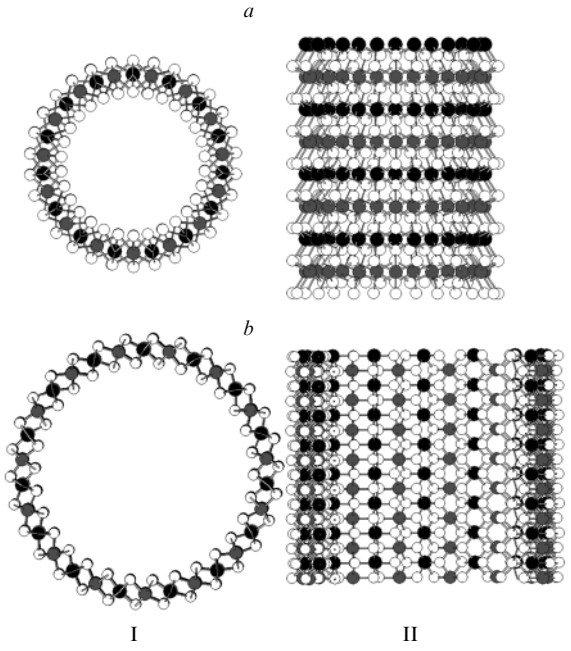


Figure 19. Structural models of zigzag (15,0) (*a*) and armchair (15,15) (*b*) titanium oxide nanotubes.[410]
Empty and solid circles represent O and Ti atoms, respectively. The model of the regular distribution of substitution elements to form rings of M atoms (model I, see the text) is illustrated by a zigzag (15,0) nanotube; the formation of bands of M atoms (model II) along the perimeter or the axis of the tubes alternating with the rings or bands composed of Ti atoms, respectively, is illustrated by an armchair (15,15) nanotube.

forbidden band gap decreases with decreasing diameters of NT, and ΔE for armchair NT are larger than those for zigzag NT.

The calculated electronic spectra of VO_2 NT also correspond to the band structures of crystalline vanadium dioxides.[409] The V3d – O2p hybrid bands are completely filled, and the Fermi level (E_F) is located in the V3d band. For armchair NT, the density of states near the Fermi level is rather low, whereas E_F for zigzag NT is in the region of a local DOS maximum. It should be noted that the analogous near-Fermi maximum of the density of states is responsible for phase instability of crystalline VO_2.[409]

The dependence of the total electronic energy E_{tot} on the diameters of TiO_2 NT is shown in Fig. 20; $E_{tot} \backsim 1/D^2$, which is indicative of a decrease in stability of nanotubes with decreasing D. Armchair nanotubes are more stable at small diameters ($D < 1$ nm),[404, 405] whereas zigzag tubes are more stable at large D. On the contrary, armchair nanotubes are more stable for all VO_2 NT. Analysis of the parameters of interatomic interactions demonstrated that the Ti – O (V – O) bonds play the major role in the nanotubes under consideration, whereas the Ti – Ti (V – V) bond populations are an order of magnitude smaller, and the O – O bonds are absent. The M = O bonds with the oxygen atoms belonging to the inner (O^{in}) or outer (O^{out}) oxygen cylinders are strongly polarised and differ in population (Table 4).[405]

Chemical modifications by introducing guest atoms or molecules into the inner cavities of NT, between the walls of multilayer NT or into intertubular regions between the adjacent nanotubes in their associates, as well as through adsorption of foreign atoms or molecules on the surface or at the ends of NT or through the replacement of atoms in NT with atoms of other elements (doping of NT), provide efficient ways of controlling the properties of oxide NT. The latter approach was used *in situ* in a number of known procedures for the preparation of NT, in particular, in the template synthesis.

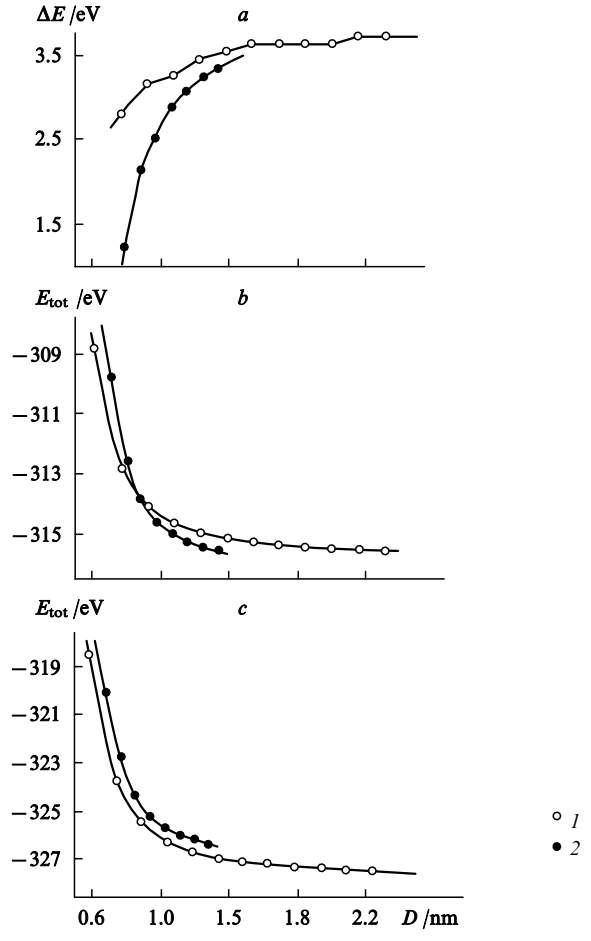


Figure 20. Plots of the forbidden band gap for TiO_2 NT (*a*) and the total band energy per $(Ti,V)O_2$ unit (*b*, *c*) *vs.* the diameters of TiO_2 (*a*, *b*) and VO_2 tubes (*c*).[404]
(*1*) An armchair configuration [(*n*,*n*) NT], (*2*) a zigzag configuration [(*n*,0) NT].

Table 4. Bond populations (e^-) for cylindrical single-layer V_2O_5 nanotubes.

Nanotubes	Bonds			
	V – O $[VO_5]^{in}$	V – O $[VO_5]^{out}$	V – O(1)^{in}	V – O(1)^{out}
(7,0)	1.673	0.856	0.921	0.856
(8,0)	1.630	0.856	0.883	0.856
(9,0)	1.614	0.856	0.867	0.856
(10,0)	1.608	0.855	0.861	0.855
(11,0)	1.602	0.855	0.859	0.855
(12,0)	1.601	0.855	0.858	0.855
(8,8)	1.239	1.035	0.855	0.847
(9,9)	1.239	1.035	0.854	0.846
(10,10)	1.239	1.035	0.854	0.845
(11,11)	1.239	1.035	0.853	0.845
(12,12)	1.239	1.035	0.853	0.845
(13,13)	1.239	1.035	0.852	0.844

Note. The populations of the bond for the V^{in} and V^{out} atoms (in VO_5 pyramids) and the pair bonds between the vanadium atoms and the terminal O(1) atoms of the V = O vanadyl groups, which form the 'outer' and 'inner' oxygen cylinders of the nanotubes, are given.

First results of quantum-chemical modelling of the electronic structures and chemical bond parameters of doped TiO_2 nanotubes were reported.[410] Silicon, germanium, vanadium and chromium were considered as elements replacing titanium, which allowed the authors [410] to discuss the results of both isoelectronic substitution (Ti ⇌ Si, Ge) and electron doping (Ti ⇌ V, Cr) of TiO_2 tubes. The structural models of the armchair (15,15) and zigzag (15,0) TiO_2 nanotubes were used as the starting models.[404, 405]

The electronic properties of (15,0) and (15,15) tubes with composition $Ti_{0.5}M_{0.5}O_2$ were analysed depending on the mode of distribution of the substitution elements M (Si, Ge, V or Cr) in thee Ti positions, which gives rise to rings (model I) or bands (model II) of M atoms along the perimeter or the axes of the tubes alternating with the rings or bands of Ti atoms, respectively (see Fig. 19). The electronic spectra of analogous TiO_2 and $(Ti_{0.5}M_{0.5})O_2$ NT for both models of ordering of the substitution atoms remain unchanged upon isoelectronic substitution (doped tubes are semiconductors), and ΔE changes by no more than 0.1 eV. The main differences concern the fine features of DOS distributions in the centre and near the lower valence band edge and are associated with the presence of (Si,Ge)p states. The electron doping (Ti ⇌ V, Cr) has a radically different effect: the lower conduction band edge is partially filled and all $(Ti_{0.5}M_{0.5})O_2$ tubes become metal-like.

The total electronic energy E_{tot} depends only slightly on the type of ordering of substitution atoms (models I or II), whereas doped armchair (15,15) $(Ti_{0.5}M_{0.5})O_2$ tubes become more stable [for 'pure' TiO_2 NT, the zigzag (15,0) configuration is energetically more favourable].[404] It was hypothesised [410] that the substitution can provide a way of changing the type of the atomic configuration of dioxide tubes. It was also expected that doping of oxide nanotubes will be accompanied by the appearance of defects, which are responsible for the difference in the morphology of real NT and the ideal model of cylinders wrapped from polyatomic layers.

In addition to tubular nanostructures, cage nanoparticles [fullerene-like molecules (FM)] based on d-metal oxides (TiO_2,

V_2O_5, Co_3O_4, MnO_2, *etc.*) have been synthesised in recent years. In the context of the present review, these nanostructures are of interest as possible prototypes of the caps of the corresponding oxide nanotubes.

The structural models of TiO_2-based FM were proposed [411, 412] and their electronic structures were calculated by quantum-chemical methods. These particles [$(TiO_2)_n$, where n = 12, 16, 36, 48 or 64] were built from fragments of the anatase (101) layer. They can be described as 'three-shell' cage molecules consisting of concentric polyhedral shells, the outer and inner shells being formed by oxygen atoms, whereas the medium shell being formed by titanium atoms (Fig. 21). The titanium and oxygen atoms have predominantly coordination numbers of 6 and 3, respectively. Each FM of stoichiometric composition includes also a group of four Ti and O atoms with coordination numbers of 5 and 2, respectively. The total energy of FM per atom (E_{tot}/N, where N is the number of atoms) decreases with increasing size of FM, *i.e.*, stability of the molecules increases. The energy difference between HOMO and LUMO of the molecules is comparable with the forbidden band gap of the crystalline and tubular forms of TiO_2. The spectrum of TiO_2 FM is characterised by molecular orbitals located between the main groups of occupied and free molecular orbitals.[411] Their appearance is associated with the change in the coordination number of the atoms occupying the vertices of polyhedral particles.

The dependence of the spectrum of $(TiO_2)_n$ FM on the coordination numbers of the atoms was simulated [412] using the $Ti_{64}O_{124}$ [*i.e.*, $(TiO_2)_{64}-4\,O$] and $Ti_{64}O_{130}$ [*i.e.*, $(TiO_2)_{64}+2\,O$] molecules. In these molecules, four oxygen atoms with a coordination number of 2 are removed or two oxygen atoms are added to complete the environment of the Ti atoms with a coordination number of 5 to an octahedron. The forbidden band gap ΔE is most substantially affected by the changes in the coordination number of the atoms (0.03 and 1.39 eV for the $Ti_{64}O_{124}$ and $Ti_{64}O_{130}$ molecules, respectively). Calculations of the orbital overlap populations (OOP) demonstrated that Ti–O interactions are the main covalent bonds in $(TiO_2)_n$ FM. Some (non-equivalent) bonds are comparable in the orbital overlap population. The orbital overlap populations of the $Ti-O^{out}(2)$ bonds increase by more than 25% compared to those of the $Ti-O^{out}(3)$ bonds as the coordination numbers of the atoms decrease. However, the total bond population of the oxygen atoms with a coordination number of 3 [$O^{out}(3)$ type] is higher than that of the atoms with a coordination number of 2 [$O^{out}(2)$] ($\sim$0.399–0.387 and $\sim$0.334 e^-, respectively).

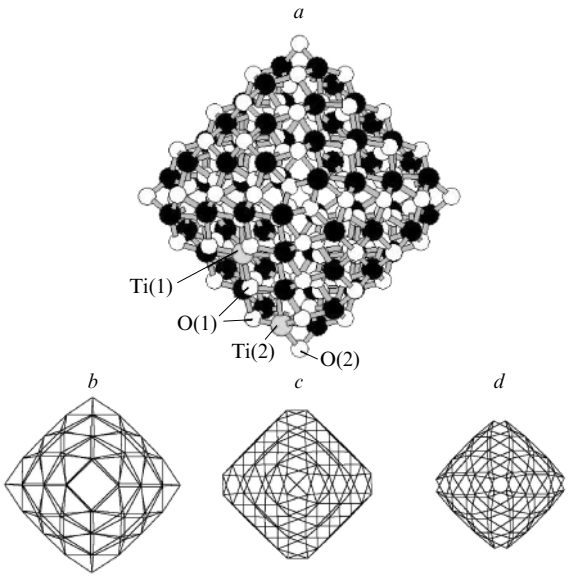


Figure 21. Structure of the fullerene-like $(TiO_2)_{64}$ molecule (*a*); the structures of the outer (*b*), medium (*c*) and inner (*d*) $(TiO_2)_{64}$ shells composed of O, Ti and O atoms, respectively.[412]
Non-equivalent types of the Ti(1), Ti(2), O(1) and O(2) atoms with coordination numbers of 6, 5, 3 and 2, respectively are shown.

b. Vanadium oxides

Compared to classical carbon NT, the tubular structures of vanadium oxides have important distinguishing features. The available VO_x nanotubes are composed of many layers (the walls of the tubes contain from a few to tens of molecular layers) and are open. Ideal concentric cylinders are rare among such tubes. The morphology of these tubes is generally similar to a roll shape, and the constituent molecular layers contain different types of defects. It is also of importance that the elemental composition of VO_x NT is determined by the procedure used for the synthesis and the resulting 'vanadium oxide' tubes should be assigned to nanotube composites, in which the VO_x molecular layers are separated by organic template layers (amines, diamines, *etc.*). These structural and compositional features of vanadium oxide tubes make it difficult to construct their atomic models and study their electronic properties.

Simplified models of vanadium oxide tubes, *viz.*, families of cylindrical structures, constructed by wrapping the V_2O_5 (010) monolayer, were proposed.[413] Orthorhombic crystals of V_2O_5 contain quasi-two-dimensional (010) layers formed by distorted VO_5 pyramids. The V_2O_5 units contain three structurally non-equivalent oxygen atoms: the terminal O(1) atoms of the vanadyl ions and the μ_2-O(2) and μ_3-O(3) atoms (Fig. 22). Wrapping of the (010) layer gives rise to tubes consisting of five coaxial cylinders ($O^{in}-V^{in}-O^{c}-V^{out}-O^{out}$). In these tubes, the outer and inner cylinders (O^{out} and O^{in}, respectively) are formed by the O(1) atoms of the vanadyl groups, and the central cylinder (O^{c}) is formed by the O(2) and O(3) atoms. These cylinders are separated by the outer and inner (with respect to O^{c}, respectively) cylinders consisting of vanadium atoms (V^{in} and V^{out}, respectively). By analogy with carbon NT, it is possible to construct three groups of quasi-one-dimensional V_2O_5 structures: achiral armchair (*n*,*n*), zigzag (*n*,0) and chiral (*n*,*m*) nanotubes.

The electronic structures of a series of (*n*,0)- and (*n*,*n*)-like V_2O_5 nanotubes with indices in the ranges from (6,0) to (12,0) and from (2,2) to (13,13) (which correspond to the ranges of the outer diameters of the tubes (D^{out}), 1.17–1.78 and 1.01–4.75 nm, respectively) were studied.[413] The valence band of the V_2O_5 (010) molecular layer, like that in the V_2O_5 crystal,[414–424] belongs to the hybrid V3d–O2p type and is completely occupied. The forbidden band gap of the V_2O_5 (010) monolayer is $\sim$ 2.5 eV. The V–O covalent bonds are the strongest bonds in this layer, the V–V bonds are an order of magnitude weaker, and interactions

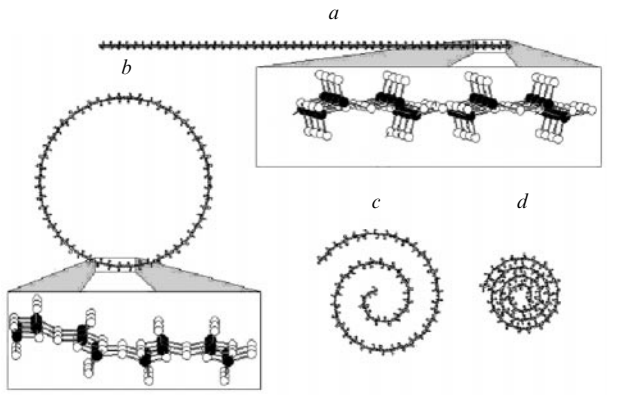


Figure 22. Atomic models of quasi-one-dimensional nanostructures of vanadium pentaoxide (cross-sections).[425]
(*a*) A monolayer, (*b*) cylindrical (26,26) NT, (*c*, *d*) roll-like NT with distances between the adjacent walls of 1.5 and 0.45 nm, respectively.

between the oxygen atoms are antibonding. There is anisotropy in the V—O bond populations: the V—O(3) and V—O(1) bonds are the strongest and weakest bonds, respectively.

The dependence of E_{tot} on the diameters of V_2O_5 NT takes the form $E_{tot} \backsim 1/D^2$ typical of nanotubular structures,[2–7] which is indicative of destabilisation of V_2O_5 tubes as their diameter decreases. For vanadium oxide tubes with $D > 1$ nm, the armchair-type atomic configurations are more stable. All cylindrical V_2O_5 NT are semiconductors. For example, ΔE for the tubes with the largest diameters (minimum wall curvature) considered in the study[411] are $\sim$2.67 and $\sim$ 2.95 eV for armchair (13,13) NT and zigzag (12,0) NT, respectively, which is comparable with ΔE ($\sim$2.5 eV) of the V_2O_5 (010) monolayer. The forbidden band gap decreases with decreasing tube diameter. It should be noted that this dependence of ΔE on the diameter is also typical of semiconducting nanotubes of layered metal dichalcogenides.[377–382] The populations of the V—O bonds depend on their orientation relative to the tube axis and the coordination mode of the atoms belonging to the outer or inner atomic cylinders (see Table 4). The populations of the $V—O^{in}$ bonds are higher than those of the $V—O^{out}$ bonds. This is indicative of high reactivity of the outer oxygen atoms of the vanadyl groups and the probable distortion of the ideal structure of the outer oxygen shell due to relaxation processes and the formation of O atom vacancies.

The experimentally observed roll morphology is reflected in particular atomic models of VO_x NT.[425] To construct these models, the ideal cylindrical zigzag (26,0) and armchair (26,26) V_2O_5 nanotubes with inner diameters of 2.958 and 8.712 nm, respectively, were cut along the axis and rolled up into helical forms shown in Fig. 22. The electronic structures of such tubes reflect the total densities of states presented in Fig. 23. It can be seen that the spectra of vanadium oxide nanorolls contain additional states near E_F, some of which, depending on the atomic configuration of the roll, can be filled. The latter fact should affect substantially, in particular, the electrophysical properties of nanostructures. This modification of the spectrum of rolls (compared to cylindrical tubes) is associated with the presence of broken bonds in their inner and outer cross-sections, the differences in the curvature radius of individual layers of the V_2O_5 molecular ribbons, which form the roll, and the interactions between the adjacent layers in the roll.

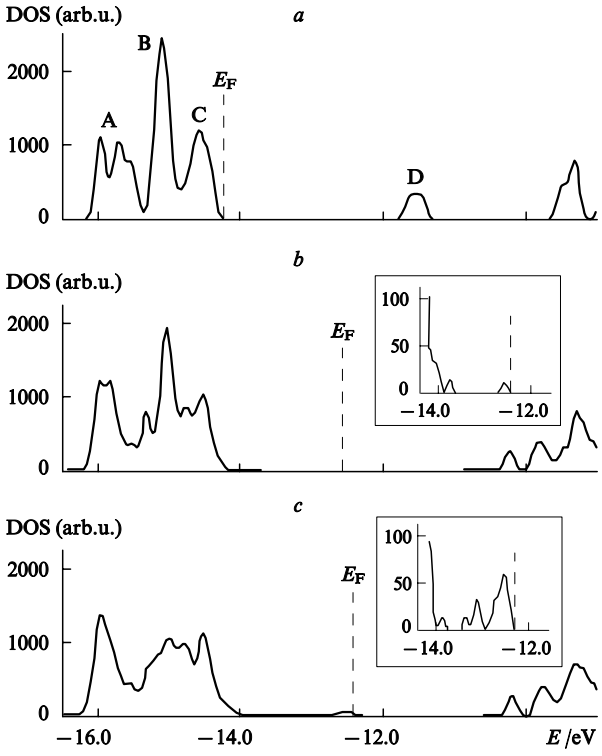


Figure 23. Total densities of states in V_2O_5 NT;[425]
(*a*) cylindrical (26,26) NT, (*b* and *c*) roll-like tubes with distances between the adjacent walls of 1.5 and 0.45 nm, respectively. The densities of states near E_F are shown in the insets.

c. Molybdenum oxides

Models of achiral NT were constructed[426] on the basis of the crystal structure of orthorhombic molybdenum trioxide (space group *Pbnm*, unit cell parameters $a = 3.92$, $b = 13.94$, $c = 3.66$ Å), which is composed of layers of edge-sharing MoO_6 octahedra. This monolayer was used to construct possible types of MoO_3 tubes from coaxial $(O—Mo—O)_\infty$ atomic cylinders with different types of helicoid ordering of the chains of MoO_6 octahedra (Fig. 24). Unlike the above-considered NT, MoO_3 tubes are perforated. Their walls contain pores inside the rings formed by the $[MoO_6]$ polyhedra, which provides an interesting possibility for intercalation with various atoms.

Calculations[426] of the electronic structures of (*n*,0)- and (*n*,*n*)-like MoO_3 nanotubes ($3 < n < 24$) showed that the forbidden band gap ($\sim$3–4 eV) depends most substantially on the atomic configuration and the tube diameter and increases with increasing diameter. The dependence of E_{tot} on D is nearly linear, *i.e.*, it

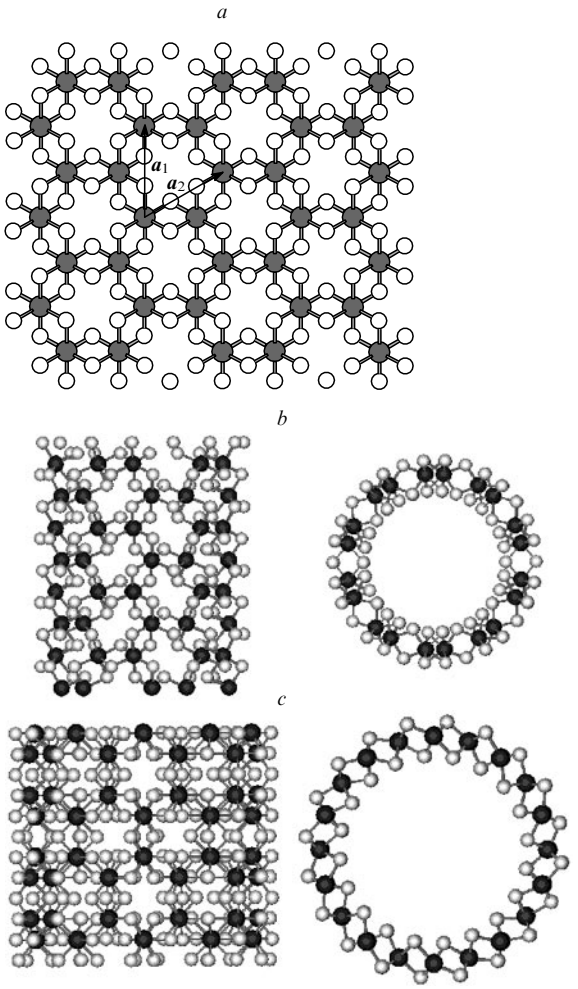


Figure 24. Structure of the molecular monolayer of molybdenum trioxide;[426]
a_1 and a_2 are the basis vectors of the network of Mo atoms (*a*). The atomic models of armchair (5,5) (*b*) and zigzag (10,0) (*c*) MoO_3 nanotubes viewed from the side and the top.

differs sharply from the analogous dependences ($\sim 1/D^2$) known for carbon and non-carbon NT of other layered compounds (BN, MoS_2, *etc.*). Evidently, this is associated mainly with the characteristic features of chemical bonding in MoO_3, primarily, with the fact that there is no pronounced anisotropy in intra- and interlayer interactions. That is why MoO_3 were prepared experimentally [358] using MoO_3/carbon NT nanotube composites as templates. Apparently, this characteristic feature is responsible for the observed [358, 359] polyhedral morphology of the $Mo-O_3$ tubes. In all MoO_3 NT, $Mo-O$ interactions play the major role,[426] whereas $Mo-Mo$ and $O-O$ covalent bonds are virtually absent.

IV. Conclusion

Nowadays, studies of transition metal oxide nanostructures of transition metal oxides are aimed primarily at developing procedures for their synthesis and investigating the morphology of the products. Titanium, vanadium and zinc oxides have been studied most extensively. Titanium-dioxide-based nanostructures have promise as photocatalysts and materials for photoelements. The tubular forms of vanadium oxides allow enhancement of the activity of catalysts and an increase in the cathode capacity of chemical current sources. Zinc oxide nanostructures, which are used in electronics, optics, photocatalysis, solar batteries and sensors, have attracted considerable attention.

A great deal of experimental and theoretical data on metal oxide nanotubes and related nanostructures have been accumulated within a short period after the synthesis of the first materials of this class. Methods for the synthesis of these materials were developed, their morphology and properties were studied, the atomic models were constructed and characteristic features of the electronic structures and chemical bonding in oxide nanotubes were revealed. Various oxide nanostructures and nanocomposites as tubes, ribbons, rods and more complex geometric forms were synthesised, and ways of modifying these properties were proposed.

The results of investigations are of importance for the development of chemistry of metal oxides at nanoscale and for an understanding of the specific properties of nanotubular oxides compared to their crystalline forms and offer considerable possibilities for the technological use of such materials.

As opposed to classical carbon nanotubes and nanotubular structures of layered inorganic compounds, the most efficient procedures for the synthesis of metal oxide nanotubes are the template and chemical methods. In modern studies, considerable attention is being given to the template method, which allows the preparation of oxides and nanocomposites of a desired geometric shape. However, the structures of the tubes thus prepared are far from the ideal cylindrical shape, and they generally include template substances. Chemical methods for the synthesis of nanotubes are also being successfully developed. Intercalation compounds as sols or gels serve as main precursors.[203] The chemical methods allow one to perform syntheses in a wide temperature range and in various solvents and to use and remove templates. The drawback of the chemical hydrothermal method is that nanostructures contain components of the reaction medium. Nowadays, it is difficult to give preference to a particular method of synthesis, because materials science and technological studies of oxide nanotubes lag behind.

In the chemistry of nanotube forms of metal oxides, the immediate aims are to devise procedures for the synthesis of nanostructures with a desired morphology, including more complex geometric forms and their associates. Hence, new methods of synthesis, which will enable one to change the size and form of nanostructures as desired, are of great importance for studies in this field. Systematic investigations of the properties of oxide nanostructures and their dependence on the size and morphology are of equal importance.

The presence of non-compensated bonds of the surface atoms of oxide nanostructures open possibilities for preparing new substances possessing unusual adsorption and chemical activity. The synthesis of complex oxide nanotubes would be expected [427] to provide new ingenious solutions of problems associated with the design of such materials.

A further development of structural and electronic models of oxide NT taking into consideration the specific features of their real morphology and composition is of great importance. This problem is directly related to elucidation of microscopic mechanisms of formation and growth of oxide NT and the processes of their association giving rise to compact materials (bundles, films or crystals).

This review has been written with the financial support of the Russian Foundation for Basic Research (Project Nos 03-03-32104 and 04-03-32111), the Joint Grant from the Russian Foundation for Basic Research and the National Natural Science Foundation of China (Grant No. 03-03-39009) and the Federal Program for the Support of Leading Scientific Schools of the Russian Federation (Grants NSh 829.2003.3 and NSh 1046.2003.3).

References

1. S Iijima *Nature (London)* **354** 56 (1991)
2. M S Dresselhaus, G Dresselhaus, P Eklund *Science of Fullerenes and Carbon Nanotube* (San-Diego: Academic Press, 1996)
3. T W Ebbesen *Carbon Nanotubes, Preparation and Properties* (New York: CRC Press, 1996)
4. R Saito, G Dresselhaus, M S Dresselhaus *Physical Properties of Carbon Nanotubes* (London: Imperial College Press, 1998)
5. K Tanaka, T Yamabe, K Fuku *The Science and Technology of Carbon Nanotubes* (Oxford: Elsevier, 1999)
6. A L Ivanovskii *Kvantovaya Khimiya v Materialovedenii. Nanotubulyarnye Formy Veshchestva* (Quantum Chemistry for Materials Science. Nanotube Forms of Substance) (Ekaterinburg: Urals Branch of Russian Academy of Sciences, 1999)
7. P J F Harris *Carbon Nanotubes and Related Structures: New Materials for the Twenty-first Century* (Cambridge: Cambridge University Press, 1999)
8. T W Ebbesen *Annu. Rev. Mater. Sci.* **24** 235 (1994)
9. R Tenne *Adv. Mater.* **7** 965 (1995)
10. T W Ebbesen *Phys. Today* **49** 26 (1996)
11. A Zettl *Adv. Mater.* **8** 443 (1996)
12. P M Ajayan *Prog. Cryst. Growth Charact. Mater.* **34** 37 (1997)
13. P M Ajayan, T W Ebbesen *Rep. Prog. Phys.* **60** 1025 (1997)
14. A V Eletskii *Usp. Fiz. Nauk* **167** 945 (1997) [*Physics-Uspekhi* **40** 899 (1997)]
15. Yu E Lozovik, A M Popov *Usp. Fiz. Nauk* **167** 751 (1997) [*Physics-Uspekhi* **40** 717 (1997)]
16. A Nikolic, V Radmilovic, M Simicic, D Koruga *Mater. Sci. Forum* **282** 83 (1998)
17. S Subramoney *Adv. Mater.* **10** 1157 (1998)
18. A L Ivanovskii *Usp. Khim.* **68** 119 (1999) [*Russ. Chem. Rev.* **68** 103 (1999)]
19. M Terrones, W K Hsu, H W Kroto, D R M Walton *Top. Curr. Chem.* **199** 189 (1999)
20. T Braun, A P Schubert, R N Kostoff *Chem. Rev.* **100** 23 (2000)
21. E G Rakov *Usp. Khim.* **69** 41 (2000) [*Russ. Chem. Rev.* **69** 35 (2000)]
22. E G Rakov *Usp. Khim.* **70** 934 (2001) [*Russ. Chem. Rev.* **70** 827 (2001)]
23. P N D'yachkov *Zh. Neorg. Khim.* **46** 93 (2001) [a]
24. M Baxendale *J. Mater. Sci.* **14** 657 (2003)
25. A V Eletskii *Usp. Fiz. Nauk* **172** 401 (2002) [*Physics-Uspekhi* **45** 369 (1997)]
26. S Iijima *Physica B* **323** 1 (2002)
27. A L Buchachenko *Usp. Khim.* **72** 419 (2003) [*Russ. Chem. Rev.* **72** 375 (2003)]
28. M Terrones, H Terrones *Philos. Trans. R. Soc. London, Ser. A* **361** 2789 (2003)
29. S B Sinnott, R Andrews *Crit. Rev. Solid State Mater. Sci.* **26** 145 (2001)

30. C N R Rao, B C Satishkumar, A Govindaraj, M Nath *Chem. Phys. Phys. Chem.* **2** 78 (2001)
31. X Blase *Comput. Mater. Sci.* **17** 107 (2000)
32. A Loiseau *Vide: Sci., Tech. Appl.* **56** 209 (2001)
33. R Tenne *Prog. Inorg. Chem.* **50** 269 (2001)
34. R Tenne, C N R Rao *Philos. Trans. R. Soc. London, Ser. A* **362** 2099 (2004)
35. E T Thostenson, Z F Ren, T W Chou *Compos. Sci. Technol.* **61** 1899 (2001)
36. V V Pokropivnyi *Porosh. Metall.* (11/12) 51 (2001)
37. V V Pokropivnyi *Porosh. Metall.* (3/4) 13 (2002)
38. A L Ivanovskii *Usp. Khim.* **71** 203 (2002) [*Russ. Chem. Rev.* **71** 175 (2002)]
39. G S Zakharova, A N Enyashin, V V Ivanovskaya, V L Volkov, A L Ivanovskii *Inzh. Fiz.* **5** 47 (2003)
40. R Tenne, L Margulis, M Genut, G Hodes *Nature (London)* **360** 444 (1992)
41. L Margulis, G Salitra, R Tenne, M Talianker *Nature (London)* **365** 113 (1993)
42. Y Feldman, E Wasserman, D J Srolovitz, R Tenne *Science* **267** 222 (1995)
43. Y Feldman, G L Frey, M Homyonfer, V Lyakhovitskaya, L Margulis, H Cohen, G Hodes, J L Hutchison, R Tenne *J. Am. Chem. Soc.* **118** 5362 (1996)
44. M Remskar, Z Skraba, F Cleton, R Sanjines, F Levy *Appl. Phys. Lett.* **69** 351 (1996)
45. M Remskar, Z Skraba, F Cleton, R Sanjines, F Levy *Surf. Rev. Lett.* **5** 423 (1998)
46. D H Galvan, R Rangel, G Alonso *Fullerene Sci. Technol.* **6** 1025 (1998)
47. D H Galvan, R Rangel, E Adem *Fullerene Sci. Technol.* **7** 421 (1999)
48. E B Mackie, D H Galvan, E Adem, S Talapatra, G Yang, A D Migone *Adv. Mater.* **12** 495 (2000)
49. L Rapoport, Y Bilik, Y Feldman, M Homyonfer, S R Cohen, R Tenne *Nature (London)* **387** 791 (1997)
50. R Sen, A Govindaraj, K Suenaga, S Suzuki, H Kataura, S Iijima, Y Achiba *Chem. Phys. Lett.* **340** 242 (2001)
51. M Chhowalla, G A J Amaratunga *Nature (London)* **407** 164 (2000)
52. A Rothschild, J Sloan, A P E York, M L H Green, J L Hutchison, R Tenne *Chem. Commun.* 363 (1999)
53. G L Frey, S Elani, M Homyonfer, Y Feldman, R Tenne *Phys. Rev. B* **57** 6666 (1998)
54. M Remskar, Z Skraba, M Regula, C Ballif, R Sanjines, F Levy *Adv. Mater.* **10** 246 (1998)
55. A Rothschild, R Popovitz-Biro, O Lourie, R Tenne *J. Phys. Chem. B* **104** 8976 (2000)
56. O Stephan, Y Bando, A Loiseau, F Willaime, N Shramachenko, T Tamiya, T Sato *Appl. Phys. A: Mater. Sci. Process.* **67** 107 (1998)
57. A Loiseau, F Willaime, N Demoncy, N Schramchenko, G Hug, C Colliex, H Pascard *Carbon* **36** 743 (1998)
58. J Cumings, A Zettl *Chem. Phys. Lett.* **316** 211 (2000)
59. Y Shimizu, Y Moriyoshi, S Komatsu, T Ikegami, T Ishigaki, T Sato, Y Bando *Thin Solid Films* **316** 178 (1998)
60. D Golberg, Y Bando, K Kurashima, T Sato *Solid State Commun.* **116** 1 (2000)
61. W Q Han, J Cumings, X S Huang, K Bradley, A Zettl *Chem. Phys. Lett.* **346** 368 (2001)
62. D Golberg, Y Bando, K Kurashima, T Sato *Scr. Mater.* **44** 1561 (2001)
63. D Golberg, Y Bando, L Bourgeois, K Kurashima, T Sato *Appl. Phys. Lett.* **77** 1979 (2000)
64. J A Hollingsworth, D M Poojary, A Clearfield, W E Buhro *J. Am. Chem. Soc.* **122** 3562 (2000)
65. X D Wang, P X Gao, J Li, C J Summers, Z L Zang *Adv. Mater.* **14** 1732 (2002)
66. C Ye, G Meng, Z Jiang, Y Wang, G Wang, L Zhang *J. Am. Chem. Soc.* **124** 15 180 (2002)
67. M Brorson, T W Hansen, C J H Jacobsen *J. Am. Chem. Soc.* **124** 11 582 (2002)
68. W K Hsu, Y Q Zhu, C B Boothroyd, I Kinloch, S Trasobares, H Terrones, N Grobert, M Terrones, R Escudero, G Z Chen, C Colliex, A H Windle, D J Fray, H W Kroto, D R M Walton *Chem. Mater.* **12** 3541 (2000)
69. M Nath, C N R Rao *Pure Appl. Chem.* **74** 1545 (2002)
70. M Nath, C N R Rao *Angew. Chem., Int. Ed.* **41** 3451 (2002)
71. D H Galvan, J H Kim, M B Maple, E Adem *Fullerene Sci. Technol.* **9** 225 (2001)
72. M Nath, S Kar, A K Raychaudhuri, C N R Rao *Chem. Phys. Lett.* **368** 690 (2003)
73. T Tsuneta, T Toshima, K Inagaki, T Shibayama, S Tanda, S Uji, M Ahlskog, P Hakonen, M Paalanen *Curr. Appl. Phys.* **3** 473 (2003)
74. J Chen, S-L Li, Z-L Tao, F Gao *Chem. Commun.* **8** 980 (2003)
75. J Chen, Z-L Tao, S-L Li *Angew. Chem., Int. Ed.* **42** 2147 (2003)
76. J Chen, S-L Li, Z-L Tao,Y T Shen, C X Cui *J. Am. Chem. Soc.* **125** 5284 (2003)
77. E Flores, A Tlahuice, E Adem, D H Galvan *Fullerene Sci. Technol.* **9** 9 (2001)
78. D H Galvan, R Rangel, E Adem *Fullerene Sci. Technol.* **8** 9 (2000)
79. M Remskar, A Mrzel, Z Skraba, A Jesih, M Ceh, J Demsar, P Stadelmann, F Levy, D Mihailovic *Science* **292** 479 (2001)
80. Y J Xiong, Y Xie, J Yang, R Zhang, C Z Wu, G A Du *J. Mater. Chem.* **12** 3712 (2002)
81. C N R Rao, A Govindaraj, F L Deepak, N A Gunari, M Nath, *Appl. Phys. Lett.* **78** 1853 (2001)
82. Z Y Jiang, Z X Xie, X H Zhang, R B Huang, L S Zheng *Chem. Phys. Lett.* **378** 313 (2003)
83. R Dominko, M Gaberscek, D Arcon, A Mrzel, M Remskar, D Mihailovic, S Pejovnik, J Jamnik *Electrochim. Acta* **48** 3079 (2003)
84. Y R Hacohen, E Grunbaum, R Tenne, J Sloan, J L Hutchison *Nature (London)* **395** 336 (1998)
85. Y R Hacohen, R Popovitz-Biro, E Grunbaum, Y Prior, R Tenne *Adv. Mater.* **14** 1075 (2002)
86. V V Ivanovskaya, A N Enyashin, N I Medvedeva, A L Ivanovskii http://xxx.lanl.gov/PS_cache/cond-mat/pdf/0304/0304230.pdf
87. O G Schmidt, K Eberl *Nature (London)* **410** 168 (2001)
88. V Y Prinz, A V Chekhovskiy, V V Preobrazhenskii, B R Semyagin, A K Gutakovsky *Nanotechnology* **13** 231 (2002)
89. C Deneke, C Muller, N Y Jin-Phillipp, O G Schmidt *Semicond. Sci. Technol.* **17** 1278 (2002)
90. H C Bao, Z Xu, H M Hong, X Ma, Z H Lu *Scr. Mater.* **50** 19 (2004)
91. D Wang, D Yu, Y Peng, Z Meng, S Zhang, Y Qian *Nanotechnology* **14** 748 (2003)
92. M S Mo, J H Zeng, X M Liu, W C Yu, S Y Zhang, Y T Qian *Adv. Mater.* **14** 1658 (2002)
93. Z P Liu, S Li, Y Yang, Z K Hu, S Peng, J B Liang, Y T Qian *New J. Chem.* **27** 1748 (2003)
94. G Wei, Y Deng, Y-H Lin, C-W Nan *Chem. Phys. Lett.* **372** 590 (2003)
95. X Y Liu, J H Zeng, S Y Zhang, R B Zheng, X M Liu, Y T Qian *Chem. Phys. Lett.* **374** 348 (2003)
96. C R Su, J M Li *Chin. Phys. Lett.* **19** 1785 (2002)
97. B J Yang, C Li, H M Hu, X G Yang, Q W Li, Y T Qian *Eur. J. Inorg. Chem.* **20** 3699 (2003)
98. O Opitz, P Zhan, I Mertig *Phys. Rev. B* **66** 245417 (2002)
99. J Bao, K Wang, Z Xu, H Zhang, Z Lu *Chem. Commun.* **2** 208 (2003)
100. M D Lay, J L Stickney *J. Am. Chem. Soc.* **125** 1352 (2003)
101. J R Ahn, Y J Kim, H S Lee, C C Hwang, B S Kim, H W Yeom *Phys. Rev. B* **66** 153403 (2002)
102. Y Li, J Wang, Z Deng, Y Wu, X Sun, D Yu, P Yang *J. Am. Chem. Soc.* **123** 9904 (2001)
103. S Su, H Liu, J M Li *Nanotechnology* **13** 746 (2002)
104. I Boustani, A Quandt, E Hernandez, A Rubio *J. Chem. Phys.* **110** 3176 (1999)
105. R Q Zhang, S T Lee, C K Law, W K Li, B K Teo *Chem. Phys. Lett.* **367** 509 (2003)
106. L A Chernozatonskii *Pis'ma Zh. Eksp. Teor. Fiz.* **74** 467 (2001) [b]
107. V G Bamburov, V V Ivanovskaya, A N Enyashin, I R Shein, N I Medvedeva, Yu N Makurin, A L Ivanovskii *Dokl. Akad. Nauk* **388** 624 (2003) [c]
108. A Quandt, A Y Liu, I Boustani *Phys. Rev. B* **64** 125 422 (2001)
109. V V Ivanovskaya, A N Enyashin, A A Sofronov, Y N Makurin, N I Medvedeva, A L Ivanovskii *J. Mol. Struct. (THEOCHEM)* **625** 9 (2003)

110. V V Ivanovskaya, A N Enyashin, A A Sofronov, Yu N Makurin, N I Medvedeva, A L Ivanovskii *Teor. Eksp. Khim.* **39** 1 (2003) [d]
111. S Gemming, G Seifert *Phys. Rev. B* **68** 075416 (2003)
112. I R Shein, V V Ivanovskaya, N I Medvedeva, A L Ivanovskii *Pis'ma Zh. Eksp. Teor. Fiz.* **76** 223 (2002) [b]
113. A N Enyashin, Yu N Makurin, A L Ivanovskii *Chem. Phys. Lett.* **387** 85 (2004)
114. V V Pokropivny *Physica C* **351** 71 (2001)
115. J Sha, J J Niu, X Y Ma, J Xu, X B Zhang, Q Yang, D Yang *Adv. Mater.* **14** 1219 (2002)
116. G D Zhan, J D Kuntz, J L Wan, A K Mukherjee *Nat. Mater.* **2** 38 (2003)
117. D B Kuang, Y P Fang, H Q Liu, C Frommen, D Fenske *J. Mater. Chem.* **13** 660 (2003)
118. J S Lee, B Min, K Cho, S Kim, J Park, Y T Lee, N S Kim, M S Lee, S O Park, J T Moon *J. Cryst. Growth* **254** 443 (2003)
119. M Hernadi, E Couteau, J W Seo, L Forro *Langmuir* **19** 7026 (2003)
120. G Gundiah, F L Deepak, A Govindaraj, C N R Rao *Top. Catal.* **24** 137 (2003)
121. G Gundiah, S Mukhopadhyay, U G Tumkurkar, A Govindaraj, U Maitra, C N R Rao *J. Mater. Chem.* **13** 2118 (2003)
122. J Zygmunt, F Krumeich, R Nesper *Adv. Mater.* **15** 1538 (2003)
123. J K Guo, J W Ning, Y B Pan *Key Eng. Mater.* **249** 1 (2003)
124. Y B Li, Y Bando, D Golberg, Y Uemura *Appl. Phys. Lett.* **83** 3999 (2003)
125. B Cheng, E T Samulski *J. Mater. Chem.* **11** 2901 (2001)
126. Q Tang, J M Shen, W J Zhou, W Zhang, W C Yu, Y T Qian *J. Mater. Chem.* **13** 3103 (2003)
127. A-W Xu, Y-P Fang, L-P You, H-Q Liu *J. Am. Chem. Soc.* **125** 1494 (2003)
128. H Du, Q Chen, R C Che, Z Y Yuan, L M Peng *Appl. Phys. Lett.* **79** 3702 (2001)
129. Q Chen, G H Du, S Zhang, L M Peng *Acta Crystallogr., Sect. B* **58** 587 (2002)
130. Q H Zhang L Gao, S Zheng J Sun *Acta Chim. Sini.* **60** 1439 (2002)
131. S Uchida, R Chiba, M Tomiha, N Masaki, M Shirai *Electrochemistry* **70** 418 (2002)
132. C Y Lin, S H Chien, J H Chao, C Y Sheu, Y C Cheng, Y J Huang, C H Tsai *Catal. Lett.* **80** 153 (2002)
133. Q H Zhang, L A Gao, J Sun, S Zheng *Chem. Lett.* **2** 226 (2002)
134. B D Yao, Y F Chan, X Y Zhang, W F Zhang, Z Y Yang, N Wang *Appl. Phys. Lett.* **82** 281 (2003)
135. S Zhang, J Zhou, Z Zhang, Z Du, A V Vorontsov, Z Jin *Chin. Sci. Bull.* **45** 1533 (2000)
136. Z R Tian, J A Voigt, J Liu, B Mckenzie, H Xu *J. Am. Chem. Soc.* **125** 12384 (2003)
137. J W Zhang, X Y Guo, Z S Jin, S L Zhang, J F Zhou, Z J Zhang *Chin. Chem. Lett.* **14** 419 (2003)
138. X M Sun, Y D Li *Chem.-Eur. J.* **9** 2229 (2003)
139. B Y Wang, X Y Guo, Z J Zhang, Y B Zhao, Z S Jin *Chem. J. Chin. Univ.* **24** 1838 (2003)
140. Y K Zhou, L Cao, F B Zhang, B L He, H L Li *J. Electrochem. Soc.* **150** A1246 (2003)
141. M Adachi, Y Murata, I Okada, S Yoshikawa *J. Electrochem. Soc.* **150** G488 (2003)
142. Q Huang, L Gao *Chem. Lett.* **32** 638 (2003)
143. S K Pradhan, P J Reucroft, F Yang, A Dozier *J. Cryst. Growth* **256** 83 (2003)
144. C Xu, Y Zhan, K Hong, G Wang *Solid State Commun.* **126** 545 (2003)
145. Z-Y Yuan, W Zhou, B-L Su *Chem. Commun.* 1202 (2002)
146. P Hoyer *Adv. Mater.* **8** 857 (1996)
147. J C Hulteen, C R Martin *J. Mater. Chem.* **7** 1075 (1997)
148. S Kobayashi, K Hanabusa, N Hamasaki, M Kimura, H Shirai, K Hanabusa *Chem. Mater.* **12** 1523 (2000)
149. S Kobayashi, N Hamasaki, M Suzuki, M Kimura, H Shirai, K Hanabusa *J. Am. Chem. Soc.* **124** 6550 (2002)
150. J H Jung, H Kobayashi, K J C van Bommel, S Shinkai, T Shimizu *Chem. Mater.* **14** 1445 (2002)
151. T Y Peng, A Hasegawa, J R Qiu, K Hirao *Chem. Mater.* **15** 2011 (2003)
152. S Fujikawa, T Kunitake *Langmuir* **19** 6545 (2003)
153. H Imai, M Matsuta, K Shimizu, H Hirashima, N Negishi *J. Mater. Chem.* **10** 2005 (2000)
154. H Imai, M Matsuta, K Shimizu, H Hirashima, N Negishi *Solid State Ionics* **151** 183 (2002)
155. R A Caruso, J H Schattka, A Greiner *Adv. Mater.* **13** 1577 (2001)
156. M Niederberger, M H Bartl, G D Stucky *J. Am. Chem. Soc.* **124** 13642 (2002)
157. A Michailowski, D AlMawlawi, G S Cheng, M Moskovits *Chem. Phys. Lett.* **349** 1 (2001)
158. S M Liu, L M Gan, L H Liu, W D Zhang, H C Zeng *Chem. Mater.* **14** 1391 (2002)
159. H Imai, Y Takei, K Shimizu, M Matsuda, H Hirashima *J. Mater. Chem.* **9** 2971 (1999)
160. N R de Tacconi, K Rajeshwar *Electrochim. Acta* **47** 2603 (2002)
161. Y Q Wang, G Q Hu, X F Duan, H L Sun, Q K Xue *Chem. Phys. Lett.* **365** 427 (2002)
162. B B Lakshmi, P K Dorhout, C R Martin *Chem. Mater.* **9** 857 (1997)
163. Y Gao, Y X Ma, H L Li *Chem. J. Chin. Univ.* **24** 1089 (2003)
164. Q Huang, L Gao *J. Mater. Chem.* **13** 1517 (2003)
165. J Sun, L A Gao, Q H Zhang *J. Mater. Sci. Lett.* **22** 339 (2003)
166. J Sun, L Gao *Carbon* **41** 1063 (2003)
167. S-W Lee, W M Sigmund *Chem. Commun.* 780 (2003)
168. M Zhang, Y Bando, K Wada *J. Mater. Res.* **16** 1408 (2001)
169. S Z Chu, K Wada, S Inoue *Adv. Mater.* **14** 1752 (2002)
170. Y Zhang, A Reller *Chem. Commun.* 606 (2002)
171. X C Song, L H Yue, B Liu, G Han, W X Chen, Z D Xu *Chin. J. Inorg. Chem.* **19** 899 (2003)
172. Y G Guo, L J Wan, C L Bai *J. Phys. Chem. B* **107** 5441 (2003)
173. V M Cepak, J C Hulteen, G Che, K B Jirage, B B Lakshmi, E R Fisher, C R Martin, H Yoneyama *Chem. Mater.* **9** 1065 (1997)
174. R V Parthasarathy, C R Martin *Nature (London)* **369** 298 (1994)
175. L Zhang, M Wan *J. Phys. Chem. B* **107** 6748 (2003)
176. D Li, Y N Xia *Nano Lett.* **3** 555 (2003)
177. D H Reneker, I Chun *Nanotechnology* **7** 216 (1996)
178. D Gong, C A Grimes, O K Varghese, W C Hu, R S Singh, Z Chen, E C Dickey *J. Mater. Res.* **16** 3331 (2001)
179. O K Varghese, D Gong, M Paulose, K G Ong, C A Grimes *Sens. Actuators, B* **93** 338 (2003)
180. O K Varghese, C A Grimes *J. Nanosci. Nanotechnol.* **3** 277 (2003)
181. O K Varghese, D W Gong, M Paulose, K G Ong, E C Dickey, C A Grimes *Adv. Mater.* **15** 624 (2003)
182. P L Chen, C T Kuo, T G Tsai, B W Wu, C C Hsu, F M Pan *Appl. Phys. Lett.* **82** 2796 (2003)
183. J J Schneider, N Czap, J Hagen, J Engstler, J Ensling, P Gutlich, U Reinoehl, H Bertagnolli, F Luis, L J de Jongh, M Wark, G Grubert, G L Honyak, R Zanoni *Chem.-Eur. J.* **6** 4305 (2000)
184. T Kasuga, M Hiramatsu, A Hoson, T Sekino, K Niihara *Langmuir* **14** 3160 (1998)
185. Y Zhu, H Li, Y Koltypin, Y R Hacohen, A Gedanken *Chem. Commun.* 2616 (2001)
186. R Marchand, L Brohan, M Tournoux *Mater. Res. Bull.* **15** 1129 (1980)
187. D S Seo, J K Lee, H Kim *J. Cryst. Growth* **229** 428 (2001)
188. Z Y Yuan, J F Colomer, B L Su *Chem. Phys. Lett.* **363** 362 (2002)
189. Z Miao, D Xu, J Ouyang, G Guo, X Zhao, Y Tang *Nano Lett.* **2** 717 (2002)
190. P Hoyer *Langmuir* **12** 1411 (1996)
191. M Zhang, Y Bando, K Wada *J. Mater. Sci. Lett.* **20** 167 (2001)
192. D K Yi, S J Yoo, D Y Kim *Nano Lett.* **2** 1101 (2002)
193. B Q Chen, W Zhou, G Du, L M Peng *Adv. Mater.* **14** 1208 (2002)
194. J J Yang, Z S Jin, X D Wang, W Li, J W Zhang, S L Zhang, X Y Guo, Z J Zhang *Dalton Trans.* **20** 3898 (2003)
195. X Sun, X Chen, Y Li *Inorg. Chem.* **41** 4996 (2002)
196. Y Mao, S Banerjee, S S Wong *Chem. Commun.* 408 (2003)
197. J J Urban, W S Yun, Q Gu, H Park *J. Am. Chem. Soc.* **124** 1186 (2002)
198. W S Yun, J J Urban, Q Gu, H Park *Nano Lett.* **2** 447 (2002)
199. P M Ajayan, O Stephan, P Redlich, C Colliex *Nature (London)* **375** 564 (1995)

200. M Giorgetti, S Passerini, W H Smyrl *Inorg. Chem.* **39** 1514 (2000)
201. H-J Muhr, F Krumeich, U P Schonholzer, F Bieri, M Niederberger, R Nesper *Adv. Mater.* **12** 231 (2000)
202. D Y Pan, S Y Zhang, Y Q Chen, J G Hou *J. Mater. Res.* **17** 1981 (2002)
203. G S Zakharova, V L Volkov *Usp. Khim.* **72** 346 (2003) [*Russ. Chem. Rev.* **72** 311 (2003)]
204. R Nesper, H-J Muhr *Chimia* **52** 571 (1998)
205. F Krumeich, H-J Muhr, M Niederberger, F Bieri, B Schnyder, R Nesper *J. Am. Chem. Soc.* **121** 8324 (1999)
206. M E Spahr, P Bitterli, R Nesper, M Muller, F Krumeich, H U Nissen *Angew. Chem., Int. Ed.* **37** 1263 (1998)
207. X Chen, X M Sun, Y D Li *Inorg. Chem.* **41** 4524 (2002)
208. R Tenne, A K Zettl *Top. Appl. Phys.* **80** 81 (2001)
209. M Niederberger, H-J Muhr, F Krumeich, F Bieri, D Günther, R Nesper *Chem. Mater.* **12** 1995 (2000)
210. F Krumeich, H-J Muhr, M Niederberger, F Bieri, R Nesper *Z. Anorg. Allg. Chem.* **626** 2208 (2000)
211. F Bieri, F Krumeich, H-J Muhr, R Nesper *Helv. Chim. Acta* **84** 3015 (2001)
212. K S Pillai, F Krumeich, H-J Muhr, M Niederberger, R Nesper *Solid State Ionics* **141 – 142** 185 (2001)
213. G T Chandrappa, N Steunou, S Cassaignon, C Bauvais, J Livage *J. Sol-Gel Sci. Technol.* **26** 593 (2003)
214. G T Chandrappa, N Steunou, S Cassaignon, C Bauvais, J Livage *Catal. Today* **78** 85 (2003)
215. W Chen, L Q Mai, Q Xu, Q Y Zhu, J F Peng *Key Eng. Mater.* **249** 145 (2003)
216. L Mai, W Chen, Q Xu, Q Zhu, C Han, J Peng *Solid State Commun.* **126** 541 (2003)
217. L Q Mai, W Chen, Q Xu, J F Peng, Q Y Zhu *Chem. Phys. Lett.* **382** 307 (2003)
218. A Dobley, K Ngala, S F Yang, P Y Zavalij, M S Whittingham *Chem. Mater.* **13** 4382 (2001)
219. J M Reinoso, H-J Muhr, F Krumeich, F Bieri, R Nesper *Helv. Chim. Acta* **83** 1724 (2000)
220. S Nordlinder, J Lindren, T Gustafsson, K Edström *J. Electrochem. Soc.* **150** E280 (2003)
221. B Azambre, M J Hudson, O Heintz *J. Mater. Chem.* **13** 385 (2003)
222. B Azambre, M J Hudson *Mater. Lett.* **57** 3005 (2003)
223. X Wang, L Liu, R Bontchev, A J Jacobson *Chem. Commun.* 1009 (1998)
224. M Wörle, F Krumeich, F Bier, H-J Muhr, R Nesper *Z. Anorg. Allg. Chem.* **628** 2778 (2002)
225. B C Satishkumar, A Govindaraj, M Nath, C N R Rao *J. Mater. Chem.* **10** 2115 (2000)
226. B C Satishkumar, A Govindaraj, E M Vogl, L Basumallick, C N R Rao *J. Mater. Res.* **12** 604 (1997)
227. N Pinna, M Willinger, K Weiss, J Urban, R Schlögl *Nano Lett.* **3** 1131 (2003)
228. H Y Xu, H Wang, Z Q Song, Y W Wang, Y C Zhang, H Yan *Chem. Lett.* **32** 444 (2003)
229. Z Gui, R Fan, X-H Chen, Y Hu, Y-C Wu *Trans. Nonferrous Met. Soc. China* **11** 324 (2001)
230. P Millet, J Y Henry, F Mila, J Galy *J. Solid State Chem.* **147** 676 (1999)
231. J Choi, J L Musfeldt, Y J Wang, H-J Koo, M-H Whagbo, J Galy, P Millet *Chem. Mater.* **14** 924 (2002)
232. M B Sahana, S A Shivashankar *J. Mater. Chem.* **13** 2254 (2003)
233. F Zhang, P Y Zavalij, M S Whittingham *J. Mater. Chem.* **9** 3137 (1999)
234. J F Xu, J F R Czerw, S Webster, D L Carroll, J Ballato, R Nesper *Appl. Phys. Lett.* **81** 1711 (2002)
235. J S Sakamoto, B Dunn *J. Electrochem. Soc.* **149** A26 (2002)
236. M E Spahr, P Strscjitzki-Bitterli, R Nesper, O Haas, P Novak *J. Electrochem. Soc.* **146** 2780 (1999)
237. S Nordlinder, K Edstrom, T Gustafsson *Electrochem. Solid-State Lett.* **4** A129 (2001)
238. C R Sides, C N Li, C J Patrissi, B Scrosati, C R Martin *MRS Bull.* **27** 604 (2002)
239. G T Kim, J Muster, V Krstic, J G Park, Y W Park, S Roth, M Burghard *Appl. Phys. Lett.* **76** 1875 (2000)
240. S Nordlinder, A Augustsson, T Schmitt, J Guo, L C Duda, J Nordgren, T Gustafsson, K Edstrlm *Chem. Mater.* **15** 3227 (2003)
241. A Augustsson, T Schmitt, L C Duda, J Nordgren, S Nordlinder, K Edström, T Gustafsson, J H Guo *J. Appl. Phys.* **94** 5083 (2003)
242. W Dong, J Sakamoto, B Dunn *J. Sol-Gel Sci. Technol.* **26** 641 (2003)
243. G R Patzke, F Krumeich, R Nesper *Angew. Chem., Int. Ed.* **41** 2446 (2002)
244. S Banerjee, A Dan, D Chakravorty *J. Mater. Sci.* **37** 4261 (2002)
245. C Gomes-Navarro, P J de Pablo, J Colchero, Y Fan, M Burghard, J Gomes-Herrero, A M Baro *Nanotechnology* **14** 134 (2003)
246. J Mittal, M Monthiox, H Allouche, O Stephan *Chem. Phys. Lett.* **339** 311 (2001)
247. J Liu, J Cai, Y-C Son, Q Gao, S L Suib, M Aindow *J. Phys. Chem. B* **106** 9761 (2002)
248. B B Lakshmi, C J Patrissi, C R Martin *Chem. Mater.* **9** 2544 (1997)
249. C Gong, D Chen, X Jiao, Q Wang *J. Mater. Chem.* **12** 1844 (2002)
250. Z J Zhang, B Q Wei, P M Ajayan *Appl. Phys. Lett.* **79** 4207 (2001)
251. M Rajamathi, M Ghosh, R Seshadri *Chem. Commun.* 1152 (2002)
252. K Matsui, T Kyotani, A Tomita *Mol. Cryst. Liq. Cryst.* **387** 225 (2002)
253. C Pham-Huu, N Keller, C Estournzhs, G Ehret, M J Ledoux *Chem. Commun.* 1882 (2002)
254. W Shenton, T Douglas, M Young, G Stubbs, S Mann *Adv. Mater.* **11** 253 (1999)
255. X Y Shi, S B Han, R J Sanedrin, F Zhou, M Selke *Chem. Mater.* **14** 1897 (2002)
256. X Y Shi, S B Han, R J Sanedrin, C Galvez, D G Ho, B Hernandez, F Zhou, M Selke *Nano Lett.* **2** 289 (2002)
257. K Matsui, B K Pradhan, T Kyotani, A Tomita *J. Phys. Chem. B* **105** 5682 (2001)
258. Y K Chen, A Chu, J Cook, M L H Green, P J F Harris, R Heesom, M Humphries, J Sloan, S C Tsang, J F C Turner *J. Mater. Chem.* **7** 545 (1997)
259. B K Pradhan, T Kyotani, A Tomita *Chem. Commun.* 1317 (1999)
260. W Wang, Y Zhan, G Wang *Chem. Commun.* 727 (2001)
261. H Q Wu, X W Wei, M W Shao, J S Gu, M Z Qu *Chem. Phys. Lett.* **364** 152 (2002)
262. C T Hsieh, J M Chen, H H Lin, H C Shih *Appl. Phys. Lett.* **82** 3316 (2003)
263. W Z Wang, Y J Zhan, X S Wang, Y K Liu, C L Zheng, G H Wang *Mater. Res. Bull.* **37** 1093 (2002)
264. G T Wu, C S Wang, X B Zhang, H S Yang, Z F Qi, W Z Li *J. Power Sources* **75** 175 (1998)
265. Z R Dai, Z W Pan, Z L Wang *Adv. Function. Mater.* **13** 9 (2003)
266. J Zhang, L Sun, H Pan, C Liao, C Yan *New J. Chem.* **26** 33 (2002)
267. B Liu, H C Zeng *J. Am. Chem. Soc.* **125** 4430 (2003)
268. X M Sun, X Chen, Z X Deng, Y D Li *Mater. Chem. Phys.* **78** 99 (2003)
269. J M Wang, L Gao *J. Mater. Chem.* **13** 2551 (2003)
270. J Zhang, L Sun, C Liao, C Yan *Chem. Commun.* 262 (2002)
271. J J Wu, S C Liu *J. Phys. Chem. B* **106** 9546 (2002)
272. L Vayssieres *Adv. Mater.* **15** 464 (2003)
273. Z Q Li, Y Xie, Y J Xiong, R Zhang, W He *Chem. Lett.* **32** 760 (2003)
274. C-F Jin, X Yuan, W-W Ge, J-M Hong, X-Q Xin *Nanotechnology* **14** 667 (2003)
275. Y Liu, Z Liu, G Wang *J. Cryst. Growth* **252** 213 (2003)
276. L Guo, Y L Ji, H Xu, P Simon, Z Wu *J. Am. Chem. Soc.* **124** 14864 (2002)
277. J Y Li, X L Chen, H Li, M He, Z Y Qiao *J. Cryst. Growth* **233** 5 (2001)
278. J Y Li, X L Chen, Z F Wei, Z Y Qiao *Chin. Phys. Lett.* **18** 1527 (2001)

279. B Y Geng, T Xie, X S Peng, Y Lin, X Y Yuan, G W Meng, L D Zhang *Appl. Phys. A: Mater. Sci. Process.* **77** 363 (2003)
280. L Dai, X L Chen, W J Wang, T Zhou, B Q Hu *J. Phys.: Condens. Matter.* **15** 2221 (2003)
281. C C Tang, S S Fan, M L de la Chapelle, P Li *Chem. Phys. Lett.* **333** 12 (2001)
282. Y Dai, Y Zhang, Q K Li, C W Nan *Chem. Phys. Lett.* **358** 83 (2002)
283. V A L Roy, A B Djurisic, W K Chan, J Gao, H F Lui, C Surya *Appl. Phys. Lett.* **83** 141 (2003)
284. Y Dai, Y Zhang, Z L Wang *Solid State Commun.* **126** 629 (2003)
285. I S Kim, G H Lee *Solid State Commun.* **123** 191 (2002)
286. C Xu, Z Liu, S Liu, G Wang *Scr. Mater.* **48** 1367 (2003)
287. J Q Hu, Q Li, N B Wong, C S Lee, S T Lee *Chem. Mater.* **14** 1216 (2002)
288. J Q Hu, Y Bando *Appl. Phys. Lett.* **82** 1401 (2003)
289. Z R Tian, J A Voigt, J Liu, B McKenzie, M J McDermott *J. Am. Chem. Soc.* **124** 12954 (2002)
290. X H Zhang, S Y Xie, Z Y Jiang, X Zhang, Z Q Tian, Z X Xie, R B Huang, L S Zheng *J. Phys. Chem. B* **107** 10114 (2003)
291. X H Zhang, S Y Xie, Z Y Jiang, Z X Xie, R B Huang, L S Zheng, J Y Kang, T Sekiguchi *Solid State Chem.* **173** 109 (2003)
292. L Guo, Y Ji, H Xu, Z Wu, P Simon *J. Mater. Chem.* **13** 754 (2003)
293. Y Zhang, N Wang, S Gao, R He, S Miao, J Liu, J Zhu, X Zhang *Chem. Mater.* **14** 3564 (2002)
294. Q Wan, K Yu, T H Wang, C L Lin *Appl. Phys. Lett.* **83** 2253 (2003)
295. X Chen, C An, J Liu, X Wang, Y Qian *J. Cryst. Growth* **253** 357 (2003)
296. Y W Wang, L D Zhang, G Z Wang, X S Peng, Z Q Chu, C H Liang *J. Cryst. Growth* **234** 171 (2002)
297. Y C Kong, D P Yu, B Zhang, W Fang, S Q Feng *Appl. Phys. Lett.* **78** 407 (2001)
298. K Park, J S Lee, M Y Sung, S Kim *Jpn. J. Appl. Phys., Part 1* **41** 7317 (2002)
299. P D Yang, H Q Yan, S Mao, R Russo, J Johnson, R Saykally, N Morris, J Pham, R He, H J Choi *Adv. Function. Mater.* **12** 323 (2002)
300. J S Lee, K Park, M I Kang, I W Park, S W Kim, W K Cho, H S Han, S Kim *J. Cryst. Growth* **254** 423 (2003)
301. K McGuire, Z W Pan, Z L Wang, D Milkie, J Menendez, A M Rao *J. Nanosci. Nanotechnol.* **2** 499 (2002)
302. J Y Lao, J Y Huang, D Z Wang, Z F Ren *Nano Lett.* **2** 235 (2003)
303. J G Wen, J Y Lao, D Z Wang, T M Kyaw, Y L Foo, Z F Ren *Chem. Phys. Lett.* **372** 717 (2003)
304. P Gao, Z L Wang *J. Phys. Chem. B* **106** 12653 (2002)
305. H J Yuan, S S Xie, D F Liu, X Q Yan, Z P Zhou, L J Ci, J X Wang, Y Gao, L Song, L F Liu, W Y Zhou, G Wang *Chem. Phys. Lett.* **371** 337 (2003)
306. J Q Hu, X L Ma, Z Y Xie, N B Wong, C S Lee, S T Lee *Chem. Phys. Lett.* **344** 97 (2001)
307. J Zhang, W Yu, L Zhang *Phys. Lett. A* **299** 276 (2002)
308. K Ogata, K Maejima, S Fujita, S Fujita *J. Cryst. Growth* **248** 25 (2003)
309. K Maejima, M Ueda, S Fujita, S Fujita *Jpn. J. Appl. Phys., Part 1* **42** 2600 (2003)
310. K S Kim, H W Kim *Physica B* **328** 368 (2003)
311. S C Liu, J J Wu *J. Mater. Chem.* **12** 3125 (2002)
312. W I Park, D H Kim, S W Jung, G C Yi *Appl. Phys. Lett.* **80** 4232 (2002)
313. M Haupt, A Ladenburger, R Sauer, K Thonke, R Glass, W Roos, J P Spatz, H Rauscher, S Riethmuller, M Moller *J. Appl. Phys.* **93** 6252 (2003)
314. M Kawakami, A B Hartanto, Y Nakata, T Okada *Jpn. J. Appl. Phys., Part 2* **42** L33 (2003)
315. M H Huang, S Mao, H Feick, H Q Yan, Y Y Wu, H Kind, E Weber, R Russo, P D Yang *Science* **292** 1897 (2001)
316. X M Sun, Z X Deng, Y D Li *Mater. Chem. Phys.* **80** 366 (2003)
317. J J Wu, S C Liu *Adv. Mater.* **14** 215 (2002)
318. J S Lee, M I Kang, S Kim, M S Lee, Y K Lee *J. Cryst. Growth* **249** 201 (2003)
319. Y Dai, Y Zhang, Y Q Bai, Z L Wang *Chem. Phys. Lett.* **375** 96 (2003)
320. Y B Li, Y Bando, T Sato, K Kurashima *Appl. Phys. Lett.* **81** 144 (2002)
321. D F Liu, D S Tang, L J Ci, X Q Yan, X Y Liang, Z P Zhou, H J Yuan, W Y Zhou, G Wang *Chin. Phys. Lett.* **20** 928 (2003)
322. C H Liu, J A Zapien, Y Yao, X M Meng, C S Lee, S S Fan, Y Lifshitz, S T Lee *Adv. Mater.* **15** 838 (2003)
323. P Hu, Y Q Liu, X B Wang, L Fu, D B Zhu *Chem. Commun.* 1304 (2003)
324. Y K Tseng, I N Lin, K S Liu, T S Lin, I C Chen *J. Mater. Res.* **18** 714 (2003)
325. S C Lyu, Y Zhang, H Ruh, H J Lee, H W Shim, E K Suh, C J Lee *Chem. Phys. Lett.* **363** 134 (2002)
326. Y Li, G S Cheng, L D Zhang *J. Mater. Res.* **15** 2305 (2000)
327. M J Zheng, L D Zhang, G H Li, W Z Shen *Chem. Phys. Lett.* **363** 123 (2002)
328. Y Li, G W Meng, L D Zhang, F Phillipp *Appl. Phys. Lett.* **76** 2011 (2000)
329. S U Yuldashev, S W Choi, T W Kang, L A Nosova *J. Korean Phys. Soc.* **42** S216 (2003)
330. H Zhang, X Ma, J Xu, J Niu, D Yang *Nanotechnology* **14** 423 (2003)
331. H Kim, W Sigmund *Appl. Phys. Lett.* **81** 2085 (2002)
332. W I Park, S W Jung, G C Yi, S H Oh, C G Park, M Kim *Jpn. J. Appl. Phys., Part 2* **41** L1206 (2002)
333. J J Wu, S C Liu, C T Wu, K H Chen, L C Chen *Appl. Phys. Lett.* **81** 1312 (2002)
334. J Q Hu, Q Li, X M Meng, C S Lee, S T Lee *Chem. Mater.* **15** 305 (2003)
335. Z Wang, X F Qian, Y Li, J Yin, Z K Zhu *J. Solid State Chem.* **178** 1589 (2005)
336. J Q Hu, Y Bando, Z W Liu *Adv. Mater.* **15** 1000 (2003)
337. B Min, J S Lee, J W Hwang, K H Keem, M I Kang, K Cho, M Y Sung, S Kim, M-S Lee, S O Park, J T Moon *J. Cryst. Growth* **252** 565 (2003)
338. Q Li, C Wang *Chem. Phys. Lett.* **375** 525 (2003)
339. C J Lee, T J Lee, S C Lyu, Y Zhang, H Ruh, H J Lee *Appl. Phys. Lett.* **81** 3648 (2002)
340. Y W Zhu, H Z Zhang, X C Sun, S Q Feng, J Xu, Q Zhao, B Xiang, R M Wang, D P Yu *Appl. Phys. Lett.* **83** 144 (2003)
341. H Kind, H Q Yan, B Messer, M Law, P D Yang *Adv. Mater.* **14** 158 (2002)
342. W I Park, Y H Jun, S W Jung, G C Yi *Appl. Phys. Lett.* **82** 964 (2003)
343. L Guo, J X Cheng, X Y Li, Y J Yan, S H Yang, C L Yang, J N Wang, W K Ge *Mater. Sci. Eng., C* **16** 123 (2001)
344. M S Arnold, P Avouris, Z W Pan, Z L Wang *J. Phys. Chem. B* **107** 659 (2003)
345. W I Park, G C Yi, J W Kim, S M Park *Appl. Phys. Lett.* **82** 4358 (2003)
346. J C Johnson, H Q Yan, R D Schaller, P B Petersen, P Yang, R J Saykally *Nano Lett.* **2** 279 (2002)
347. N I Kovtyukhova, B R Martin, J K N Mbindyo, P A Smith, B Razavi, T S Mayer, T E Mallouk *J. Phys. Chem. B* **105** 8762 (2001)
348. X D Bai, P X Gao, Z L Wang, E G Wang *Appl. Phys. Lett.* **82** 4806 (2003)
349. J Wang, H B Chen, H He, Y Cai, J D Lin, J Yi, H B Zhang, D W Liao *Chin. Chem. Lett.* **13** 1217 (2002)
350. Y Y Wu, H Q Yan, P D Yang *Top. Catal.* **19** 197 (2002)
351. T Xu, C S Xie *Prog. Org. Coat.* **46** 297 (2003)
352. L F Dong, J Jiao, D W Tuggle, J M Petty, S A Elliff, M Coulter *Appl. Phys. Lett.* **82** 1096 (2003)
353. Y W Heo, V Varadarajan, M Kaufman, K Kim, D P Norton, F Ren, P H Fleming *Appl. Phys. Lett.* **81** 3046 (2002)
354. Z X Zheng, Y Y Xi, P Dong, H G Huang, J Z Zhou, L L Wu, Z H Lin *Phys. Chem. Commun.* **5** 63 (2002)
355. C N R Rao, B C Satishkumar, A Govindaraj *Chem. Commun.* 1581 (1997)
356. F Miyaji, Y Tatematsu, Y Suyama *J. Ceram. Soc. Jpn.* **109** 924 (2001)
357. Z Q Shen, L L He, E D Wu, Y Y Fan, J F He, H M Cheng, D X Li, H Q Ye *J. Mater. Res.* **17** 2761 (2002)

358. Y Li, Y Bando *Chem. Phys. Lett.* **364** 484 (2002)
359. M Niederberger, F Krumeich, H-J Muhr, M Müller, R Nesper *J. Mater. Chem.* **11** 1941 (2001)
360. X M Wei, H C Zeng *J. Phys. Chem. B* **107** 2619 (2003)
361. Y W Wang, C H Liang, G Z Wang, T Gao, S X Wang, J C Fan, L D Zhang *J. Mater. Sci. Lett.* **20** 1687 (2001)
362. X S Peng, X F Wang, Y W Wang, C Z Wang, G W Meng, L D Zhang *J. Phys. D: Appl. Phys.* **35** L101 (2002)
363. X Liu, C Li, S Han, J Han, C W Zhou *Appl. Phys. Lett.* **82** 1950 (2003)
364. W T Dong, C S Zhu *Opt. Mater. (Amsterdam)* **22** 227 (2003)
365. F D Morrison, L Ramsay, J F Scott *J. Phys.: Condens. Matter.* **15** L527 (2003)
366. Y Q Zhu, W Hu, W K Hsu, M Terrones, N Grobert, J P Hare, H W Kroto, D R M Walton, H Terrones *Chem. Phys. Lett.* **309** 327 (1999)
367. W B Hu, Y Q Zhu, W K Hsu, B H Chang, M Terrones, N Grobert, H Terrones, J P Hare, H W Kroto, D R M Walton *Appl. Phys. A* **70** 231 (2000)
368. K Lee, W S Seo, J T Park *J. Am. Chem. Soc.* **125** 3408 (2003)
369. Y Miyamoto, A Rubio, M L Cohen, S G Louie *Phys. Rev. B* **50** 4976 (1994)
370. T Kar, M Cuma, S Scheiner *J. Mol. Struct.* **556** 275 (2000)
371. C Y Zhi, X D Bai, E G Wang *Appl. Phys. Lett.* **80** 3590 (2002)
372. T Kar, J Pattanayak, S Scheiner *J. Phys. Chem. A* **107** 8630 (2003)
373. T Yoshioka, H Suzuura, T Ando *J. Phys. Soc. Jpn.* **72** 2656 (2003)
374. M Terrones, D Golberg, N Grobert, T Seeger, M Reyes-Reyes, M Mayne, R Kamalakaran, P Dorozhkin, Z C Dong, H Terrones, M Ruhle, Y Bando *Adv. Mater.* **15** 1899 (2003)
375. L Wirtz, A Rubio, R A de la Concha, A Loiseau *Phys. Rev. B* **68** 045425 (2003)
376. S Guerini, P Piquini *Microelectr. J.* **34** 495 (2003)
377. G Seifert, H Terrones, M Terrones, G Jungnickel, T Frauenheim *Phys. Rev. Lett.* **85** 146 (2000)
378. G Seifert, H Terrones, M Terrones, T Frauenheim *Solid State Commun.* **114** 245 (2000)
379. G Seifert, H Terrones, M Terrones, T Frauenheim *Solid State Commun.* **115** 635 (2000)
380. G Seifert, T Kohler, R Tenne *J. Phys. Chem B* **106** 2497 (2002)
381. V V Ivanovskaya, A N Enyashin, N I Medvedeva, Yu N Makurin, A L Ivanovskii *Internet Electron J. Mol. Design* **2** 499 (2003)
382. V V Ivanovskaya, A N Enyashin, N I Medvedeva, A L Ivanovskii *Phys. Status Solidi B* **238** R1 (2003)
383. B W Smith, M Monthioux, D E Luzzi *Nature (London)* **396** 323 (1998)
384. B Burteaux, A Claye, B W Smith, M Monthioux, D E Luzzi, J E Fischer *Chem. Phys. Lett.* **310** 21 (1999)
385. B W Smith, M Monthioux, D E Luzzi *Chem. Phys. Lett.* **315** 31 (1999)
386. B W Smith, D E Luzzi *Chem. Phys. Lett.* **321** 169 (2000)
387. D E Luzzi, B W Smith *Carbon* **38** 1751 (2000)
388. D J Hornbaker, S J Kahng, S Misra, B W Smith, A T Johnsos, E J Mele, D E Luzzi, A Yazdani *Science* **295** 828 (2002)
389. X Liu, T Pichler, A Knupfer, M S Golden, J Fink, H Kataura, Y Achiba, K Hirahara, S Iijima *Phys. Rev. B* **65** 045 419 (2002)
390. S Bandow, M Takizawa, K Hirahara, M Yudasaka, S Iijima *Chem. Phys. Lett.* **337** 48 (2001)
391. H Kataura, Y Maniwa, T Kodama, K Kikuchi, K Hirahara, K Suenaga, S Iijima, S Suzuki, Y Achiba, W Kratschmer *Synth. Met.* **121** 1195 (2001)
392. K Hirahara, S Bandow, K Suenaga, T Okazaki, H Shinohara, S Iijima *Phys. Rev. B* **64** 115420 (2001)
393. K Hirahara, K Suenaga, S Bandow, H Kato, T Okazaki, H Shinohara, S Iijima *Phys. Rev. Lett.* **85** 5384 (2000)
394. E Hernandez, V Meunier, B W Smith, R Rurali, H Terrones, M B Nardelli, M Terrones, D E Luzzi, J C Charlier *Nano Lett.* **3** 1037 (2003)
395. J Lee, H Kim, S J Kahng, G Kim, Y W Son, J Ihm, H Kato, Z W Wang, T Okazaki, H Shinohara, Y Kuk *Nature (London)* **415** 1005 (2002)
396. V V Ivanovskaya, A A Sofronov, A L Ivanovskii *Teor. Eksp. Khim.* **37** 331 (2001) [d]
397. A A Sofronov, V V Ivanovskaya, Yu N Makurin, A L Ivanovskii *Chem. Phys. Lett.* **351** 35 (2002)
398. A L Ivanovskii *Zh. Neorg. Khim.* **48** 945 (2003) [a]
399. T Pichler, X Liu, M Knupfer, J Fink *New J. Phys.* **5** 156 (2003)
400. T Yamaguchi, N Ishii, K Tashiro, T Aida *J. Am. Chem. Soc.* **125** 13934 (2003)
401. M Otani, S Okada, A Oshiyama *Phys. Rev. B* **68** 125424 (2003)
402. T Seeger, Th Köhler, T Frauenheim, N Grobert, M Rühle, M Terrones, G Seifert *Chem. Commun.* 34 (2002)
403. N Grobert, T Seeger, G Seifert, M Rühle *J. Ceram. Proc. Res.* **4** 1 (2003)
404. V V Ivanovskaya, A N Enyashin, A L Ivanovskii *Mendeleev Commun.* 5 (2003)
405. V V Ivanovskaya, A N Enyashin, N I Medvedeva, A L Ivanovskii http://xxx.lanl.gov/PS_cache/cond-mat/pdf/0211/0211441.pdf
406. S Shin, S Suga, M Taniguchi, M Fujisawa, H Kanzaki, A Fujimori, H Daimon Y Ueda, K Kosuge, S Kachi *Phys. Rev. B* **41** 4993 (1990)
407. R Asahi, Y Taga, W Mannstadt, A J Freeman *Phys. Rev. B* **61** 7459 (2000)
408. S P Kowalczyk, F R McFeely, L Ley, V T Gritsyna, D A Shirley *Solid State Commun.* **23** 161 (1977)
409. M F Guelfucci *J. Phys. Chem. Solids* **62** 1961 (2001)
410. A N Enyashin, V V Ivanovskaya, Yu N Makurin, V G Bamburov, A L Ivanovskii *Dokl. Akad. Nauk* **391** 496 (2003) [c]
411. V V Ivanovskaya, A N Enyashin, A L Ivanovskii *Zh. Strukt. Khim.* **45** 158 (2004) [e]
412. V V Ivanovskaya, A N Enyashin, A L Ivanovskii *Zh. Neorg. Khim.* **49** 285 (2004) [a]
413. V V Ivanovskaya, A N Enyashin, A A Sofronov, Yu N Makurin, N I Medvedeva, A L Ivanovskii *Solid State Commun.* **126** 489 (2003)
414. A Chakrabarti, K Hermann, R Druzinic, M Witko, F Wagner, M Petersen *Phys. Rev. B* **59** 10 583 (1999)
415. K Hermann, M Witko, R Druzinic, A Chakrabarti, B Tepper, M Elsner, A Gorschluter, H Kuhlenbeck, H J Freund *J. Electron. Spectrosc. Relat. Phenom.* **98 – 99** 245 (1999)
416. M Demeter, M Neumann, W Reichelt *Surf. Sci.* **454** 41 (2000)
417. K Hermann, A Chakrabarti, R Druzinic, M Witko *Phys. Status Solidi A* **173** 195 (1999)
418. I Loa, A Grzechnik, U Schwarz, K Syassen, M Hanfland, R K Kremer *J. Alloys Compd.* **317** 103 (2001)
419. J P Perdew, Y Wang *Phys. Rev. B* **45** 13244 (1992)
420. C Kolczewski, K Hermann *J. Chem. Phys.* **118** 7599 (2003)
421. A Michalak, M Witko, K Hermann *Surf. Sci.* **375** 385 (1997)
422. V Eyert, K H Hock *Phys. Rev. B* **57** 12727 (1998)
423. K Hermann, M Witko, R Druzinic *Faraday Discuss.* **114** 53 (1999)
424. K Hermann, M Witko, R Druzinic, R Tokarz *Appl. Phys. A: Mater. Sci. Process.* **72** 429 (2001)
425. A N Enyashin, V V Ivanovskaya, Yu N Makurin, A L Ivanovskii http://xxx.lanl.gov/PS_cache/cond-mat/pdf/0303/0309179.pdf
426. A N Enyashin, V V Ivanovskaya, Yu N Makurin, A L Ivanovskii *Mendeleev Commun.* 94 (2004)
427. V L Volkov, G S Zakharova, V M Bondarenka *Kserogeli Prostykh i Slozhnykh Polivanadatov* (Xerogels of Simple and Complex Polyvanadates) (Ekaterinburg: Urals Branch of the Russian Academy of Sciences, 2001)

[a] — *Russ. J. Inorg. Chem. (Engl. Transl.)*
[b] — *J. Exp. Theor. Phys. Lett. (Engl. Transl.)*
[c] — *Dokl. Chem. (Engl. Transl.)*
[d] — *Theor. Exp. Chem. (Engl. Transl.)*
[e] — *Russ. J. Struct. Chem. (Engl. Transl.)*